

**Harnessing lignin-degrading fungal peroxidases to
enhance the valorization of lignocellulosic biomass**

(リグノセルロース系バイオマスの高価値化に向けたリグニン
分解ペルオキシダーゼの活用)

Kenneth Sze Kai TEO

Supervisor

Prof. Masato Katahira

Graduate School of Energy Science

Institute of Advanced Energy

Kyoto University

Table of contents

Chapter 1

General introduction

1.1. Renewable energy	2
1.2. Lignocellulosic biomass	3
1.2.1 Cellulose	5
1.2.2 Hemicellulose	6
1.2.3 Lignin	7
1.3 Lignocellulosic biomass to biofuels and biochemicals	9
1.3.1 Biofuels	9
1.3.1.1 Bioethanol	10
1.3.2 Biochemicals	11
1.4 Pretreatment of lignocellulosic biomass	12
1.4.1 Physical pretreatment methods	12
1.4.2 Chemical pretreatment methods	13
1.4.3 Biological pretreatment methods	14
1.5 White-rot fungi	15
1.5.1 Laccase	16
1.5.2 Manganese peroxidase	17
1.5.3 Lignin peroxidase	18
1.5.4 Versatile peroxidase	20
1.6 Research objectives	20
1.7 References	23

Chapter 2

Understanding manganese peroxidase-catalyzed conversion of the lignin structure and its application for the polymerization of Kraft lignin

2.1 Introduction	40
2.2 Results and discussion	42
2.2.1 Analysis of reaction products by RP-HPLC	42
2.2.2 Analysis of compounds contained in P1-5 by SEC	45
2.2.3 NMR analysis of GGE	47

2.2.4 NMR analysis of a compound present in P1	53
2.2.5 Application of CsMnP for KL polymerization	59
2.3 Conclusions	65
2.4 Experimental procedures	65
2.4.1 Cloning and expression of CsMnP in <i>Pichia pastoris</i> , and preparation of crude CsMnP	
2.4.2 Activity assaying of CsMnP	67
2.4.3 Reaction of GGE with CsMnP	67
2.4.4 Analysis and separation of reaction products by RP-HPLC	68
2.4.5 Molecular weight analysis of reaction products by SEC	69
2.4.6 Structural analysis of the reaction product by 2D NMR	69
2.4.7 Polymerization of KL by CsMnP	70
2.4.8 Estimation of total phenolic content in KL	71
2.4.9 Molecular weight analysis of KL by SEC	71
2.4.10 Structural analysis of KL by 2D NMR	72
2.5 References	72

Chapter 3

Enhanced depolymerization of beech wood lignin and its removal with peroxidases through continuous separation of lignin fragments

3.1 Introduction	82
3.2 Results	85
3.2.1 Peroxidase-catalyzed lignin depolymerization in batch and membrane bioreactors	
3.2.2 Analysis of aromatic products released into the aqueous phase	86
3.2.3 Identification of the depolymerized products in the filtrate	89
3.2.4 Lignin removal from MBW through the peroxidase-catalyzed reaction	94
3.2.5 Molecular weight distribution of lignin in the solid residues	97
3.2.6 Analysis of lignin substructures in the solid residues by NMR spectroscopy	101
3.2.7 Enzymatic hydrolysis of solid residues	107
3.3 Discussion	108
3.4 Conclusions	112
3.5 Experimental procedures	113

3.5.1 Preparation of milled beech wood	113
3.5.2 Preparation of crude MnP and LiP	114
3.5.3 Peroxidase-catalyzed lignin degradation in the batch bioreactor	115
3.5.4 Peroxidase-catalyzed lignin degradation in the membrane bioreactor	116
3.5.5 SEC of the products released into the aqueous phase	117
3.5.6 GCMS analysis of the depolymerized products in the filtrate	118
3.5.7 Chemical composition analysis of the solid residues	119
3.5.8 SEC for solid residues	121
3.5.9 Structural analysis of MBW solid residue by 2D NMR	122
3.5.10 Enzymatic hydrolysis of solid residues	123
3.6 References	124

Chapter 4

Enhancing bioethanol production from rice straw through environmentally-friendly delignification using versatile peroxidase

4.1 Introduction	133
4.2 Results and discussion	136
4.2.1 Optimization of VP expression for activity	136
4.2.2 Optimizing VP enzymatic activity using monomeric and dimeric substrates	138
4.2.3 Delignification of RS using VP	142
4.2.4 Effect of VP treatment on enzymatic saccharification of RS	143
4.2.5 Molecular weight analysis of delignified RS	146
4.2.6 FTIR spectroscopy analysis of raw and delignified RS	147
4.2.7 Morphological characterization of raw and delignified RS	149
4.2.8 Effect of VP treatment on ethanol production from RS	150
4.3 Conclusions	153
4.4 Experimental procedures	153
4.4.1 Cloning and expression of VP gene in <i>Pichia pastoris</i>	153
4.4.2 Optimizing the expression of VP	154
4.4.3 Production of VP	155
4.4.4 Enzymatic activity assessment of VP using monomeric substrates	156
4.4.5 Enzymatic activity assessment of VP using dimeric substrates	157
4.4.6 Preparation of rice straw	158

4.4.7 VP-catalyzed delignification of rice straw	158
4.4.8 Composition analysis of rice straw by the Klason lignin method	159
4.4.9 HPLC analysis	160
4.4.10 Molecular weight analysis of treated rice straw	161
4.4.11 Structural morphology analysis of treated rice straw	162
4.4.12 Fourier transform infrared spectroscopy analysis of treated rice straw	162
4.4.13 Enzymatic saccharification of treated rice straw	163
4.4.14 Simultaneous saccharification and fermentation of treated rice straw	163
4.5 References	164
Chapter 5	
Conclusions	173
List of publications	177
List of presentations	178
Acknowledgements	180

List of abbreviations

- NHE: normal hydrogen electrode
- MnP: manganese peroxidase
- LiP: lignin peroxidase
- VP: versatile peroxidase
- H₂O₂: hydrogen peroxide
- GGE: guaiacylglycerol-beta-guaiacyl ether
- SGE: syringylglycerol-beta-guaiacyl ether
- VGE: veratrylglycerol-beta-guaiacyl ether
- RP-HPLC: reverse-phase high performance liquid chromatography
- 2D NMR: two-dimensional nuclear magnetic resonance
- HSQC: heteronuclear single quantum coherence spectroscopy
- HMBC: heteronuclear multiple bond correlation
- SEC: size-exclusion chromatography
- GCMS: gas chromatography mass spectrometry
- FTIR: fourier transform infrared spectroscopy
- SEM: scanning electron microscope
- KL: Kraft lignin
- M_n: number-average molecular weight
- M_w: weight -average molecular weight
- M_p: peak molecular weight
- GAE: gallic-acid equivalent
- DMP: 2,6-dimethoxyphenol
- VA: veratryl alcohol
- MBW: milled beech wood
- MWCO: molecular weight cut-off
- RC: regenerated cellulose
- LP: percentage of lignin
- RES: solid residues
- CEL: cellulolytic enzyme lignin
- TA: total amount
- SSF: simultaneous saccharification and fermentation

Chapter 1

General Introduction

1.1 Renewable energy

Energy is the cornerstone of our present society, and it will undoubtedly maintain its critical role in shaping our future. Global energy demand had risen in tandem with technological advancements, population growth, and economic expansion since the onset of the industrial revolution in the 17th century.^{1,2} To meet this ever-growing demand, fossil fuels, such as oil, natural gas, and coal, have played a central role.³ However, it is important to acknowledge that fossil fuels are finite and non-renewable resources. While fossil fuels have been instrumental in driving global industrialization due to their affordability, convenience, and reliability, their prolonged use has taken a toll on the environment.^{3,4} This is primarily evident in the alarming increase in greenhouse gas emissions, contributing to global warming experienced worldwide.^{3,4}

In response to this environmental crisis, the international community has united through agreements like the Kyoto Protocol and the Paris Agreement.⁵ These global accords have urged the governments worldwide to shift their energy policies away from polluting fossil fuels and towards cleaner, renewable energy sources.⁶ As a result, renewable energy such as solar, hydropower, bioenergy, geothermal, and wind energy have experienced substantial growth in worldwide adoption.⁷ Unlike fossil fuels, renewable energy harnesses the power of natural cycles, offering a cleaner and more sustainable alternative.⁸

Among these sustainable energy options, biofuels stand out as an attractive alternative due to their chemical similarity to fossil fuels.⁹ Biofuels are derived from renewable biological sources (lignocellulosic biomass) such as corn, woody biomass, algae, soybeans, and palm oils.¹⁰ Biofuels like biodiesel and bioethanol have gained widespread popularity,

especially in Brazil and United States, where they are often blended with conventional fossil fuels and used in transportation sector.¹¹ In addition to their renewability, biofuels have the potential to alleviate the adverse environmental impacts associated with fossil fuels by reducing overall greenhouse gas emissions and pollutants.^{12,13}

1.2 Lignocellulosic biomass

Lignocellulosic biomass, a complex organic material found abundantly worldwide, acting as a natural storehouse of solar energy, harnessed by plants through photosynthesis process.¹⁴ In this process, plants absorb sunlight, extract carbon dioxide from the atmosphere, and draw water from the ground. These inputs are then transformed into glucose, a versatile molecule that serves as the fuel for plant growth.^{15,16}

Lignocellulosic biomass displays diverse forms and compositions, reflecting the planet's rich biodiversity.¹⁷⁻¹⁹ Broadly, it can be categorized into the following groups. Woody Biomass: This category encompasses materials such as wood residues, sawdust, and forest debris obtained from trees, shrubs, and woody plants.²⁰ Agricultural Biomass: This category includes materials from various crops and agricultural residues, such as corn stover, wheat straw, and sugarcane bagasse.^{20,21}

The Earth is home to a vast amount of biomass across various ecosystems, ranging from forests to oceans. Estimates suggest that the world's total biomass reserves amount to approximately 1.8 trillion tons on land and 4 billion tons in aquatic environments.^{22,23} The sheer abundance and versatility of lignocellulosic biomass position itself as a promising and sustainable resource for producing valuable biofuels and biochemicals.^{24,25} Additionally,

another significant advantage of utilizing lignocellulosic biomass for energy production is that any carbon dioxide released into the atmosphere essentially constitutes recycled carbon.^{17,20} This carbon originally came from the atmosphere during the plants' growth phase through photosynthesis.^{14,25} This unique carbon recycling process renders lignocellulosic biomass a carbon-neutral resource, meaning it neither increases nor decreases the overall levels of carbon dioxide in the atmosphere.^{17,18,24} To fully tap into this potential, it is essential to gain a comprehensive understanding of the diverse chemical compositions present in lignocellulosic biomass.

Lignocellulosic biomass typically consists of three primary components: cellulose, hemicellulose, and lignin (Figure 1.1).²⁶ The distribution of these components can vary significantly among different sources and types of biomass.²⁷ By harnessing these chemical compounds, we can establish integrated biorefineries capable of producing substantial quantities of valuable biofuels and biochemicals from lignocellulosic biomass.²⁸

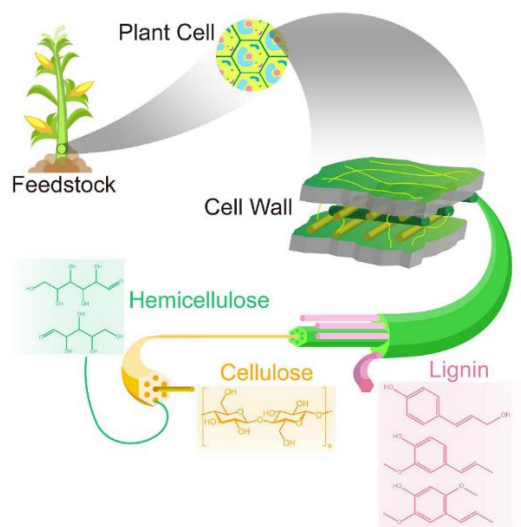


Figure 1.1. Composition of lignocellulosic biomass.²⁶

1.2.1 Cellulose

Cellulose, the most abundant organic polymer found in nature, makes up a significant portion of lignocellulosic biomass, comprising approximately 40-60% of its weight.²⁹ Cellulose is a complex polysaccharide that serves as the primary component of the plant cell wall, imparting stiffness and stability to it.³⁰ It consists of a linear homopolymer composed of β -D-glucopyranose units linked together via β -1,4 glycosidic bonds, with cellobiose as the fundamental repeating unit (see Figure 1.2).³¹ These cellulose chains organize themselves into microfibrils, which further assemble into cellulose fibrils.^{32,33} The cohesion between neighboring cellulose chains is facilitated by hydrogen bonds and van der Waal's forces, resulting in parallel alignment and the formation of a crystalline structure, which limits enzyme accessibility.^{34,35}

Cellulose materials find widespread applications in various manufacturing industries, including textiles, pharmaceuticals, and industrial sugar production.³⁶ They are used as building materials in the form of wood, in the production of paper products, and for manufacturing cotton, linen, and rayon for clothing, as well as cellulose acetate for packaging films.³⁷ Cellulose and its derivatives are known for their strength, reproducibility, recyclability, and biocompatibility, making them suitable for a range of biomedical applications, such as blood purification membranes.^{38,39}

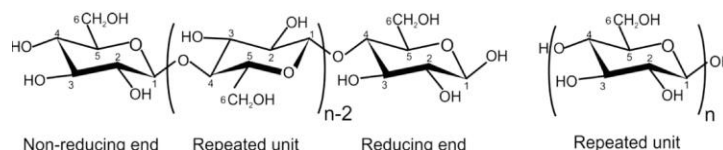


Figure 1.2. Structure of cellulose. Left: cellulose chain's nonreducing and reducing ends. Right: the repeating unit (anhydroglucose).³¹

1.2.2 Hemicellulose

Hemicelluloses, a diverse group of biopolymers, constitute approximately 20-40% of the total biomass weight and ranked as the second most abundant branched hetero biopolymers.⁴⁰ Hemicellulose is situated beneath cellulose fibers and plays a crucial role in tightly linking microfibrils through non-covalent attractions. It also forms complex bonds, both covalent and non-covalent, with lignin, contributing to the overall structural strength of the biomass.⁴¹

Unlike cellulose, hemicellulose is a form of dietary fiber derived from a heterogeneous group of sugars. This includes d-xylose, d-mannose, and d-galactose in the hemicellulose backbone chain, as well as l-arabinose, d-galactose, and 4-O-methyl-d-glucuronic acid in the hemicellulose side chains.^{42,43} The structure of hemicellulose is more complex than that of cellulose, characterized by numerous branches, with acetyl groups being the most prevalent. In hardwoods, hemicellulose mainly consists of pentose subunits, such as xylose (see Figure 1.3).⁴⁵ In softwoods, hemicellulose consists of hexose subunits, including glucose, mannose, and galactose.^{46,47} Generally, hemicellulose is amorphous, soft, and can be hydrolyzed by dilute acids, bases, or hemicellulase enzymes. Its amorphous nature, low degree of polymerization, and susceptibility to pretreatment processes make hemicellulose valuable in various industrial applications, including hydrogels, drug carriers, and cosmetics.^{48,49}

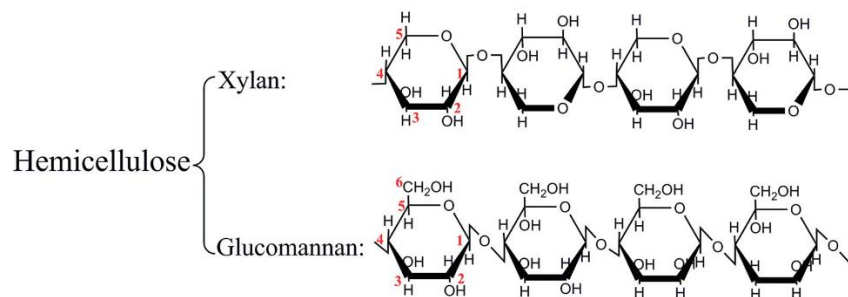


Figure 1.3. Structure of hemicellulose (xylan and glucomannan).⁴⁵

1.2.3 Lignin

Lignin is the most abundant aromatic biopolymer on Earth.⁵⁰ It plays a crucial role in providing structural reinforcement and resilience to plant tissues and is vital for water and nutrient transport.⁵¹ Lignin's remarkable mechanical properties make it an essential hydrophobic strengthening agent, which, in turn, complicates the hydrolysis process and enhances the recalcitrance of lignocellulose.⁵² Additionally, lignin acts as a protective barrier, shielding plant cells from enzymatic and chemical attacks, due to its higher resistance to degradation compared to polysaccharides.^{53,54}

Lignin is the most complex renewable three-dimensional biopolymer containing various functional groups, including phenylpropane, methoxy, and non-carbohydrate polyphenolic substances. It contributes to approximately 10-25% of the weight of lignocellulosic biomass.⁵⁵

The biosynthesis of lignin is a complex process consisting of three stages: (i) the creation of lignin monomers, (ii) their transport to the apoplast (the area between plant cells), and (iii) polymerization.^{9,56-59} During monomer formation, three types of monolignols are generated through the phenylalanine/tyrosine metabolic pathway in a plant's cell wall:

sinapyl alcohol (S), coniferyl alcohol (G), and p-coumaryl alcohol (H).^{57,58,60-63} Different plant types have varying compositions of these monolignols. Softwood, for instance, primarily contains G-type lignin, with up to 95% of G-units. Hardwood, on the other hand, mainly consists 46-75% of S-units and 25-50% of G-units. Grass has a composition of 5-33% H-units, 33-80% of G-units, and 20-54% of S-units.⁶¹⁻⁶³

These monolignols then undergo random polymerization, resulting in the formation of the complex and diverse structure known as lignin.⁶⁴ Two major types of linkages connect the units: ether linkages (β -O-4' and 4-O-5') and carbon-carbon (β -5', β -1', and β - β ') linkages (see Figure 1.4).⁶⁵ Among these, β -O-4' ether linkages account for approximately 50% of the total linkages in native lignin, along with an additional 5-12% consisting of β - β ', 1-9% of 5-5', and β -1' linkages.⁶⁵ Consequently, the destruction of β -O-4', which is the most reactive linkage, represents the critical step in lignin conversion.⁶⁶⁻⁶⁸

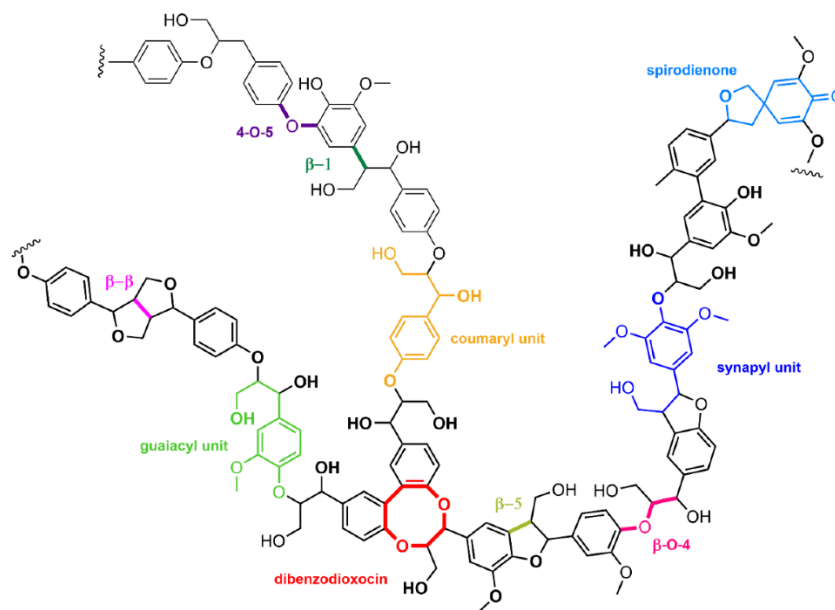


Figure 1.4. Lignin structure with their constituting units and interunit bonds.⁵⁷

1.3 Lignocellulosic biomass to biofuels and biochemicals

1.3.1 Biofuels

The term 'biofuel' refers to fuel obtained from renewable living materials, such as plants and animals.⁶⁹ Biofuels serve as energy carriers and non-fossil fuels that store the energy derived from organic biomass, including plants, animals, and microorganisms.⁶⁹ Biofuels can take various forms: (1) liquid, like bioethanol and biodiesel; (2) solid, including charcoal, wood pellets, and fuelwood; and (3) gas, such as biogas.⁷⁰ The categorization of biofuels is based on their biomass feedstock source and the technology used in their production, dividing them into first- to fourth-generation biofuels.^{71,72}

First-generation biofuels primarily originate from edible parts of plants.⁷³ Notable examples of first-generation biofuels include biodiesel, ethanol, biofuel gasoline, and biogas.⁷⁴ Currently, these first-generation biofuels are primarily produced using agricultural feedstocks with high polysaccharide contents such as sugarcane, corn, and sugar beets.⁷⁵ However, this approach has faced criticism from the global community due to ethical concerns related to the debate over using food crops for fuel production and the expansion of large farmlands for this purpose.⁶³

Second-generation biofuels are derived from non-edible plants or non-edible parts of plants.⁷⁶ Abundant non-edible lignocellulosic biomass, such as grasses, forest residues, and agricultural waste, serves as the feedstock for second-generation biofuel production.⁷⁷ Examples of second-generation biofuels include bioethanol, butanol, and mixed alcohols.^{78,79}

Third-generation biofuels are derived from photosynthetic microbes, particularly microalgae.⁸⁰ Fourth-generation biofuels are produced from genetically modified photosynthetic microbes, such as cyanobacteria, algae, and fungi.⁸¹

1.3.1.1 Bioethanol

Bioethanol, a prominent biofuel, holds great promise as an eco-friendly alternative to conventional fuels especially in the energy and transportation sector.⁸² It also serves as both a precursor and a highly efficient organic solvent for synthesizing various valuable chemicals and composites.⁸³

Derived from lignocellulosic biomass, bioethanol emerges as a particularly promising, environmentally friendly biofuel choice. It offers numerous advantages, including a high octane rating, a low boiling point, and high energy content comparable to traditional fuels.⁸⁴ Notably, vehicles can run on gasoline blended with up to 85% (v/v) bioethanol without any modifications, presenting a significant opportunity to reduce greenhouse gas emissions and petroleum consumption.⁸⁴

Generally, the production of bioethanol involves microbial fermentation, primarily utilizing carbohydrates from plants rich in sugars, such as corn, sugarcane, or lignocellulosic biomass.⁸⁵ The production process consists of three key steps: (1) pretreatment to separate lignin from cellulose, (2) hydrolysis of cellulose to obtain fermentable sugars, and (3) fermentation to convert sugars into ethanol, followed by distillation for ethanol purification.⁸⁶

Despite its advantages, the widespread industrialization of bioethanol has been limited to a few countries like Brazil and the USA due to the high energy consumption in

pretreatment, fermentation, and separation processes.⁸⁷ A significant challenge is the elevated processing cost, making the process economically unfeasible. Therefore, the development of an efficient pretreatment method that removes lignin while minimizing sugar content loss are critical in addressing this challenge.

1.3.2 Biochemicals

Lignocellulosic biomass has the potential to not only supplement but also potentially replace petroleum-based chemical feedstocks and raw materials.⁸⁸ Lignocellulosic biomass comprises cellulose and hemicellulose, the carbohydrate components, which are used in bioenergy production and the synthesis of essential low-molecular organic chemicals, including ethanol, methanol, acetic acid, formic acid, and 5-hydroxymethyl furfural.⁸⁹ While a considerable amount of research focuses on valorization of cellulose and hemicellulose, lignin, unfortunately, tends to receive less attention due to its highly recalcitrant properties. Nevertheless, the economic feasibility of biorefineries largely depends on efficiently harnessing all three components: cellulose, hemicellulose, and lignin.⁹⁰ Consequently, recent research have emphasized towards unlocking lignin's potential for the production of valuable biochemicals.

Lignin, formed through the radical polymerization of monolignols, holds significant promise as a source of aromatic chemical feedstocks and products.⁹¹ For example, bioproducts like vanillin, guaiacol, carbon-based nanomaterials, bioplastics, dyes, and aerogels can all be derived from lignin.^{92,93} These lignin-derived bioproducts serve as sustainable alternatives to petroleum-based counterparts, offering both cost-effectiveness and

renewability while simultaneously addressing concerns related to the production of non-biodegradable products and ecological pollution.⁹⁴

1.4 Pretreatment of lignocellulosic biomass

Efficient production of biofuels and biochemicals from lignocellulosic biomass necessitates an effective pretreatment process. The primary objective of pretreatment is to break down cellulose, hemicellulose, and lignin found within lignocellulosic biomass.⁹⁵ This breakdown enables their subsequent conversion into valuable bioproducts with higher efficiency.⁹⁵ Additionally, maintaining the native structure of these biomass components during pretreatment is essential to preserve their functionality for subsequent conversion to bioproducts.⁹⁶ Furthermore, factors such as energy consumption and economic feasibility of the pretreatment method is pivotal in determining its suitability for industrial applications.⁹⁷

In general, pretreatment approaches can be broadly categorized into three main categories: physical, chemical, and biological methods.⁹⁸

1.4.1 Physical pretreatment methods

Physical pretreatments involve disrupting the lignocellulose structure without introducing substantial chemical alterations to the individual cell wall components.⁹⁹ These treatments make use of various mechanical tools and techniques such as millers, grinders, screws, or microwave radiation.¹⁰⁰ One of the common methods employed in physical pretreatment is reducing the size of biomass particles through comminution, which includes dry, wet, vibratory, and compression-based ball milling.¹⁰⁰

The goal of physical pretreatment is to enhance the digestibility of enzymes by increasing the surface area accessible to the cell wall in relation to its volume.⁹⁹ In certain cases, extensive ball milling can lead to the decrystallization of cellulose and a reduction in the degree of polymerization, subsequently increasing hydrolysis efficiency.¹⁰¹ However, it is important to note that merely reducing particle size is often insufficient to significantly boost the rate of enzymatic hydrolysis.¹⁰¹ Moreover, as the desired particle size decreases, the cost of size reduction rises exponentially, potentially making the process economically impractical in commercial applications.⁹⁹ Consequently, it is common practice to follow physical pretreatment with chemical or biological treatments to avoid the need for extreme particle size reduction.⁹⁹

1.4.2 Chemical pretreatment methods

Chemical pretreatment stands as one of the most prevalent methods for breaking down lignocellulosic biomass.¹⁰² It harnesses a range of chemical agents such as organic solvents (1,4-dioxane) and alkaline (sodium hydroxide) to break apart the stubborn components of lignocellulosic biomass, with the ultimate goal of transforming this feedstock into optimal substrates for bioproduct production.¹⁰²

One key objective of chemical pretreatment is to modify or eliminate lignin while simultaneously reducing cellulose crystallinity.^{99,102} While chemical pretreatment methods have proven effective in enhancing the digestibility of lignocellulosic biomass, they do come with noteworthy downsides. These methods are often burdened by substantial costs and environmental concerns due to the significant quantities of chemical residues that necessitate

safe handling and disposal post-pretreatment.¹⁰³ Moreover, chemical pretreatment typically prioritizes the extraction of cellulose and hemicellulose, which often result in detrimental structural alterations to native lignin.¹⁰³ Consequently, this structural change makes it challenging to find further applications for lignin.

1.4.3 Biological methods

Biological pretreatment of lignocellulosic biomass emerges as a highly promising and environmentally friendly alternative to chemical pretreatment methods.¹⁰⁴ Its distinctive non-destructive nature minimizes structural alterations, especially in lignin, making it an attractive choice.¹⁰⁴ This approach is renowned for its simplicity, cost-effectiveness, and eco-friendly attributes, as it demands lower energy input (lower reaction temperatures) and avoids the use of harsh chemicals.¹⁰⁴

The biological pretreatment process employ bacteria, fungi, or their enzymes to break down the intricate structure of lignocellulosic materials before further processing.¹⁰⁵ Among them, fungi, particularly white-rot fungi, have exhibited remarkable effectiveness in pretreating lignocellulosic biomass.¹⁰⁶ Pretreatment of lignocellulosic biomass with white-rot fungi enhanced the accessibility of cellulose and hemicellulose for enzymatic hydrolysis, a critical step in biofuel production.¹⁰⁶ For instance, when rice straw undergoes fungal pretreatment using white-rot fungi, a significant portion of lignin was removed with minimal loss in cellulose and hemicellulose content.^{106,107} The lignin removal significantly enhanced the subsequent saccharification process, leading to a higher bioethanol yield.^{107,108} Additionally, the lignin removed during the process holds inherent value as it can be further

processed into valuable biochemicals.¹⁰⁹

Consequently, biological pretreatment holds the potential to fully utilize all three components (cellulose, hemicellulose, and lignin) within lignocellulosic biomass, establishing a complete biorefinery process.

1.5 White-rot fungi

The selective removal of lignin from lignocellulose has long been a central goal in unlocking the potential of plant biomass. In nature, this process plays a critical role in recycling terrestrial carbon and relies on the actions of microorganisms such as white-rot fungi.¹⁰⁷ Unlike many thermochemical industrial processes, certain white-rot fungi possess the remarkable ability to selectively break down lignin while preserving the integrity of the polysaccharides, all without causing environmental harm.¹¹⁰ Consequently, these selective white-rot fungi are gaining increasing attention for their potential applications in biotechnological fields such as biopulping and biofuel production.¹⁰⁷⁻¹¹⁰

These fungi employ a combination of extracellular ligninolytic enzymes, organic acids, mediators, and accessory enzymes to accomplish the complex task of degrading lignin.¹¹⁰ The primary enzymes responsible for this selective lignin degradation are collectively referred to as ligninolytic enzymes. Generally, there are four key ligninolytic enzymes involved in the process: laccase, manganese peroxidase, lignin peroxidase, and versatile peroxidase.¹¹¹

1.5.1 Laccase

Laccase (EC 1.10.3.2; Lac) is an extracellular enzyme containing copper, which facilitates the reduction of molecular oxygen to water while simultaneously catalyzing the one-electron oxidation of various substrates.¹¹² These substrates include diphenols, methoxy-substituted monophenols, aromatics, and aliphatic amines.^{113,114} Laccase is a glycosylated protein with a molecular weight ranging from 60 to 90 kDa.¹¹⁴ Since its initial discovery in the sap of the Japanese lacquer tree *Rhus vernicifera*, numerous laccase isozymes have been isolated from a variety of sources, including bacteria, fungi, plants, and insects.¹¹⁵ Laccase is distinct from peroxidase enzymes in that it does not require hydrogen peroxide (H₂O₂) but relies on oxygen for its catalytic reactions.¹¹⁶

Fungal laccases generally possess a redox potential of ≤ 800 mV vs. NHE, making them effective at oxidizing the phenolic subunits found in lignin.¹¹⁷ Conversely, non-phenolic subunits with higher redox potentials (>1400 mV vs. NHE) are resistant to oxidation by laccase alone.¹¹⁷ However, when laccase is combined with a suitable mediator, its oxidizing capacity can be extended to non-phenolic lignin structures.¹¹⁷

Figure 1.5 (a) illustrates the direct oxidation (in the absence of a mediator) of a substrate by laccase, while Figure 1.5 (b) demonstrates the indirect oxidation (in the presence of a mediator) of the substrate by laccase.¹¹⁸ In a laccase/mediator system, the oxidized mediator exhibits a high redox potential, enabling it to oxidize non-phenolic substrates through either electron transfer or radical hydrogen atom transfer mechanisms.¹¹⁸ Due to its versatility, laccase finds wide application in the food industry, pulp industry, and synthetic chemistry.

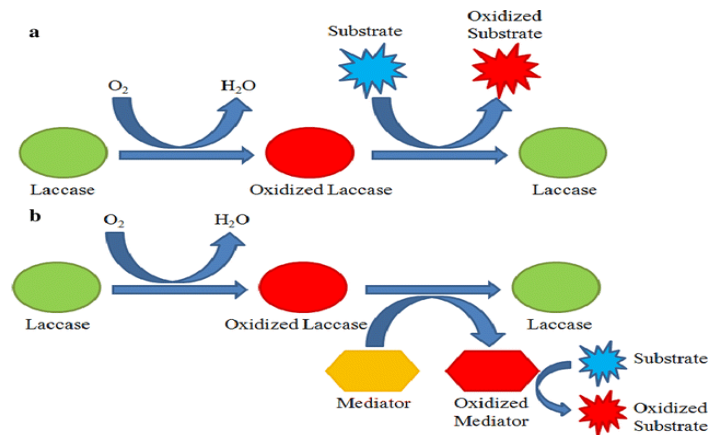


Figure 1.5. Catalytic mechanism of Lac (a) without mediator (b) with mediator.¹¹⁸

1.5.2 Manganese peroxidase

Manganese peroxidase (EC 1.11.1.13; MnP) is a heme-containing glycoprotein that was initially identified in 1985 in *Phanerochaete chrysosporium*.¹¹⁹ Belonging to the class II heme peroxidase family, MnP relies on the presence of hydrogen peroxide (H_2O_2) to initiate its enzymatic activity.¹²⁰ Like other ligninolytic enzymes, MnP is secreted extracellularly. MnP is particularly proficient at oxidizing phenolic lignin, although it can also oxidize non-phenolic lignin in the presence of mediators.¹²⁰ This enzyme is primarily produced by basidiomycetous fungi, with *Ceriporiopsis subvermispora* being the sole species known to contain genes for all three MnP subfamilies.^{120,121} MnP takes on various forms, with molecular sizes ranging from 38 to 62.5 kDa and comprises approximately 350 amino acid residues.¹²² Intriguingly, MnP shares a relatively similar sequence with another ligninolytic enzyme, lignin peroxidase (LiP), with a sequence similarity of around 43%.¹²³

As depicted in Figure 1.6, when MnP encounters H_2O_2 , it undergoes oxidation, forming a Fe^{4+} -oxo-porphyrin-radical complex referred to as MnP compound I.¹²⁴ MnP

compound I catalyzes the oxidation of a manganese ion and is subsequently reduced to MnP compound II.¹²⁴ MnP compound II is then further reduced back to its native resting state, during which another manganese ion undergoes oxidation. These oxidized manganese ions play a crucial role in the oxidation of lignin substrates, enabling MnP to oxidize a diverse range of substrates, both phenolic and non-phenolic.¹²⁵ Industries such as biopulping, biobleaching, and bioremediation have harnessed the capabilities of MnP in their processes.¹²⁶

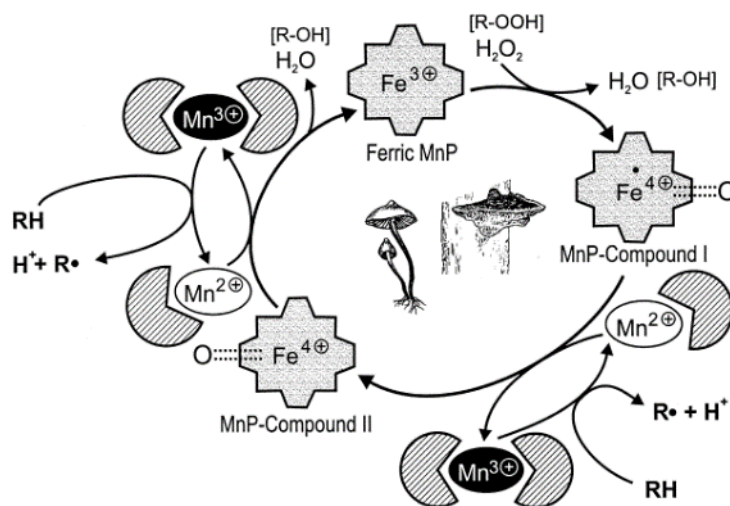


Figure 1.6. Catalytic cycle of MnP.¹²⁴

1.5.3 Lignin peroxidase

Lignin peroxidase (EC 1.11.1.14; LiP), also known as ligninase, is a glycosylated heme protein belonging to the class II fungal secretory peroxidases.¹²⁷ It typically has a molecular weight ranging from 37 to 50 kDa.¹²⁸ Its discovery dates back to 1983 in the fungus *P. chrysosporium*, and since then, various isozymes of LiP have been identified and sequenced in different fungi.¹²⁸ Some species possess multiple LiP isoenzymes, with

Trametes versicolor, for instance, having as many as 16.¹²⁹ For a considerable time, LiP was regarded as one of the most crucial enzymes in lignin degradation, exhibiting oxidative activity towards both phenolic and non-phenolic lignin.¹³⁰ Unlike MnP, LiP does not rely on manganese ions for its catalytic reactions. Instead, LiP's high redox potential allows it to directly oxidize non-phenolic lignin, a task that enzymes with lower redox potentials like MnP and Lac cannot accomplish without mediators.¹³¹ Like other peroxidases, LiP also requires H₂O₂ to initiate its catalytic activity.¹²⁸

The catalytic cycle of LiP can be divided into three key steps, as illustrated in Figure 1.7.¹³² Initially, LiP is oxidized by H₂O₂, resulting in the formation of a high redox potential intermediate known as compound I oxo-ferryl.¹³² Compound I then oxidizes a substrate while acquiring an electron to become compound II. The final step involved compound II oxidizing another substrate and returning to its resting ferric state, marking the completion of one oxidative cycle of LiP.^{132,133} Thanks to its high redox potential, LiP has garnered significant attention for its applications in scientific research, industry, and biotechnology.¹³⁴

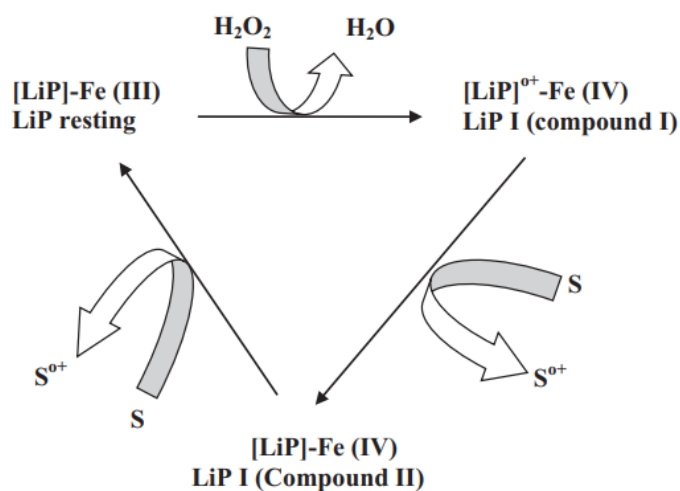


Figure 1.7. Catalytic cycle of LiP.¹³²

1.5.4 Versatile peroxidase

Versatile peroxidase (EC 1.11.1.16; VP), initially identified in the white-rot fungus *Pleurotus eryngii*, is a relatively recent addition to the family of lignin-degrading peroxidases.¹³⁵ It is exclusively found in fungi of the *Pleurotus*, *Bjerkandera*, and *Lepista* genera.¹³⁴ VP is often described as a hybrid enzyme, as it possesses the oxidative capabilities of both LiP and MnP.¹³² Similar to LiP, VP can directly oxidize lignin with high redox potential that is non-phenolic in nature.¹³⁶ Furthermore, VP has a unique Mn²⁺ catalytic site, akin to MnP, which facilitates the oxidation of manganese ions, subsequently aiding in the oxidation of phenolic lignin compounds.¹³²⁻¹³⁶

Because of its hybrid attributes, VP demonstrates a distinct dual oxidative capacity. This enables the enzyme to efficiently oxidize compounds with varying redox potentials, including phenolic and non-phenolic lignin, as well as diazo compounds, in a non-selective manner, using H₂O₂ as an oxidizing agent.¹³¹⁻¹³² These exceptional characteristics have sparked significant interest in VP for a wide range of biotechnological applications, such as designing biosensors, creating analytical kits, enhancing paper and pulp bleaching processes, and engaging in bioremediation efforts.¹³⁶

1.6 Research objectives

The development of a cost-effective and efficient biorefinery system for lignocellulosic biomass has been a long-standing challenge. A major hurdle lies in the complexity of extracting valuable chemical compounds from lignin during the biomass pretreatment process while simultaneously maximizing the yield of fermentable sugars

through saccharification.

In this study, I focused on the pretreatment phase of lignocellulosic biomass, employing a biological pathway due to its non-destructive nature and significantly reduced environmental impact compared to other methods. Specifically, I harnessed the capabilities of three ligninolytic peroxidases derived from white-rot fungi to catalyze lignin depolymerization in native biomass. My objectives were to obtain valuable aromatic monomers and enhance lignin removal from lignocellulosic biomass, ultimately improving the efficiency of saccharification for hemicellulose and cellulose.

To achieve these goals, I utilized a heterologous expression system to produce large quantities of MnP from *Ceriporiopsis subvermispora*, LiP from *Phanerochaete chrysosporium*, and VP from *Pleurotus eryngii* in *Pichia pastoris*. Subsequently, I assessed the catalytic activity of these peroxidases towards aromatic monomers and lignin model dimers.

Specifically, I conducted an extensive analysis on MnP using a guaiacyl-type lignin model dimer (GGE) as my substrate of interest. This thorough investigation encompassed a series of analytical techniques, including reverse-phase high-performance liquid chromatography (RP-HPLC), two-dimensional nuclear magnetic resonance spectroscopy (2D NMR), and size-exclusion chromatography (SEC). These analyses were employed to study the products resulting from MnP's catalytic activity on GGE, allowing us to propose a comprehensive reaction mechanism describing the interaction between MnP and GGE. Furthermore, I ventured into exploring the potential of MnP for the valorization of Kraft lignin. To achieve this, I compared the characteristics of MnP-polymerized Kraft lignin with

those of untreated Kraft lignin. My examination involved assessing the total phenolic content using the Folin-Ciocalteu method, tracking changes in molecular weight through SEC, and scrutinizing structural alterations using 2D NMR. In sum, my research delved into both the mechanistic intricacies of MnP's action on lignin model dimer and its potential for enhancing the value of Kraft lignin.

Continuing my investigation, I proceeded to apply MnP and LiP for catalyzing lignin depolymerization in beech wood within a commercial batch bioreactor. To further enhance the efficiency of lignin depolymerization, I introduced a novel membrane bioreactor, as previously reported by Steinmetz *et al.*¹³⁷ I then meticulously compared the results obtained from this approach with those from a conventional batch bioreactor. In my pursuit of deeper insights, I employed a range of analytical techniques to analyze the products generated during the lignin depolymerization process. These techniques included gas chromatography mass spectrometry (GCMS) to identify the specific products formed, Klason lignin quantification to evaluate the extent of delignification achieved, SEC to explore changes in lignin molecular weight, and enzymatic hydrolysis experiments to assess alterations in saccharification efficiency. This comprehensive suite of analyses provided a detailed understanding of the impact of MnP and LiP on lignin depolymerization in beech wood performed using batch and membrane bioreactors.

In the final phase of my research, I utilized VP to pretreat rice straw using the membrane bioreactor, with the primary goal of reducing the lignin content within the lignocellulosic biomass. Following this pretreatment step, I rigorously evaluated the effects of delignification by VP using a multi-pronged approach. First, I utilized SEC to examine

changes in lignin molecular weight. Additionally, Fourier transform infrared spectroscopy (FTIR) was employed to investigate changes in chemical functional groups within the rice straw after VP pretreatment. Furthermore, I employed scanning electron microscopy (SEM) to probe changes in surface morphology. Subsequently, I assessed the saccharification efficiency of the pretreated rice straw and quantified the resulting enhancement in bioethanol yield when compared to untreated straw samples. This study provided valuable insights into the effectiveness of VP in improving the overall efficiency of this bioconversion process, marking a significant contribution to the field of lignocellulosic biomass utilization.

1.7 References

1. J. R. Bas, D. C. Enrica, S. W. Ian, Amplification of future energy demand growth due to climate change. *Nat. Commun.* 2019, **10**, 2762.
2. N. Rabindra, P. Nirash, Energy security, electricity, population and economic growth: The case of a developing South Asian resource-rich economy. *Energy Policy* 2019, **132**, 771-781.
3. S. Shahriar, T. Erkan, When will fossil fuel reserves be diminished? *Energy Policy* 2009, **37**, 181-189.
4. J. W. Donald, A. K. Jain, Concerns about climate change and the role of fossil fuel use. *Fuel Process Technol.* 2001, **71**, 99-119.
5. E. C. Pischke *et. al.*, From Kyoto to Paris: Measuring renewable energy policy regimes in Argentina, Brazil, Canada, Mexico and the United States. *Energy Res. Soc. Sci.* 2019, **50**, 82-91.

6. J. B. Skjærseth, S. Andresen, G. Bang, G. M. Heggelund, The Paris agreement and key actors' domestic climate policy mixes: comparative patterns. *Int. Environ. Agreem-P.* 2021, **21**, 59-73.
7. W. Strielkowski, L. Civin, E. Tarkhanova, M. Tvaronavičienė, Y. Petrenko, Renewable Energy in the Sustainable Development of Electrical Power Sector: A Review. *Energies* **14**(24), 8240.
8. T. Kåberger, Progress of renewable electricity replacing fossil fuels. *Global Energy Interconnection* 2018, **1**, 48-52
9. H. Zhang, P. Zhang, T. Wu, H. Ruan, Bioethanol Production Based on *Saccharomyces cerevisiae*: Opportunities and Challenges. *Fermentation* 2023, **9**(8), 709.
10. M. A. H. Khan *et. al.*, Investigation of Biofuel as a Potential Renewable Energy Source. *Atomsphere* 2021, **12**(10), 1289.
11. D. Neupane, Biofuels from Renewable Sources, a Potential Option for Biodiesel Production. *Bioengineering* 2023, **10**(1), 29.
12. H. K. Jeswani, A. Chilvers, A. Azapagic, Environmental sustainability of biofuels: a review. *Proc. R. Soc. A* 2020, **476**.
13. S. J. M. Algayyim *et. al.*, Sugarcane Biomass as a Source of Biofuel for Internal Combustion Engines (Ethanol and Acetone-Butanol-Ethanol): A Review of Economic Challenges. *Energies* 2022, **15**(22), 8644.
14. J. Y. Zhu, X. S. Zhuang, Conceptual net energy output for biofuel production from lignocellulosic biomass through biorefining. *Prog. Energ. Combust.* 2012, **38**(4), 583-598.

15. C. E. Wong, Z. W. N. Teo, L. Shen, H. Yu, Seeing the lights for leafy greens in indoor vertical farming. *Trends Food Sci. Tech.* 2020, **106**, 48-63.
16. T. Liu, Glucose Fuel Cells and Membranes: A Brief Overview and Literature Analysis. *Sustainability* 2022, **14**(14), 8376.
17. M. Mujtaba *et. al.*, Lignocellulosic biomass from agricultural waste to the circular economy: a review with focus on biofuels, biocomposites and bioplastics. *J. Clean Prod.* 2023, **402**, 136815.
18. M. Ni, D. Y.C. Leung, M. K.H. Leung, K. Sumathy, An overview of hydrogen production from biomass. *Fuel Process Technol.* 2006, **87**(5), 461-472.
19. A. Burland, M. V. Conssel, Towards Managing Biodiversity of European Marginal Agricultural Land for Biodiversity-Friendly Biomass Production. *Agronomy* 2023, **13**(6), 1651.
20. L. Jara-Cobos, M. Abril-González, V. Pinos-Vélez, Production of Hydrogen from Lignocellulosic Biomass: A Review of Technologies. *Catalysts* **13**(4), 766.
21. N. Dutta, M. Usman, G. Luo, S. Zhang, An Insight into Valorization of Lignocellulosic Biomass by Optimization with the Combination of Hydrothermal (HT) and Biological Techniques: A Review. *Sustain. Chem.* 2022, **3**(1), 35-55.
22. A. Tursi, A review on biomass: importance, chemistry, classification, and conversion. *Biofuel Res. J.* 2019, **6**(2), 962-979.
23. WBA Global Bioenergy Statistics 2018. World Bioenergy Association.
24. H. Chum *et. al.*, IPCC Special Report on Renewable Energy Sources and Climate Change Mitigation. Cambridge University Press 2011.

25. G. Habert, Y. Bouzidi, C. Chen, A. Jullien, Development of a depletion indicator for natural resources used in concrete. *Resour. Conserv. Recycl.* 2010, **54**(6), 364-376.
26. B. Zheng, S. Yu, Z. Chen, Y. Huo, A consolidated review of commercial-scale high-value products from lignocellulosic biomass. *Front. Microbiol.* 2022, **13**.
27. C. L. Williams, T. L. Westover, R. M. Emerson, J. S. Tumuluru, C. Li, Sources of Biomass Feedstock Variability and the Potential Impact on Biofuels Production. *Bioenerg. Res.* 2016, **9**, 1-14.
28. M. Llamas, S. Greses, J. A. Magdalena, C. González-Fernández, E. Tomás-Pejó, Microbial co-cultures for biochemicals production from lignocellulosic biomass: A review. *Bioresource Technol.* 2023, **386**, 129499.
29. H. K. Sharma, C. Xu, W. Qin, Biological pretreatment of lignocellulosic biomass for biofuels and bioproducts: an overview. *Waste Biomass Valori.* 2019, **10**, 235-251.
30. M. Ochoa-Villarreal, E. Aispuro-Hernández, I. Vargas-Arispuro, M. Á. Martínez-Téllez, Plant Cell Wall Polymers: Function, Structure and Biological Activity of Their Derivatives. *InTech, Polymerization* 2012.
31. A. Etale, A. J. Onyianta, S. R. Turner, S. J. Eichhorn, Cellulose: A Review of Water Interactions, Applications in Composites, and Water Treatment. *Chem. Rev.* 2023, **123**(5), 2016-2048.
32. P. McKendry, Energy production from biomass (part 1): overview of biomass. *Bioresour. Technol.* 2002, **83**, 37-46.
33. K. Robak, M. Balcerek, Review of second generation bioethanol production from residual biomass. *Food Technol. Biotech.* 2018, **56**, 174-187.

34. L.M.J. Kroon-Batenburg, K. Kroon, The crystal and molecular structures of cellulose I and II. *Glycoconjugate J.* 1997, **14**, 677-690.
35. M. Abhilash, D. Thomas, Biopolymers for Biocomposites and Chemical Sensor Applications. *Biopolymer Composites in Electronics* 2017, 405-435.
36. S. Gopi, P. Balakrishnan, D. Poovathankandy, S. Thomas, General scenarios of cellulose and its use in the biomedical field. *Mater. Today Chem.* 2019, **13**, 59-78.
37. J. Rojas, E. Azevedo, Functionalization and crosslinking of microcrystalline cellulose in aqueous media: A safe and economic approach. *Int. J. Pharm. Sci. Rev. Res.* 2011, **8**(1), 28-36.
38. D. Klemm, B. Heublein, H. Fink, A. Bohn, Cellulose: fascinating biopolymer and sustainable raw material. *Angew. Chem. Int. Ed.* 2005, **44**, 3358- 3393.
39. T. Heinze, Cellulose: structure and properties. Cellulose Chemistry and Properties: Fibers, Nanocelluloses and Advanced Materials. *Adv. Polym. Sci.* 2015, **271**. Springer, Cham..
40. A. K. Chandel, V. K. Garlapati, A. K. Singh, F. A. F. Antunes, S. S. D. Silva, The path forward for lignocellulose biorefineries: bottlenecks, solutions, and perspective on commercialization. *Bioresour. Technol.* 2018, **264**, 370-381.
41. J. G. Speight, Non-fossil fuel feedstocks. The Refinery of the Future (Second Edition), Gulf Professional Publishing 2020, 343-389.
42. L. Mišurcová, S. Škrovánková, D. Samek, J. Ambrožová, L. Machů, Health Benefits of Algal Polysaccharides in Human Nutrition. *Adv. Food Nutr. Res.* 2012, **66**, 75-145.
43. T. R. Mota, D. M. Oliveira, R. Marchiosi, O. Ferrarese-Filho, W. D. Santos, Plant cell wall composition and enzymatic deconstruction. *Bioengineering* 2018, **5**, 63-77.

44. N. Kumar, A. Dixit, Management of biomass. Nanotechnology for Rural Development, Elsevier 2021, 97-140.
45. X. Zhang, W. Yang, W. Blasiak, Modeling Study of Woody Biomass: Interactions of Cellulose, Hemicellulose, and Lignin. *Energy Fuels* 2011, **25** (10), 4786-4795.
46. O. Benaïmeche, N. T. Seghir, Ł. Sadowski, M. Mellas, The Utilization of Vegetable Fibers in Cementitious Materials. *Encyclopedia of Renewable and Sustainable Materials*, Elsevier 2020, **2**, 649-662.
47. N. Ahmad, M. R. Zakaria, Oligosaccharide From Hemicellulose. *Lignocellulose for Future Bioeconomy*, Elsevier 2019, 135-152.
48. A. Zoghlami, G. Paës, Lignocellulosic Biomass: Understanding Recalcitrance and Predicting Hydrolysis. *Front. Chem.* 2019, **7**.
49. J. Baruah *et al.*, Recent Trends in the Pretreatment of Lignocellulosic Biomass for Value-Added Products. *Front. Energy Res.* 2018, **6**.
50. A. Dastpak, Solubility study of lignin in industrial organic solvents and investigation of electrochemical properties of spray-coated solutions. *Ind. Crop. Prod.* 2020, **148**, 112310.
51. J. Yang, Y. C. Ching, C. H. Chuah, Applications of Lignocellulosic Fibers and Lignin in Bioplastics: A Review. *Polymers* 2019, **11**(5), 751.
52. H. Luo, M. M. Abu-Omar, Sustainable Energy Technologies and Sustainable Chemical Processes. *Encyclopedia of Sustainable Technologies*, Elsevier 2017, 573-585.
53. A. Tribot *et al.*, Wood-lignin: Supply, extraction processes and use as bio-based material. *Eur. Polym. J.* 2019, **112**, 228-240.

54. M. C. Dias, Mandacaru cactus as a source of nanofibrillated cellulose for nanopaper production. *Int. J. Biol. Macromol.* 2023, **235**, 123850.
55. Z. Jin, K. S. Katsumata, T. B. T. Lam, K. Iiyama, Covalent linkages between cellulose and lignin in cell walls of coniferous and nonconiferous woods. *Biopolymers* 2006, **83**(2), 103-110.
56. W. Boerjan, J. Ralph, M. Baucher, Lignin biosynthesis. *Annu. Rev. Plant Biol.* 2003, **54**, 519-546.
57. L. Djakovitch, N. Essayem, M. Eternot, F. Rataboul, A Landscape of Lignocellulosic Biopolymer Transformations into Valuable Molecules by Heterogeneous Catalysis in C'Durable Team at IRCELYON. *Molecules* 2021, **26** (22), 6796.
58. L. Serrano, J. A. Cecilia, C. García-Sancho, A. García, Lignin Depolymerization to BTXs. *Topics Curr. Chem.* 2019, **377**, 26.
59. J. S. Amthor, Efficiency of Lignin Biosynthesis: a Quantitative Analysis. *Ann. Bot.* 2003, **91**(6), 673-695.
60. C. Liu, Deciphering the Enigma of Lignification: Precursor Transport, Oxidation, and the Topochemistry of Lignin Assembly. *Mol. Plant* 2012, **5**(2), 304-317.
61. X. Duo, W. Li, C. Zhu, X. Jiang, H. Chang, H. Jameel, Cleavage of aryl-ether bonds in lignin model compounds using a Co-Zn-beta catalyst. *RSC Adv.* 2020, **10**, 43599-43606.
62. R. Yadav *et. al.*, Lignin derived carbon fiber and nanofiber: Manufacturing and applications. *Composites Part B: Engineering* 2023, **255**, 110613.
63. V. Poursorkhabi, Processing, carbonization, and characterization of lignin based electrospun carbon fibers: a review. *Front. Energy Res.* 2020, **8**, 208.

64. V. Ashokkumar *et al.*, Recent advances in lignocellulosic biomass for biofuels and value-added bioproducts - A critical review. *Bioresour. Technol.* 2022, **344**, 126195.
65. J. Baruah *et al.*, Recent trends in the pretreatment of lignocellulosic biomass for value-added products. *Front. Energy Res.* 2018, **6**, 141.
66. C. Li, X. Zhao, A. Wang, G. W. Huber, T. Zhang, Catalytic Transformation of Lignin for the Production of Chemicals and Fuels. *Chem. Rev.* 2015, **115**(21), 11559-11624.
67. F. Vásquez-Garay, I. Carrillo-Varela, C. Vidal, P. Reyes-Contreras, M. Faccini, R. T. Mendonça, A review on the lignin biopolymer and its integration in the elaboration of sustainable materials. *Sustainability* 2021, **13**(5), 2697.
68. A. Zoghalmi, G. Paës, Lignocellulosic Biomass: Understanding Recalcitrance and Predicting Hydrolysis. *Front. Chem.* 2019, **7**, 874.
69. M. Balk, P. Sofia, A. T. Neffe, N. Tirelli, Lignin, the Lignification Process, and Advanced, Lignin-Based Materials. *Int. J. Mol. Sci.* 2023, **24**(14), 11668.
70. S. A. Afolalu *et al.*, Biofuel, a sustainable renewable source of energy—A review. *IOP Conf. Series: Earth and Environmental Science* 2021, **665**, 012040.
71. A. K. Rai *et al.*, Recent Developments in Lignocellulosic Biofuels, a Renewable Source of Bioenergy. *Fermentation* 2022, **8**(4), 161.
72. M. Hannon, J. Gimpel, M. Tran, B. Rasala, S. Mayfield, Biofuels from algae: challenges and potential. *Biofuels* 2010, **1**(5), 763-784.
73. P. Cavelius, S. Engelhart-Straub, N. Mehlmer, J. Lercher, D. Awad, T. Brück, The potential of biofuels from first to fourth generation. *Plos Biol.* 2023, **21**(3).

74. S. J. Malode, K. K. Prabhu, R. J. Mascarenhas, N. P. Shetti, T. M. Aminabhavi, Recent advances and viability in biofuel production. *Energy Conversion and Management: X* 2021, **10**, 100070.
75. G. Itskos *et. al.*, Energy and the Environment. Environment and Development, Elsevier 2016, 363-452.
76. A. H. Hirani, N. Javed, M. Asif, S. K. Basu, A. Kumar, A review on first-and second-generation biofuel productions. *Biofuels: Greenhouse Gas Mitigation and Global Warming*, Springer New Delhi 2018, 141-154.
77. Y. Dahman, C. Dignan, A. Fiayaz, A. Chaudhry, An introduction to biofuels, foods, livestock, and the environment. *Biomass, Biopolymer-Based Materials, and Bioenergy*, Woodhead Publishing 2019, 241-276.
78. P. Wang, X. Lü, General introduction to biofuels and bioethanol. *Advances in 2nd Generation of Bioethanol Production*, Woodhead Publishing 2012, 1-7.
79. M. Perea-Moreno, E. Samerón-Manzano, A. Perea-Moreno, Biomass as renewable energy: Worldwide research trends. *Sustainability* 2019, **11**(3), 863.
80. S.N. Naik, V. V. Goud, P. K. Rout, A. K. Dalai, Production of first and second generation biofuels: A comprehensive review. *Renew. Sustain. Energy Rev.* 2010, **14**(2), 578-597.
81. N. Rafa, S. F. Ahmed, I. An. Badruddin, M. Mofijur, S. Kamangar, Strategies to Produce Cost-Effective Third-Generation Biofuel From Microalgae. *Front. Energy Res.* 2021, **9**, 749968.

82. K. Gorla, R. Kothari, H. M. Singh, A. Singh, V.V. Tyagi, Biohydrogen: potential applications, approaches, and hurdles to overcome. Handbook of Biofuels, Academic Press 2022, 399-418.
83. M. Balat, H. Balat, Recent trends in global production and utilization of bio-ethanol fuel. *Appl. Energ.* 2009, **86**(11), 2273-2282.
84. H. Xiang *et al.*, Catalytic conversion of bioethanol to value-added chemicals and fuels: A review. *Resources Chemicals and Materials* 2022, **1**(1), 47-68.
85. R. Sindhu *et al.*, Biofuel Production From Biomass. Current Developments in Biotechnology and Bioengineering, Elsevier 2019, 79-92.
86. T. J. Tse, D. J. Wiens, M. J. T. Reaney, Production of Bioethanol—A Review of Factors Affecting Ethanol Yield. *Fermentation* 2021, **7**(4), 268.
87. R. C. Anyanwu, C. Rodriguez, A. Durrant, A. G. Olabi, Micro-Macroalgae Properties and Applications. Reference Module in Materials Science and Materials Engineering, Elsevier B.V. 2018.
88. N. Sarkar, S. K. Ghosh, S. Bannerjee, K. Aikat, Bioethanol production from agricultural wastes: An overview. *Renew. Energ.* 2012, **37**(1), 19-27.
89. F. H. Isikgor, C.R. Becer, Lignocellulosic biomass: a sustainable platform for the production of bio-based chemicals and polymers. *Polym. Chem-UK.* 2015, **6**(25), 4497-4559.
90. A. Devi *et al.*, Lignocellulosic Biomass Valorization for Bioethanol Production: a Circular Bioeconomy Approach. *BioEnergy Research* 2022, **15**, 1820-1841.

91. M. Alherech *et. al.*, From Lignin to Valuable Aromatic Chemicals: Lignin Depolymerization and Monomer Separation via Centrifugal Partition Chromatography. *ACS Cent. Sci.* 2021, **7**(11), 1831-1837.
92. S. Sethupathy *et. al.*, Lignin valorization: Status, challenges and opportunities. *Bioresour. Technol.* 2022, **347**, 126696.
93. A. Boarino, H. Klok, Opportunities and Challenges for Lignin Valorization in Food Packaging, Antimicrobial, and Agricultural Applications. *Biomacromolecules* 2023, **24**(3), 1065-1077.
94. A.T.W.N. Hendriks, G. Zeeman, Pretreatments to enhance the digestibility of lignocellulosic biomass. *Bioresour. Technol.* 2009, **100**(1), 10-18.
95. K. H. Kim, C. G. Yoo, Challenges and Perspective of Recent Biomass Pretreatment Solvents. *Front. Chem. Eng.* 2021, **3**, 785709.
96. B. Zhang, X. Liu, J. Bao, High solids loading pretreatment: The core of lignocellulose biorefinery as an industrial technology – An overview. *Bioresour. Technol.* 2023, **369**, 128334.
97. Y. Zheng, J. Zhao, F. Xu, Y. Li, Pretreatment of lignocellulosic biomass for enhanced biogas production. *Prog. Energ. Combust.* 2014, **42**, 35-53.
98. F. R. Amin *et. al.*, Pretreatment methods of lignocellulosic biomass for anaerobic digestion. *AMB Express* 2017, **7**, 72.
99. S.P.S. Chundawat, V. Balan, L. D. Sousa, B.E. Dale, Thermochemical pretreatment of lignocellulosic biomass. *Bioalcohol Production* 2010, 24-72.

100. Y. Yu, H. Wu, Effect of ball milling on the hydrolysis of microcrystalline cellulose in hot-compressed water. *Environmental and Energy Engineering, AIChE J.*, 2011, **57**, 793.
101. M. Galbe, O. Wallberg, Pretreatment for biorefineries: a review of common methods for efficient utilisation of lignocellulosic materials. *Biotechnology for Biofuels* 2019, **12**, 294.
102. M. J. Gan, Y. Q. Niu, X. J. Qu, C. H. Zhou, Lignin to value-added chemicals and advanced materials: extraction, degradation, and functionalization. *Green Chem.* 2022, **24**, 7705-7750.
103. S. Chen, X. Zhang, D. Singh, H. Yu, X. Yang, Biological pretreatment of lignocellulosics: Potential, progress and challenges. *Biofuels* 2010, **1**, 177-199.
104. M. Saritha, A. Arora, Lata, Biological Pretreatment of Lignocellulosic Substrates for Enhanced Delignification and Enzymatic Digestibility. *Indian J. Microbiol.* 2012, **52**(2), 122-130.
105. X. Li *et. al.*, Improving enzymatic hydrolysis of lignocellulosic biomass by bio-coordinated physicochemical pretreatment—A review. *Energy Rep.* 2022, **8**, 696-709.
106. G. Erven *et. al.*, Elucidation of In Situ Ligninolysis Mechanisms of the Selective White-Rot Fungus *Ceriporiopsis subvermispota*. *ACS Sustainable Chem. Eng.* 2019, **7**(19), 16757-16764.
107. J. Rencoret, A. Pereira, J. C. Rio, A. T. Martinez, A. Gutierrez, Delignification and Saccharification Enhancement of Sugarcane Byproducts by a Laccase-Based Pretreatment. *ACS Sustainable Chem. Eng.* 2017, **5**(8), 7145-7154.

108. S. Zhang *et. al.*, Enzymatic hydrolysis of corn stover lignin by laccase, lignin peroxidase, and manganese peroxidase. *Bioresour. Technol.* 2022, **361**, 127699.
109. H. Suryadi *et. al.*, Biodelignification of lignocellulose using ligninolytic enzymes from white-rot fungi. *Heliyon* 2022, **8**(2), e08865.
110. S. Kim *et. al.*, Mushroom Ligninolytic Enzymes—Features and Application of Potential Enzymes for Conversion of Lignin into Bio-Based Chemicals and Materials. *Appl. Sci.* 2021, **11**(13), 6161.
111. G. Janusz *et. al.*, Laccase Properties, Physiological Functions, and Evolution. *Int. J. Mol. Sci.* 2020, **21**(3), 966.
112. S. Ncanana, S. Burton, Oxidation of 8-hydroxyquinoline catalyzed by laccase from *Trametes pubescens* yields an antioxidant aromatic polymer. *Journal of Molecular Catalysis B: Enzymatic* 2007, **44**(2), 66-71.
113. B. Viswanath, B. Rajesh, A. Janardhan, A. P. Kumar, G. Narasimha, Fungal Laccases and Their Applications in Bioremediation. *Enzyme Res.* 2014, **2014**, 163242.
114. M. D. Cannatelli, A. J. Ragauskas, Two Decades of Laccases: Advancing Sustainability in the Chemical Industry. *Chem. Rec.* 2017, **17**, 122-140.
115. H. D. Kyomuhimbo, H. G. Brink, Applications and immobilization strategies of the copper-centred laccase enzyme; a review. *Heliyon* 2023, **9**(2), e13156.
116. R. Hilgers *et. al.*, Understanding laccase/HBT-catalyzed grass delignification at the molecular level. *Green Chem.* 2020, **22**, 1735-1746.
117. K. Agrawal, V. Chaturvedi, P. Verma, Fungal laccase discovered but yet undiscovered. *Bioresources and Bioprocessing* 2018, **5**, 4.

118. M. Hussaan, Amna, M. T. Javed, M. S. Akram, S. Ali, Physiological and molecular basis of bioremediation of micropollutants. *Handbook of Bioremediation*, Elsevier 2021, 447-464.
119. M. Lin, T. Nagata, M. Katahira, High yield production of fungal manganese peroxidases by *E. coli* through soluble expression, and examination of the activities. *Protein Expres. Purif.* 2018, **145**, 45-52.
120. D. Floudas *et. al.*, The *Paleozoic* origin of enzymatic lignin decomposition reconstructed from 31 fungal genomes. *Science* 2012, **336**, 6089.
121. P. Chowdhary, N. More, A. Yadav, R. N. Bharagava, Ligninolytic Enzymes: An Introduction and Applications in the Food Industry. *Enzymes in Food Biotechnology* 2019, 181-195.
122. A. T. Martinez, Molecular biology and structure-function of lignin-degrading heme peroxidases. *Enzyme Microb. Tech.* 2002, **30**(4), 425-444.
123. M. Hofrichter, Review: Lignin conversion by manganese peroxidase (MnP). *Enzyme Microb. Tech.* 2002, **30**(4), 454-466.
124. P. Chowdhary, G. Shukla, G. Raj, L. F. R. Ferreira, R. N. Bharagava, Microbial manganese peroxidase: a ligninolytic enzyme and its ample opportunities in research. *SN Appl. Sci.* 2019, **1**, 45.
125. Kumar, A.; Arora, P. K. Biotechnological Applications of Manganese Peroxidases for Sustainable Management. *Front. Environ. Sci.* 2022, 10, 875157.
126. A. Kumar, R. Chandra, Ligninolytic enzymes and its mechanisms for degradation of lignocellulosic waste in environment. *Heliyon* 2020, **6**(2), e03170.

127. M. Asgher, M. J. Asad, H. N. Bhatti, R. L. Legge, Hyperactivation and thermostabilization of *Phanerochaete chrysosporium* lignin peroxidase by immobilization in xerogels. *World Journal of Microbiology and Biotechnology* 2007, **23**, 525-531.
128. C. A. Reddy, An overview of the recent advances on the physiology and molecular biology of lignin peroxidases of *Phanerochaete chrysosporium*. *J. Biotechnol.* 1993, **30**(1), 91-107.
129. K. Hilden, M. R. Makela, Role of Fungi in Wood Decay. *Reference Module in Life Sciences* 2018.
130. X. Wang, B. Yao, X. Su, Linking Enzymatic Oxidative Degradation of Lignin to Organics Detoxification. *Int. J. Mol. Sci.* 2018, **19**(11), 3373.
131. A. O. Falade *et. al.*, Lignin peroxidase functionalities and prospective applications. *Microbiologyopen* 2017, **6**(1), e00394.
132. H. Wariishi, J. Huang, H.B. Dunford, M.H. Gold, Reactions of Lignin Peroxidase Compounds I and II with Veratryl Alcohol. *J. Biol. Chem.* 1991, **266**(31), 20694-20699.
133. A. K. Singh *et. al.*, Structural insights, biocatalytic characteristics, and application prospects of lignin-modifying enzymes for sustainable biotechnology. *Int. J. Biol. Macromol.* 2023, **242**, 124968.
134. V. Saez-Jimenez *et. al.*, Improving the pH-stability of Versatile Peroxidase by Comparative Structural Analysis with a Naturally-Stable Manganese Peroxidase. *Plos one* 2015, **10**(11), e0143267.
135. M. Perez-Boada *et. al.*, Versatile Peroxidase Oxidation of High Redox Potential Aromatic Compounds: Site-directed Mutagenesis, Spectroscopic and Crystallographic

- Investigation of Three Long-range Electron Transfer Pathways. *J. Mol. Biol.* 2005, **354**(2), 385-402.
136. W. D. H. Schneider, M. Camassola, R. C. Fontana, How ligninolytic enzymes can help in the degradation of biomass polysaccharides, cleavage, and catalytic mechanisms? Polysaccharide-degrading Biocatalysts, Academic Press 2023, 177-190.
137. E. Rodríguez, O. Nuero, F. Guillén, A.T. Martínez, M.J. Martínez, Degradation of phenolic and non-phenolic aromatic pollutants by four *Pleurotus* species: The role of laccase and versatile peroxidase. *Soil Biol. Biochem.* 2004, **36**(6), 909-916.
138. O. D.V. Biko, M. Viljoen-Bloom, W. H. Zyl, Microbial lignin peroxidases: Applications, production challenges and future perspectives. *Enzyme Microb. Tech.* 2020, **141**, 109669.
139. V. Steinmertz, M. Villain-gambier, A. Klem, I. Ziegler, S. Dumarcay and D. Trebouet, In-situ extraction of depolymerization products by membrane filtration against lignin condensation. *Bioresour. Technol.* 2020, **311**, 123530.

Chapter 2

Understanding manganese peroxidase-catalyzed conversion of the lignin structure and its application for the polymerization of Kraft lignin

Reproduced from Ref. *ACS Sustain. Chem. Eng.*, 2024 with permission from the American Chemical Society. (DOI:10.1021/acssuschemeng.3c05635)

2.1 Introduction

Currently, there are two main sources of lignin available worldwide: native lignin and technical lignin.^{1,2} Native lignin refers to the lignin naturally occurring in plant cells, while technical lignin is generated as a byproduct during industrial processes. Among the various types of technical lignin, Kraft lignin (KL) stands out as a widely available lignin byproduct produced from the Kraft process in the pulp and paper industries, obtained by treating wood chips in a mixture of sodium hydroxide and sodium sulfide under high temperature and pressure. Traditionally, due to its high calorific value, KL has been primarily burnt for energy generation.^{3,4} However, with the growing interest in lignin valorization, KL has emerged as a potential raw material for the synthesis of high value-added products. In this context, understanding the properties and potential applications of KL has become crucial in the quest for sustainable and economically viable utilization of lignin resources.

KL is typically abundant in phenolic compounds resulting from the cleavage of ether linkages in lignin during the Kraft process.³ Additionally, KL exhibits a diverse range of molecular weights and a variety of functional groups.⁴ This variation in its chemical composition, molecular structure, and molecular weight distribution can present challenges for specific applications.⁴ Consequently, effective utilization of KL necessitates the modification of its chemical properties to tailor it for specific requirements. Researchers have demonstrated that polymerizing KL enables the synthesis of lignin-based biomaterials, such as hydrogels and dispersants.^{5,6} Presently, chemical treatments, such as oxidative treatment, are employed to modify the chemical properties of KL by capitalizing on its high phenolic content.⁴ However, these chemical methods often require harsh reaction temperatures, which may not always be economically feasible.⁷ As an alternative approach, researchers are

investigating biocatalytic pathways involving the use of natural enzymes to achieve the desired structural modification of KL. Biocatalytic methods offer advantages in terms of sustainability and environmental friendliness compared to traditional chemical treatments.

Manganese peroxidase (MnP) distinguishes itself through its remarkable functional versatility, offering numerous industrial applications, including pulp delignification, biobleaching, and pollutant degradation.⁸⁻¹² Furthermore, MnP exhibits higher selectivity in modifying bonds within the lignin structure compared to other ligninolytic enzymes, making it a promising biocatalyst for lignin valorization.¹¹ MnP can be classified as short, long, and extra-long subfamilies based on the length of their predicted C-terminal tail.^{13,14}

Ceriporiopsis subvermispota is a highly esteemed white-rot fungus known for its remarkable lignin-modifying capabilities.¹³⁻¹⁵ Among white-rot fungi, *C. subvermispota* stands out due to the presence of all three subfamilies of MnP (short, long, and extra-long) in its genome, a unique characteristic.^{14,16} Despite the absence of LiP and VP, *C. subvermispota* displays effective lignin modification with notable selectivity, suggesting that MnP plays a significant role in its ligninolytic activity.¹³⁻¹⁵ Therefore, comprehending the enzymatic properties of MnP as to lignin holds great potential for harnessing its inherent abilities as a biocatalyst for lignin valorization.

In this study, I focused on MnP117436, a MnP derived from *C. subvermispota* (CsMnP). MnP117436 was specifically selected due to its high abundance within the long MnP subfamily of *C. subvermispota*, particularly when cultivated in a medium containing aspen wood.¹⁷ Here, I aimed to elucidate the enzymatic properties of this CsMnP as to lignin and investigate its potential as a biocatalyst for the polymerization of Kraft lignin (KL). To

achieve this, I examined the enzymatic properties of CsMnP using guaiacylglycerol- β -guaiacyl ether (GGE) as a phenolic β -O-4' type lignin model compound. The progress of the reaction was monitored using reverse-phase high performance liquid chromatography (RP-HPLC). Additionally, I characterized the reaction products through size-exclusion chromatography (SEC) and two-dimensional nuclear magnetic resonance (2D NMR) spectroscopy analyses. Furthermore, I assessed the ability of CsMnP to catalyze the polymerization of KL and analyzed the resulting products using a combination of the Folin-Ciocalteu method, SEC, and NMR spectroscopy.

2.2 Results and Discussion

2.2.1 Analysis of reaction products by RP-HPLC

I investigated the enzymatic properties of CsMnP towards the phenolic subunits in lignin using guaiacylglycerol- β -guaiacyl ether (GGE), a phenolic lignin model dimer, as the substrate. To gain insight into the products resulting from the conversion of GGE catalyzed by CsMnP, I employed a RP-HPLC system to separate the products based on their hydrophobic characteristics (Figure 2.1A). In the absence of H₂O₂, only the peak corresponding to GGE (Figure 2.1A, red trace) was detected on the chromatogram. Following the addition of H₂O₂, a gradual reduction in the intensity of the GGE peak and the appearance of new product peaks (P1-5) were observed over the course of the reaction. I estimated the GGE content at each time point by analyzing the peak area of GGE on the RP-HPLC chromatogram (Figure 2.1B). The results showed a gradual decrease in GGE content over the reaction time, from 100% at 0 h to 22% at 48 h (Figure 2.1B). Particularly, a rapid decrease in GGE content was observed during the initial 12 h of the reaction, indicating that

the reaction proceeded rapidly at the early stage of the incubation.

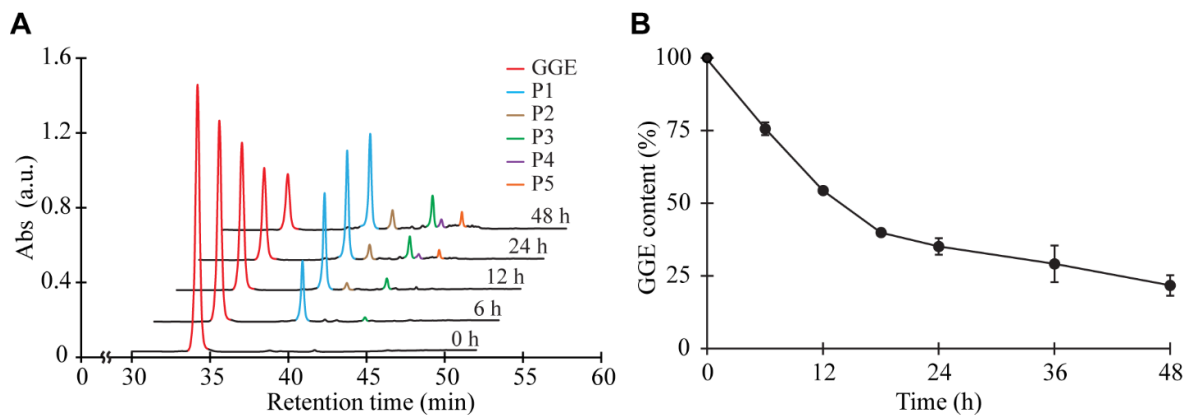


Figure 2.1. Reverse-phase high performance liquid chromatography (RP-HPLC) analysis of the reaction mixture of *CsMnP* and GGE. (A) RP-HPLC chromatograms of the reaction mixture collected at different reaction time points (0, 6, 12, 24, and 48 h). The peaks corresponding to GGE and reaction product peaks 1 to 5 (P1 to P5) are denoted based on their retention time. GGE was eluted at 34.2 min (red trace), P1 at 39.5 min (cyan trace), P2 at 40.9 min (brown trace), P3 at 43.5 min (green trace), P4 at 44.0 min (purple trace), and P5 at 45.3 min (orange trace). (B) The GGE content at each reaction time point is plotted. The GGE content at each reaction time point was deduced from the peak area on the chromatogram. The GGE content at 0 h was defined as 100%.

The intensity of P1 increased steadily from 0 to 24 h, after which it slightly decreased (Figure 2.2A). This suggests that a compound in P1 might undergo further reactions, leading to the formation of other products catalyzed by *CsMnP*. In the meantime, the intensities of P2-5 exhibited a continuous increase from 0 to 48 h (Figure 2.2B-D). After 48 h of incubation, the predominant product peak was P1, followed by P3, P2, P5, and P4 (in decreasing order).

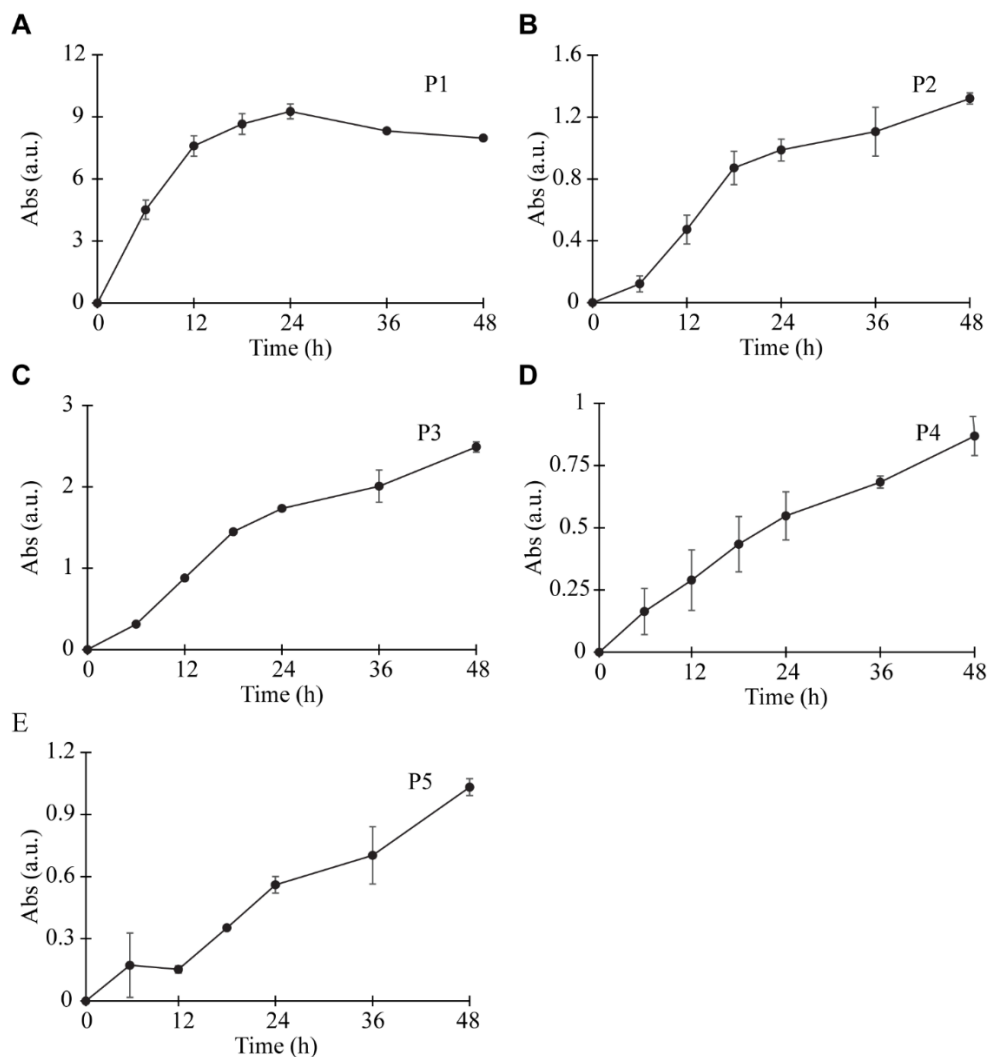


Figure 2.2. Evolution of the intensity of product peaks P1 (A), P2 (B), P3 (C), P4 (D), and P5 (E) obtained on RP-HPLC of the reaction mixtures of CsMnP and GGE at different reaction time points (0, 6, 12, 18, 24, 36, and 48 h).

I also investigated the influence of various chemical compounds on the conversion of GGE by CsMnP (Table 2.1). When the reaction was conducted without additional MnSO₄ (case 4), the conversion of GGE was 51%. Comparatively, the inclusion of 2 mM MnSO₄ (case 1) increased the conversion of GGE to 64%, indicating the beneficial role of additional manganese ions in enhancing the catalytic activity of CsMnP for lignin structure

modification.¹⁸ Furthermore, it is noteworthy that *CsMnP* exhibited no catalytic conversion of GGE in the absence of H₂O₂ (case 5), underscoring the essentiality of H₂O₂ for the enzymatic activity of *CsMnP*.

Table 2.1. The degree of conversion of GGE by *CsMnP* after 24 h^a

Case	GGE	<i>CsMnP</i>	MnSO ₄	H ₂ O ₂	Remaining GGE (%) ^b	Converted GGE (%)
1	+	+	+	+	35.7 ± 1.4	64.3 ± 1.4
2	-	+	+	+	ND	ND
3	+	-	+	+	100.0 ± 2.5	0.0 ± 2.5
4	+	+	-	+	48.9 ± 0.8	51.1 ± 0.8
5	+	+	+	-	100.0 ± 1.1	0.0 ± 1.1

^aIn case 1, the reaction was performed at room temperature in a 500 µL reaction mixture containing 1 mM GGE, 0.694 mU *CsMnP*, 2 mM MnSO₄, 0.5 mM DSS-d₆, 10% D₂O, and 0.125 mM H₂O₂. Then, 0.125 mM H₂O₂ was added every 6 h until 24 h. In cases 2-5, the reactions were performed under the same conditions except for a lack of some component in each case. ^bThe remaining GGE content was deduced from the peak area of GGE on the RP-HPLC chromatogram. The GGE content at 0 h was defined as 100%. The mean and standard deviation were obtained from two independent experiments. ND = not detected.

2.2.2 Analysis of compounds contained in P1-5 by SEC

Following the identification of five major product peaks (P1-5) through RP-HPLC, I conducted further investigations to determine the molecular weight of the compound present in each peak using SEC. Initially, I separated P1-5 based on their elution profile on RP-HPLC, collecting P1 from 39.2-40.5 min, P2 from 40.8-41.5 min, P3 from 43.1-43.9 min, P4 from 43.9-44.4 min, and P5 from 45.2-45.6 min. Subsequently, individual analysis of P1-5 was performed using SEC.

Table 2.2 presents the molecular weights of the compounds identified in P1 to P5 as determined by SEC analysis. Remarkably, the molecular weights of the compounds in P1 to

P5 displayed an increasing trend, consistent with the observed increase in hydrophobic characteristics in the RP-HPLC chromatogram. The compound in P1 displayed a M_n of 656, approximately twice the molecular weight of GGE (320), which contains two aromatic rings (dimer). This suggests that the compound in P1 is a tetramer, containing four aromatic rings. The compound in P2 was estimated to consist of five aromatic rings (pentamer), followed by P3 and P4, which contained six aromatic rings (hexamer), and P5, which contained seven aromatic rings (heptamer).

Table 2.2. SEC analysis to deduce the number-average molecular weights (M_n) of the compounds in P1 to P5 obtained by RP-HPLC

Compound	M_n	Estimated number of aromatic rings
GGE	320	Two
Compound in P1	656	Four
Compound in P2	748	Five
Compound in P3	887	Six
Compound in P4	975	Six
Compound in P5	1107	Seven

I propose that *CsMnP* mediates a radical coupling reaction between GGEs, leading to the formation of compounds containing even numbers of aromatic rings (P1: four, P3 and P4: six) through the establishment of carbon-carbon and/or ether interunit linkages. Similar polymerization reactions have been reported for laccase^{19,20} and VP²¹ using GGE as a substrate. Meanwhile, the formation of compounds containing odd numbers of aromatic rings (P2: five and P5: seven) can be attributed to two potential mechanisms. Firstly, *CsMnP* may catalyze the cleavage of the ether linkage within the compounds containing an even number

of aromatic rings (P3 and P4), resulting in the liberation of a monomeric product and subsequent formation of a compound containing an odd number of aromatic rings (P2). A similar phenomenon was observed during the conversion of GGE by VP, where it was hypothesized that the odd-numbered heptamer was produced through the release of a monomer from an octamer via ether bond cleavage.²¹ Secondly, CsMnP might cleave the ether linkage within GGE itself, generating a single aromatic ring that subsequently undergoes polymerization with the compounds containing even numbers of aromatic rings (P1 or P3/P4), leading to the formation of compounds containing odd numbers of aromatic rings (P2 or P5).

2.2.3 NMR analysis of GGE

I acquired 2D ^1H - ^{13}C HSQC (Figure 2.3) and HMBC (Figure 2.4) spectra for GGE and assigned the signals accordingly. Firstly, I referred to previous studies for signal assignment of GGE,^{22,23} and subsequently employed the HMBC spectra with $^nJ_{\text{CH}} = 5$ and 8 Hz for confirmation. The aromatic and aliphatic regions of the HSQC spectrum are shown in Figure 2.3A, while the chemical structures of GGE with a phenolic ring labeled as "A," a non-phenolic phenoxy ring as "B," and a glycerol chain as "C" are depicted in Figure 2B.

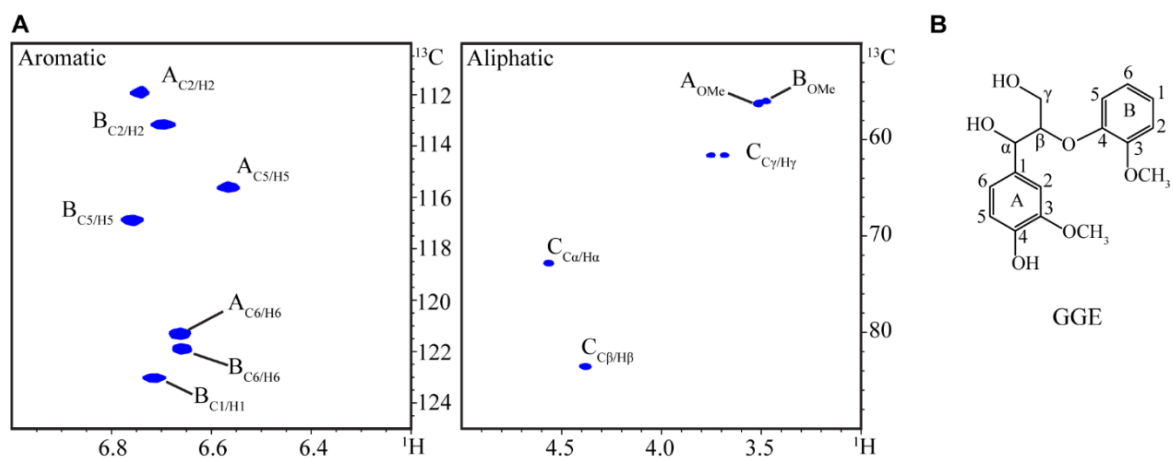


Figure 2.3. (A) Aromatic (left) and aliphatic (right) regions of 2D ^1H - ^{13}C HSQC spectrum of GGE. (B) Chemical structure of GGE. The signal assignments are summarized in Table 2.3.

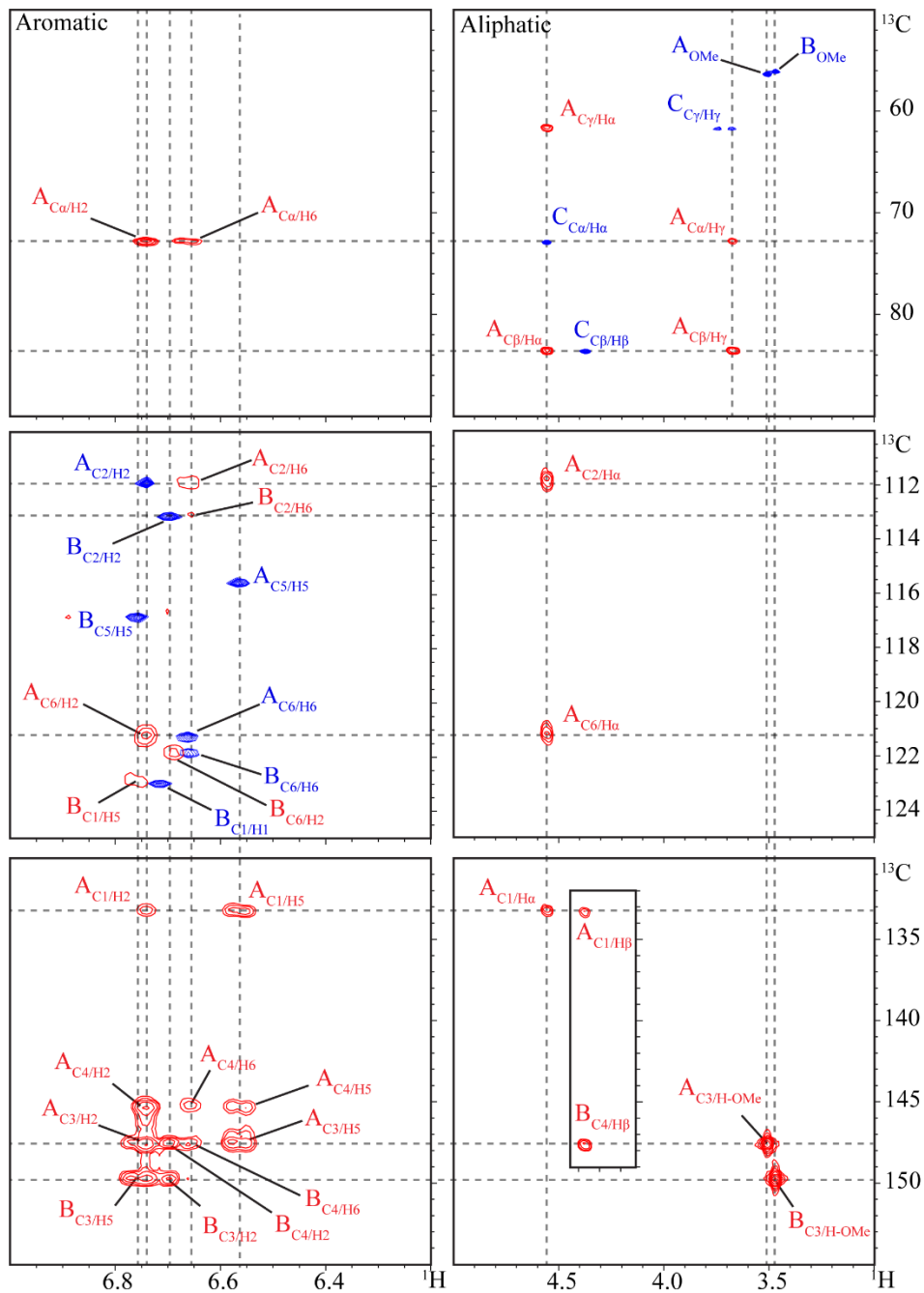


Figure 2.4. Superimposition of the 2D ^1H - ^{13}C HSQC (blue) and HMBC (red) spectra of GGE. The aromatic (left) and aliphatic (right) regions are shown. The HMBC signals acquired using $^n\text{J}_{\text{CH}} = 5$ Hz are shown. Inset in the bottom right spectrum, the HMBC signals acquired using $^n\text{J}_{\text{CH}} = 8$ Hz are shown. The signal assignments are given in Table 2.3.

Table 2.3. The signal assignments of the 2D ^1H - ^{13}C HSQC spectrum of GGE

Label	δ_C/δ_H (ppm/ppm)	Assignment
B _{OMe}	56.1/3.47	C/H in methoxy groups of non-phenolic ring B of GGE
A _{OMe}	56.3/3.50	C/H in methoxy groups of phenolic ring A of GGE
C _{Cγ/Hγ1}	61.7/3.67	C _{γ} /H γ 1 in β -O-4' substructures
C _{Cγ/Hγ2}	61.7/3.74	C _{γ} /H γ 2 in β -O-4' substructures
C _{Cγ/Hα}	61.7/4.55	C _{α} /H γ in β -O-4' substructures
C _{Cα/Hγ1}	72.9/3.67	C _{α} /H γ in β -O-4' substructures
C _{Cα/Hα}	72.9/4.55	C _{α} /H α in β -O-4' substructures
C _{Cα/H$_6$}	72.9/6.66	C _{α} /H $_6$ in A-ring
C _{Cα/H$_2$}	72.9/6.74	C _{α} /H $_2$ in A-ring
C _{Cβ/Hγ1}	83.6/3.67	C _{β} /H γ in β -O-4' substructures
C _{Cβ/Hβ}	83.6/4.37	C _{β} /H β in β -O-4' substructures
C _{Cβ/Hα}	83.6/4.55	C _{β} /H α in β -O-4' substructures
A _{C$_2$/Hα}	111.9/4.55	C $_2$ /H α in A-ring
A _{C$_2$/H$_6$}	111.9/6.66	C $_2$ /H $_6$ in A-ring
A _{C$_2$/H$_2$}	111.9/6.74	C $_2$ /H $_2$ in A-ring
B _{C$_2$/H$_6$}	113.1/6.66	C $_2$ /H $_6$ in B-ring
B _{C$_2$/H$_2$}	113.1/6.70	C $_2$ /H $_2$ in B-ring
A _{C$_5$/H$_5$}	115.6/6.57	C $_5$ /H $_5$ in A-ring
B _{C$_5$/H$_5$}	116.8/6.76	C $_5$ /H $_5$ in B-ring
A _{C$_6$/Hα}	121.2/4.55	C $_6$ /H α in A-ring
A _{C$_6$/H$_6$}	121.2/6.66	C $_6$ /H $_6$ in A-ring
A _{C$_6$/H$_2$}	121.2/6.74	C $_6$ /H $_2$ in A-ring
B _{C$_6$/H$_6$}	121.9/6.66	C $_6$ /H $_6$ in B-ring
B _{C$_6$/H$_2$}	121.9/6.70	C $_6$ /H $_{1,2}$ in B-ring
B _{C$_1$/H$_1$}	123.0/6.72	C $_1$ /H $_1$ in B-ring
B _{C$_1$/H$_5$}	123.0/6.76	C $_1$ /H $_1$ in B-ring
A _{C$_1$/Hα}	133.2/4.55	C $_1$ /H α in A-ring
A _{C$_1$/H$_5$}	133.2/6.57	C $_1$ /H $_5$ in A-ring
A _{C$_1$/H$_2$}	133.2/6.74	C $_1$ /H $_2$ in A-ring
A _{C$_4$/H$_5$}	145.2/6.57	C $_4$ /H $_5$ in A-ring
A _{C$_4$/H$_6$}	145.2/6.66	C $_4$ /H $_6$ in A-ring

A _{C4/H2}	145.2/6.74	C ₄ /H ₂ in A-ring
A _{C3/H-OMe}	147.4/3.50	C ₃ /H _{OMe} in A-ring
A _{C3/H5}	147.4/6.57	C ₃ /H ₅ in A-ring
A _{C3/H2}	147.4/6.74	C ₃ /H ₂ in A-ring
B _{C4/H6}	147.5/6.66	C ₄ /H ₆ in B-ring
B _{C4/H2}	147.5/6.70	C ₄ /H ₂ in B-ring
B _{C3/H-OMe}	149.8/3.47	C ₃ /H _{OMe} in B-ring

In the aliphatic region ($\delta_H = 5.0\text{-}3.0$ ppm) of the HSQC spectrum, I observed six signals (Figure 2.3A) and assigned them based on prior studies.²³ Specifically, the signals at $\delta_C/\delta_H = 56.3/3.50$ and $56.1/3.47$ ppm were attributed to A_{OMe} and B_{OMe}, respectively. Additionally, two signals at $\delta_C/\delta_H = 61.7/3.67$ and $61.7/3.74$ ppm corresponded to C_{C γ /H γ 1} and C_{C γ /H γ 2}, respectively. The remaining two signals at $\delta_C/\delta_H = 72.9/4.55$ and $83.6/4.37$ ppm were assigned to C_{C α /H α} and C_{C β /H β} , respectively.

In the aromatic region ($\delta_H = 7.0\text{-}6.2$ ppm) of the HSQC spectrum, I identified seven signals (Figure 2.3A) and assigned them following previous studies.²³ Specifically, the signals at $\delta_C/\delta_H = 111.9/6.74$, $115.6/6.57$, and $121.2/6.66$ ppm were attributed to A_{C2/H2}, A_{C5/H5}, and A_{C6/H6}, respectively. Furthermore, four additional signals at $\delta_C/\delta_H = 113.1/6.70$, $116.8/6.76$, $121.9/6.66$, and $123.0/6.72$ ppm were assigned to B_{C2/H2}, B_{C5/H5}, B_{C6/H6}, and B_{C1/H1}, respectively.

In the aliphatic region ($\delta_H = 5.0\text{-}3.0$ ppm) of the HMBC spectra, I observed six signals in the top-right and middle-right of Figure 2.4, each connecting two HSQC signals. The HMBC signal at $\delta_C/\delta_H = 72.9/3.67$ ppm connected the HSQC signals C_{C γ /H γ 1} and C_{C α /H α} , while that at $\delta_C/\delta_H = 83.6/3.67$ ppm connected the HSQC signals C_{C γ /H γ 1} and C_{C β /H β} (Figure 2.4). Therefore, these HMBC signals were attributed to C_{C α /H γ 1} and C_{C β /H γ 1}, respectively. In terms

of the symmetry of the HMBC spectrum, the HMBC signals at $\delta_C/\delta_H = 61.7/4.55$ and $83.6/4.55$ ppm (Figure 2.4) were assigned to $C_{C\gamma/H\alpha}$ and $C_{C\beta/H\alpha}$, respectively. In other words, the presence of these HMBC signals confirmed the assignment of the HSQC signals mentioned above (Figure 2.3A). Furthermore, the HMBC signals at $\delta_C/\delta_H = 111.9/4.55$ and $121.2/4.55$ ppm connected the HSQC signals $C_{C\alpha/H\alpha}$ and $A_{C2/H2}$, and $C_{C\alpha/H\alpha}$ and $A_{C6/H6}$, respectively, and were therefore assigned to $A_{C2/H\alpha}$ and $A_{C6/H\alpha}$ (Figure 2.4), confirming the HSQC signal assignments in Figure 2.3A.

In the aromatic region ($\delta_H = 7.0$ - 6.2 ppm) of the HMBC spectra, I identified seven signals in the top-left and middle-left of Figure 2.4, each connecting two HSQC signals. Considering the symmetry of the HMBC spectrum, the HMBC signals at $\delta_C/\delta_H = 72.9/6.74$ and $72.9/6.66$ ppm were assigned to $A_{C\alpha/H2}$ and $A_{C\alpha/H6}$ (Figure 2.4). The presence of these HMBC signals validated the HSQC signal assignments in Figure 2.3A. The HMBC signal at $\delta_C/\delta_H = 111.9/6.66$ ppm connected the HSQC signals $A_{C6/H6}$ and $A_{C2/H2}$, while that at $\delta_C/\delta_H = 113.1/6.66$ ppm connected the HSQC signals $B_{C6/H6}$ and $B_{C2/H2}$ (Figure 2.4). Therefore, these HMBC signals were attributed to $A_{C2/H6}$ and $B_{C2/H6}$, respectively. Considering the symmetry of the HMBC spectrum, the HMBC signals at $\delta_C/\delta_H = 121.2/6.74$ and $121.9/6.70$ ppm were assigned to $A_{C6/H2}$ and $B_{C6/H2}$, respectively. Furthermore, the HMBC signal at $\delta_C/\delta_H = 123.0/6.76$ ppm connected the HSQC signals $B_{C5/H5}$ and $B_{C1/H1}$, and was therefore assigned to $B_{C1/H5}$. Again, the presence of these HMBC signals confirmed the HSQC signal assignment in Figure 2.3A.

All the signals observed in the bottom panels of Figure 2.4 (aliphatic and aromatic regions) of the HMBC spectra were correlation signals involving the quaternary carbons,

specifically positions 1, 3, and 4 for ring A, and positions 3 and 4 for ring B. From these signals, the assignments of the quaternary carbons were made.

The detailed signal assignment of the HSQC and HMBC spectra of GGE is presented in Figure 2.4 and Table 2.3.

2.2.4 NMR analysis of a compound present in P1

To determine the chemical structure of the predominant compound in the P1 fraction, I utilized 2D ^1H - ^{13}C HSQC and HMBC spectra (Figure 2.5).

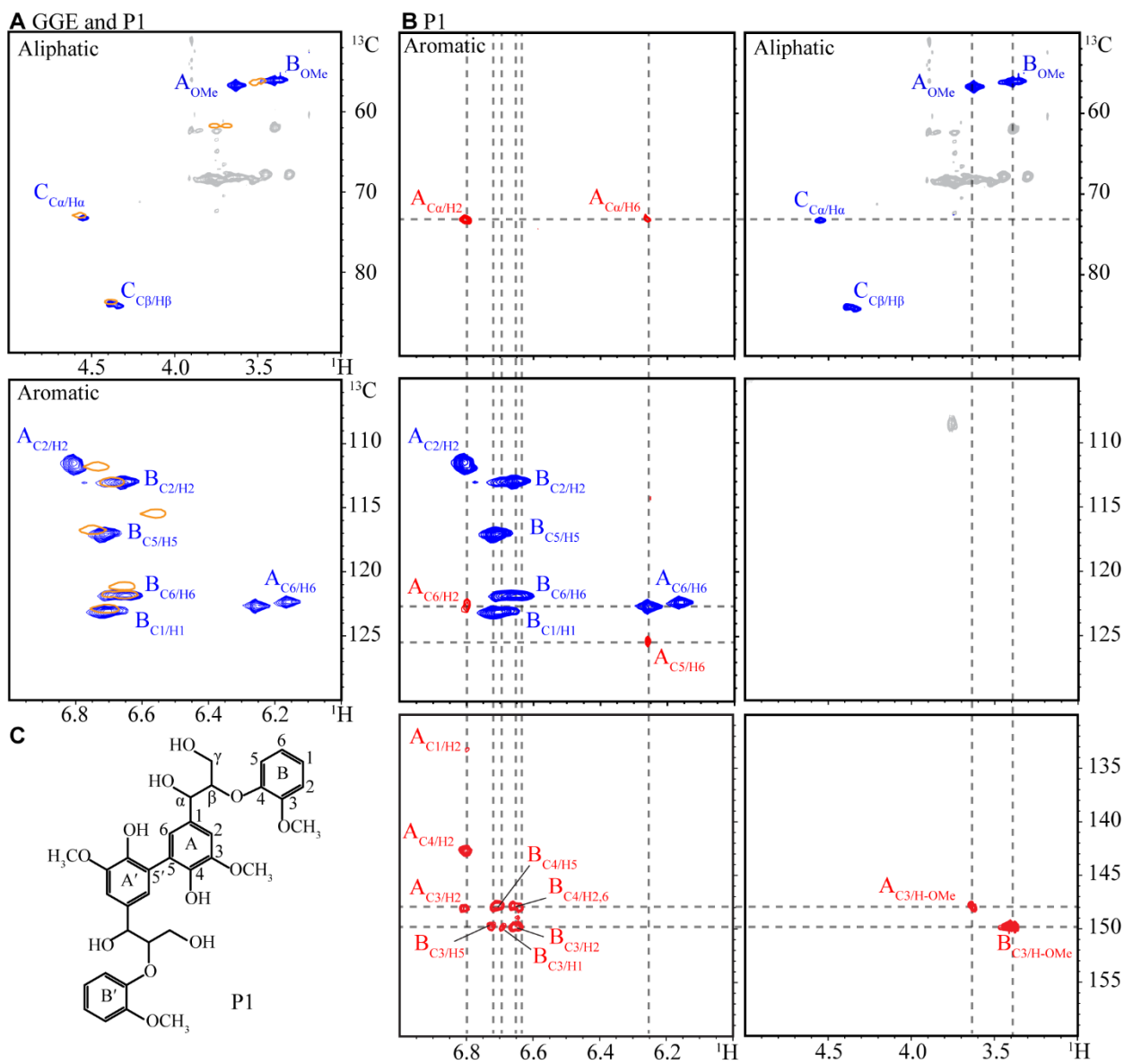


Figure 2.5. (A) Superimposition of the 2D ^1H - ^{13}C HSQC spectra of GGE (orange) and P1 (blue). (B) Superimposition of the 2D ^1H - ^{13}C HSQC (blue) and 2D ^1H - ^{13}C HMBC (red) spectra of P1. The grey signals were not assigned. The signal assignments are summarized in Table 2.4. (C) The chemical structure of the compound present in P1 deduced from the analysis.

Table 2.4. The signal assignments of the 2D ^1H - ^{13}C HSQC and HMBC spectra of P1

Label	δ_C/δ_H (ppm/ppm)	Assignment	Relative to A ₂
B _{OMe}	56.1/3.38	C/H in methoxy groups of non-phenolic ring B of P1	
A _{OMe}	56.7/3.62	C/H in methoxy groups of phenolic ring A of P1	
A _{Cα/Hα}	73.1/4.55	C α /H α in β -O-4' substructures	
A _{Cα/H₆}	73.1/6.25	C α /H ₆ in A-unit	
A _{Cα/H₂}	73.1/6.80	C α /H ₂ in A-unit	
A _{Cβ/Hβ}	84.0/4.40	C β /H β in β -O-4' substructures	
A _{C₂/H₂}	111.5/6.80	C ₂ /H ₂ in A-unit	1.00
B _{C₂/H₂}	113.1/6.66	C ₂ /H ₂ in B-unit	1.15
B _{C₅/H₅}	117.2/6.73	C ₅ /H ₅ in B-unit	1.05
B _{C₆/H₆}	121.9/6.66	C ₁ /H ₁ in B-unit	1.00
A _{C₆/H₆}	122.3/6.16 and 122.7/6.25	C ₆ /H ₆ in A-unit	0.51 0.60
A _{C₆/H₂}	122.7/6.80	C ₆ /H ₂ in A-unit	
B _{C₁/H₁}	123.1/6.72	C ₆ /H ₆ in B-unit	1.06
A _{C₅/H₆}	125.4/6.25	C ₅ /H ₆ in A-unit	
A _{C₁/H₂}	133.1/6.80	C ₁ /H ₂ in A-unit	
A _{C₄/H₂}	142.7/6.80	C ₄ /H ₂ in A-unit	
B _{C₄/H_{2,6}}	147.7/6.66	C ₄ /H _{2,6} in B-unit	
B _{C₄/H₅}	147.7/6.73	C ₄ /H ₅ in B-unit	
A _{C₃/H-OMe}	148.1/3.62	C ₃ /H _{OMe} in A-unit	
A _{C₃/H₂}	148.1/6.80	C ₃ /H ₂ in A-unit	
B _{C₃/H-OMe}	149.7/3.38	C ₃ /H _{OMe} in B-unit	
B _{C₃/H₂}	149.7/6.66	C ₃ /H ₂ in B-unit	
B _{C₃/H₁}	149.7/6.72	C ₃ /H ₁ in B-unit	
B _{C₃/H₅}	149.7/6.73	C ₃ /H ₅ in B-unit	

Initially, I compared the HSQC spectra of P1 and GGE (Figure 2.5A). In the aliphatic region, I observed the signals of P1 with similar, if not identical, ^1H and ^{13}C chemical shifts

to the A_{OMe}, B_{OMe}, C_{C α /H α} , and C_{C β /H β} signals of GGE (Figure 2.5A). Based on this resemblance, I attributed these signals of P1 to A_{OMe} ($\delta_C/\delta_H = 56.7/3.62$ ppm), B_{OMe} ($\delta_C/\delta_H = 56.1/3.38$ ppm), C_{C α /H α} ($\delta_C/\delta_H = 73.1/4.55$ ppm), and C_{C β /H β} ($\delta_C/\delta_H = 84.0/4.40$ ppm). Similarly, in the aromatic region, the signals of P1 exhibited identical ¹H and ¹³C chemical shifts to the B_{C2/H2}, B_{C5/H5}, B_{C6/H6} and B_{C1/H1} signals of GGE (Figure 2.5A). These signals of P1 were assigned to B_{C2/H2} ($\delta_C/\delta_H = 113.1/6.66$ ppm), B_{C5/H5} ($\delta_C/\delta_H = 117.2/6.73$ ppm), B_{C6/H6} ($\delta_C/\delta_H = 121.9/6.66$ ppm), and B_{C1/H1} ($\delta_C/\delta_H = 123.1/6.72$ ppm). Additionally, a signal of P1 closely resembling the A_{C2/H2} signal of GGE was identified (Figure 2.5A). Consequently, I assigned this signal of P1 to A_{C2/H2} ($\delta_C/\delta_H = 111.5/6.80$ ppm). Then, it was noted that a signal corresponding to A_{C5/H5} of GGE was absent in the P1 spectrum. Thus far, it is evident that the structure of a compound in the P1 fraction is closely related to that of GGE. In the subsequent analysis, I identified the signal corresponding to position 5, along with the signal corresponding to position 6 of the phenolic ring A of P1.

In the P1 HSQC spectrum (Figure 2.5A), I observed two new signals ($\delta_C/\delta_H = 122.3/6.16$ and $122.7/6.25$ ppm) that were not present in the GGE spectrum. In the P1 HMBC spectrum (Figure 2.5B, top-left), I identified two signals ($\delta_C/\delta_H = 73.1/6.80$ and $73.1/6.25$ ppm) with correlations to the C α of HSQC. The first signal, $\delta_C/\delta_H = 73.1/6.80$ ppm, exhibited a correlation with A_{C2/H2} in the HSQC, and was therefore assigned to A_{C α /H2}. Consequently, I assigned the other signal, $\delta_C/\delta_H = 73.1/6.25$ ppm, to A_{C α /H6}. As a result, one of the two new signals in the P1 HSQC spectrum, $\delta_C/\delta_H = 122.7/6.25$ ppm, was assigned to A_{C6/H6} (Figure 2.5B).

Assignments for the chemical shifts of carbons at positions 1, 3, 4, and 6 of ring A

were based on the resemblance in the HMBC spectrum between GGE and P1, illustrated at the bottom left of Figure 2.5B. Moreover, the chemical shift of carbon at position 2 of ring A had been previously assigned, as explained earlier. The HMBC signal at $\delta_C/\delta_H = 125.4/6.25$ ppm indicated a two or three bond correlation between the proton at position 6 of ring A and the carbon at position either 1, 2, 4, or 5 of the same ring, A. As $\delta_C = 125.4$ ppm differed from the chemical shift of already assigned carbons at positions 1, 2, and 4 of ring A, the HMBC signal at $\delta_C/\delta_H = 125.4/6.25$ ppm was attributed to $A_{C5/H6}$. Then, it turned out that a HSQC signal for the position 5 of ring A of P1 was not present. Therefore, I concluded that the proton of position 5 of ring A of P1 had undergone deprotonation.

Next, I analyzed the relative intensities of the HSQC signals of P1 (Table 2.4). All signals of rings A and B were observed to be close to 1, except for the two new signals ($\delta_C/\delta_H = 122.3/6.16$ and $122.7/6.25$ ppm) with approximately 0.5 intensity, respectively. Since the latter signal was assigned to $A_{C6/H6}$, I concluded that the former one also corresponds to $A_{C6/H6}$. The differences in chemical shifts are probably due to conformational variations. The molecular weight analysis of P1 indicated that the compound in P1 contains four aromatic rings (Table 2.2). Since no HSQC signal other than the signals corresponding to rings A and B was observed, it is supposed that the structure of P1 is symmetrical, except for the C_6/H_6 moiety of ring A.

Based on my analysis of HSQC and HMBC signals for P1, I propose that the primary compound in P1 has a chemical structure consisting of two GGE portions connected by a 5-5' linkage (Figure 2.5C). Several lines of evidence support this conclusion: Firstly, the SEC analysis of P1 indicated a molecular weight consistent with two GGE portions. Secondly, the

disappearance of the HSQC correlation for A₅ (Figure 2.5A) suggests the deprotonation of position 5 of the phenolic ring A of P1, which is indicative of the formation of a 5-5' linkage. Lastly, I observed a shift in the ¹³C chemical shift for position 5 of phenolic ring A of P1 from $\delta_C = 115.6$ (GGE) to 125.4 ppm (P1). This observation aligns with a previous NMR study by Ralph *et al.*, where the formation of a 5-5' carbon-carbon interunit linkage of identical dimers resulted in a downfield perturbation of the carbon directly involved in the formation of the interunit linkage.²⁴ In conclusion, I revealed that a radical coupling reaction occurred between two GGE molecules at C₅ in phenolic ring A, resulting in the formation of P1, a 5-5' biphenyl GGE (Figure 2.5C).

In my proposed reaction mechanism involving CsMnP and GGE (illustrated in Figure 2.6), the catalytic activity of CsMnP is initiated in the presence of H₂O₂, CsMnP compound I being formed. CsMnP compound I then oxidizes Mn²⁺ to Mn³⁺ and generates CsMnP compound II.²⁵⁻²⁷ Similarly, CsMnP compound II oxidizes Mn²⁺ to produce Mn³⁺ and reverts to ferric CsMnP, completing the catalytic cycle of CsMnP. The chelated Mn³⁺ ions produced by CsMnP act as diffusible redox mediators, facilitating the oxidation of the phenolic substrate (phenolic ring A) in GGE. This oxidation leads to the abstraction of a hydrogen atom from the OH group on GGE, resulting in the formation of a GGE radical. Subsequently, a radical coupling reaction occurs between two GGE radicals at C₅ on phenolic ring A, yielding a 5-5' biphenyl GGE. Further catalytic activity of CsMnP leads to additional reactions, ultimately yielding products such as P2-5.

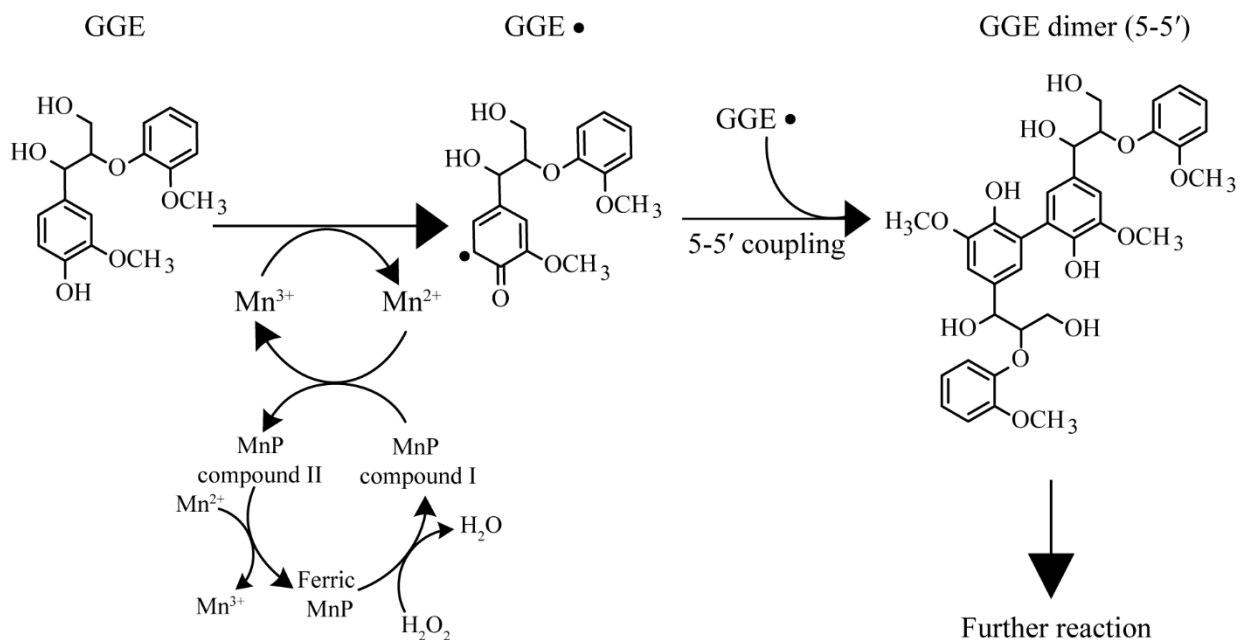


Figure 2.6. A proposed reaction scheme for the conversion of GGE catalyzed by *CsMnP* and the catalytic cycle of *CsMnP*.²⁵⁻²⁷

2.2.5 Application of *CsMnP* for KL polymerization

Having observed the polymerization ability of *CsMnP* as to a guaiacyl-type phenolic lignin dimer, I further explored its potential for polymerizing KL. To compare the characteristics of untreated KL (KL) and *CsMnP*-treated KL (*CsMnP*-KL), I conducted analyses to determine their total phenolic contents using the Folin-Ciocalteu method, estimated their molecular weights through SEC analysis, and performed structural analysis using NMR spectroscopy.

Before initiating the enzymatic reaction with H_2O_2 , the phenolic content of KL was determined to be 168.1 mg GAE/g KL (Table 2.5). After 24 hours of reaction, the phenolic content of *CsMnP*-KL had decreased by 37% to 106.7 mg GAE/g KL. These findings suggest that *CsMnP* initiated the oxidation of phenolic OH groups in KL, leading to the formation of

highly reactive phenoxy radicals.²⁸⁻³⁰ These radicals can undergo cross-reactions, establishing new interunit linkages and causing the reduction in the phenolic content of KL.^{28,29}

Table 2.5. The phenolic contents, number-average (M_n) and weight-average (M_w) molecular weights, and polydispersity (M_w/M_n) of untreated KL and CsMnP-treated KL (CsMnP-KL)^a

Sample	Phenolic content ^b (mg GAE/g KL)	M_n	M_w	M_w/M_n
KL				
0 h	166.2 ± 3.1	2844	14036	4.93
24 h	165.3 ± 4.6	2872	14389	5.01
CsMnP-KL				
0 h	168.1 ± 5.9	3521	18831	5.35
24 h	106.7 ± 4.5	15586	68574	4.40

^aReaction was performed at 30 °C for 24 h in a 50 mL reaction mixture containing 0.5 g KL, 2 mM MnSO₄, 0.25 mM H₂O₂, and with or without 5 U CsMnP. Then, 0.25 mM H₂O₂ was added every 12 h until 24 h. ^bThe phenolic content was expressed as mg gallic acid equivalent (GAE) per 1 g of KL. The mean and standard deviation were obtained from two independent experiments.

Subsequently, I conducted SEC analysis to determine the molecular weights of KL and CsMnP-KL (Table 2.5). After 24 hours of reaction, the M_n and M_w of CsMnP-KL had increased, while the polydispersity decreased from 5.35 to 4.4. Specifically, the M_w of CsMnP-KL exhibited a 3.6-fold increase, increasing from 18,831 to 68,574. These results indicate that CsMnP effectively catalyzed the polymerization of KL, resulting in the formation of various new interunit linkages and the subsequent increase in M_w . Similar increases in the M_w have been reported when laccase was employed for KL polymerization.^{29,31-33} The higher molecular weight of CsMnP-KL enables new applications,

such as lignin-based hydrogels, lignin-based dispersants, and thermoplastic blends, enhancing thermal and mechanical performance.³⁴⁻³⁶

Next, I employed NMR spectroscopy to investigate the chemical structures of KL and CsMnP-treated KL (CsMnP-KL). The HSQC spectra of KL and CsMnP-KL are shown in Figures 2.7A and 2.7B, respectively, with the aliphatic and aromatic regions depicted in the upper and lower panels, respectively. Signal assignments were made with reference to relevant literature sources.³⁷⁻³⁹ In the aliphatic region, I identified HSQC correlations corresponding to the methoxy group (-OMe), phenylcoumaran (B), resinol (C), diresinol (C''), β -O-4' (A), and xylan (X) present in KL (Figure 2.7). Additionally, correlations corresponding to the guaiacyl-unit (G) were observed in the aromatic region.

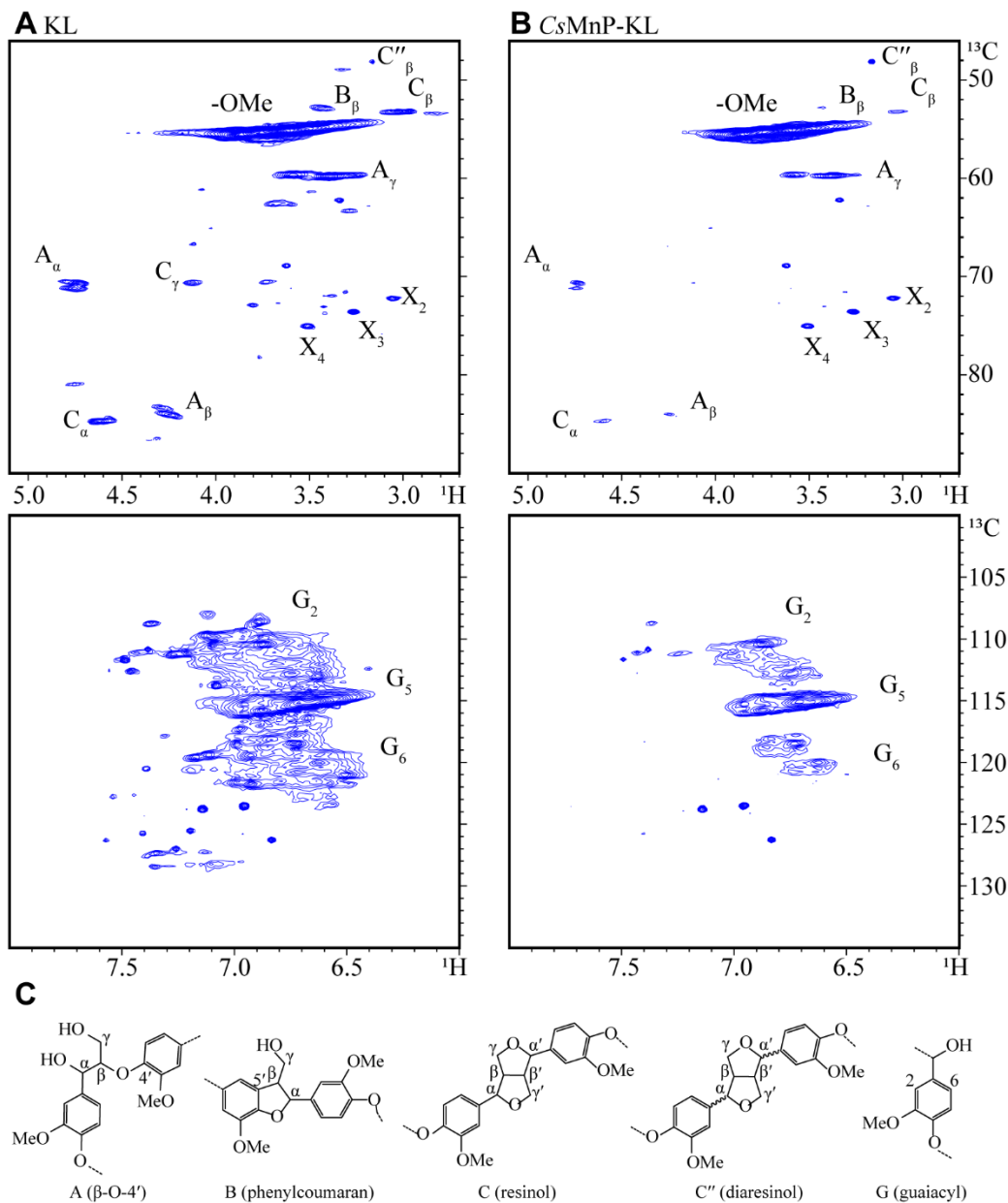


Figure 2.7. 2D ^1H - ^{13}C HSQC spectra of untreated (A) and CsMnP-treated (B) Kraft lignins (KLs). The aliphatic (top) and aromatic (bottom) regions are shown. (C) The lignin substructures identified in HSQC spectra. The signal assignments are summarized in Table 2.6.

Table 2.6. The signal assignments of the 2D ^1H - ^{13}C HSQC spectra of untreated KL and *CsMnP*-treated KL (*CsMnP*-KL)

Label	δ_C/δ_H (ppm/ppm)	Assignment
C''_β	48.8/3.19	C_β/H_β in diaresinol substructures
B_β	53.3/3.46	C_β/H_β in phenylcoumaran substructures
C_β	53.5/3.06	C_β/H_β in resinol substructures
-OMe	55.6/3.73	C/H in methoxy groups
A_γ	59.5-59.7/3.4-3.7	C_γ/H_γ in β -O-4' substructures
A_α	70.9/4.71	C_α/H_α in β -O-4' substructures
C_γ	71.0/3.79 and 4.16	C_γ/H_γ in resinol substructures
X_2	73.0/3.08	C_2/H_2 in xylan
X_3	74.3/3.34	C_3/H_3 in xylan
X_4	75.9/3.52	C_4/H_4 in xylan
A_β	83.5/4.27	C_β/H_β in β -O-4' substructures
C_α	84.9/4.64	C_α/H_α in resinol substructures
G_2	110.9/6.98	C_2/H_2 in guaiacyl unit
G_5	114.9/6.77	C_5/H_5 in guaiacyl unit
G_6	119.0/6.80	C_6/H_6 in guaiacyl unit

Following a 24-hour reaction, the signal intensities of phenylcoumaran, resinol, β -O-4', and guaiacyl in *CsMnP*-KL exhibited a decrease compared to those of KL (Table 2.7). Meanwhile, the signal intensities of xylan and diaresinol remained largely unaffected by *CsMnP* treatment. The reduction in signal intensities for β -O-4', phenylcoumaran, and resinol can be attributed to the cleavage of these substructures during treatment with *CsMnP*. This is consistent with the previous study that demonstrated the cleavage of the β -aryl ether and β - β' resinol substructures when alkali lignin was treated with a commercial bacterial laccase.³³

Table 2.7. The relative amount of the lignin substructures present in CsMnP-treated KL (CsMnP-KL) to those for untreated KL

Label	Relative amount (%)
-OMe	59.7
β -O-4' (A)	43.8
Phenylcoumaran (B)	30.4
Resinol (C)	32.6
Diaresinol (C'')	98.8
Xylan (X)	99.1
Guaiacyl (G)	43.5

^aThe relative amount of lignin substructures was calculated using Eq (2.1) below, based on the volume integrals of the signals in the HSQC spectrum. The amount of lignin substructures present in untreated KL was defined as 100%. Each signal volume was normalized based on the signal volume for DSS-d₆.

Equation 2.1. The relative amount of lignin substructures present in CsMnP-KL as to those for untreated KL was determined based on the volume integrals of the signals in the HSQC spectrum. $\int S_{CsMnP-KL}$ is the volume integral of the signals for the lignin substructure present in CsMnP-KL. $\int S_{KL}$ is the volume integral of the signals for the lignin substructure present in untreated KL.

$$\text{Relative amount (\%)} = \frac{\int S_{CsMnP-KL}}{\int S_{KL}} \times 100\% \quad (2.1)$$

The reduction in signal intensity of the guaiacyl-unit suggests the deprotonation of the benzenic ring in KL and polymerization, which aligns with the results obtained on SEC analysis (Table 2.5). Similar trends of involving decreased or vanished aromatic proton signals in NMR spectra have been noted in laccase-catalyzed polymerization of

lignosulfonates^{40,41} and kraft lignin^{7,29,33,34}. In these studies, the researchers attributed this phenomenon to the creation of polymerized structures through α -5', 5-5', and 4-O-5' linkages.

Collectively, the outcomes of total phenolic content quantification, SEC analysis, and NMR analysis consistently indicate CsMnP-catalyzed polymerization of KL.

2.3 Conclusions

In conclusion, my study using GGE and KL as substrates provides strong evidence for the effectiveness of CsMnP as a biocatalyst for lignin phenolic subunit polymerization. The results clearly show that CsMnP catalyzed the formation of a biphenyl GGE linked at the 5-5' position of the phenolic ring, and also generated compounds up to heptamer length, indicating that polymerization was the primary reaction. Additionally, CsMnP demonstrated a remarkable ability to polymerize KL, resulting in a substantial 3.6-fold increase in molecular weight and a noteworthy 37% reduction in phenolic content. NMR analysis provided insights into the role of CsMnP in facilitating polymerization reactions on KL. These significant findings shed new light on the enzymatic properties of CsMnP and highlight its potential as a biocatalyst for lignin-based product synthesis through polymerization reactions.

2.4 Experimental procedures

2.4.1 Cloning and expression of CsMnP in *Pichia pastoris*, and preparation of crude CsMnP

The DNA template encoding the MnP enzyme from *Ceriporiopsis subvermispora*

(designated as CsMnP, Joint Genome Institute protein code CsMnP10: 117436) was synthesized by Thermo Fisher Scientific. The CsMnP gene was amplified through polymerase chain reaction (PCR) and then ligated with the pPICZ α A vector (Invitrogen, USA) using *Kpn*I and *Not*I restriction sites. Subsequently, the resulting pPICZ α A-CsMnP vector was linearized with *Sac*I and introduced into *P. pastoris* X-33 (Invitrogen, USA) by electroporation. The transformants were cultured on YPDS agar medium (1% yeast extract, 2% peptone, 2% glucose, 1 M sorbitol, 2% agar, and 100 μ g/mL zeocin) for three days at 30 °C. The positive clones were selected by performing colony PCR, a 1 mL-scale expression check, and an activity assay.

To produce CsMnP, a single colony of the confirmed transformant was inoculated into 100 mL of BMGY medium (1% yeast extract, 2% peptone, 1.34% yeast nitrogen base with ammonium sulfate, 0.1 M potassium phosphate (pH 6), 0.4 μ g/mL biotin, and 1% glycerol) in a 500 mL baffled flask. The culture was then incubated at 30 °C and 200 rpm shaking until the optical density at 600 nm (OD₆₀₀) reached 6.0. To induce the expression of CsMnP, the cells were harvested by centrifugation at 3,500 \times g for 5 min and resuspended in BMMY medium (1% yeast extract, 2% peptone, 1.34% yeast nitrogen base with ammonium sulfate, 0.1 M potassium phosphate (pH 6), 0.4 μ g/mL biotin, and 0.5% methanol) supplemented with 1 mM CaCl₂, which was pre-cooled at 15 °C, to achieve an OD₆₀₀ of 1.0. The induction was carried out at 15 °C. During the induction phase, 0.5% methanol and 0.2% hemin stock solution (10 mg/mL hemin in a 0.1 M NH₄OH solution) were added every 12 h. After 72 h, the supernatant containing the secreted CsMnP was collected by centrifugation at 8,000 \times g for 30 min. Subsequently, the supernatant was filtered with a 300-kDa cut-off

membrane (Pall, USA) using a Minimate TFF system (OAPMP110, Pall) to eliminate cell debris. The resulting cell-free supernatant was concentrated 40-fold and buffer-exchanged to 50 mM sodium malonate (pH 5) with a 10-kDa cut-off membrane (Pall, USA). This solution, referred to as crude *CsMnP*, was stored at 4 °C for future use.

2.4.2 Activity assaying of *CsMnP*

The enzymatic activity of crude *CsMnP* was determined employing 2,6-dimethoxyphenol (DMP) as the substrate. The reaction was conducted at 25 °C in a total volume of 200 μ L, with 50 mM sodium malonate (pH 5), 10 μ L of crude *CsMnP*, 1 mM DMP, 1 mM $MnSO_4$, and 0.1 mM H_2O_2 . To monitor the formation of the product (coerulignone), the increase in visible light absorbance at 469 nm was measured using an Infinite[®] 200 PRO (TECAN) spectrophotometer. The amount of coerulignone was determined using the molar absorption coefficient of coerulignone ($\epsilon_{469} = 53,200/M\text{ cm}$).⁴² In this study, one unit (U) of enzyme activity was defined as the amount of *CsMnP* required to catalyze the production of 1 μ mol of coerulignone per minute under the specified assay conditions.

2.4.3 Reaction of GGE with *CsMnP*

The enzymatic reaction of *CsMnP* with guaiacylglycerol- β -guaiacyl ether (GGE, TCI, Japan) was performed in a 1 mL reaction mixture containing 50 mM sodium malonate (pH 5), 1 mM GGE, 0.694 mU *CsMnP*, and 2 mM $MnSO_4$. The reaction was initiated by adding 0.125 mM H_2O_2 and conducted at 25 °C. Then, 0.125 mM H_2O_2 was added once every 6 h. A total of seven samples were prepared for the reaction, which was terminated by heating at

95 °C for 10 min at 0, 6, 12, 18, 24, 36, and 48 h, respectively. Following termination, all samples were frozen and stored until further analysis. Two independent experiments were performed to obtain the mean and standard deviation.

To analyze the individual reaction products, a large-scale enzymatic reaction was carried out for 48 h using the same reaction composition. The reaction mixture volume was adjusted to 25 mL.

2.4.4 Analysis and separation of reaction products by RP-HPLC

The reaction mixture collected at each time point was subjected to analysis using a RP-HPLC system (Shimadzu, Japan) equipped with an SPD-20A UV-Vis detector set to detect absorbance at 280 nm. To prepare the samples for analysis, acetonitrile (ACN) was added to a final concentration of 5%, and the resulting mixture was filtered through a 0.2 µm polytetrafluoroethylene (PTFE) membrane. For analysis, 20 µL of the filtered sample was injected into a TSKgel ODS-80T_M (6.0 × 150 mm, Tosoh, Japan) analytical column, which was maintained at 45 °C throughout the analysis. The mobile phases consisted of water (eluent A) and ACN (eluent B), both containing 0.1% trifluoroacetic acid. The elution profile used was as follows: an isocratic step at 5% B for 0-5 min, a linear gradient from 5% to 40% B over 5-15 min, a linear gradient from 40% to 95% B over 15-40 min, an isocratic step at 95% B for 40-45 min, a linear gradient from 95% to 5% B over 45-46 min, and an isocratic step at 5% B for 47-52 min. The flow rate was set at 0.5 mL/min. The GGE content was determined based on the peak area on the chromatogram.

For further analysis, a 15 mL portion of the reaction mixture collected at 48 h was

concentrated by lyophilization, and the resulting concentrate was dissolved in 1 mL of 5% ACN. The solution was then filtered through a 0.2 μm PTFE membrane. Subsequently, 100 μL of the filtered sample was injected into the RP-HPLC system and separated using the same elution profile as described earlier. The reaction products were individually collected, lyophilized, and subjected to analysis by SEC and 2D NMR.

2.4.5 Molecular weight analysis of reaction products by SEC

To determine the molecular weights of the reaction products, each sample obtained from the RP-HPLC as explained in the last paragraph of the previous section was dissolved in tetrahydrofuran (THF). Subsequently, the samples were filtered through a 0.2 μm PTFE filter and injected into an HPLC system equipped with an SPD M20A photodiode array detector. Three TSKgel SuperMultiporeHZ-M analytical columns (4.6 \times 150 mm, Tosoh) were connected in tandem for the analysis. The detection was done at 280 nm.

The analysis was performed at 40 $^{\circ}\text{C}$ using THF as the mobile phase, at a flow rate of 0.35 mL/min. To estimate the molecular weights of the reaction products, a calibration curve was constructed utilizing a series of polystyrene standards (PStQuickC, weight average molecular weight (M_w) = 5970-2110000, Tosoh), 1-(3,4-Dimethoxyphenyl)-2-(2-methoxyphenoxy)-1,3-propanediol (M_w = 334), and vanillin (M_w = 152).⁴³ These standards aided in the determination of the molecular weights of the reaction products.

2.4.6 Structural analysis of the reaction product by 2D NMR

The reaction product obtained on RP-HPLC as explained above was dissolved in 270

μL of D_2O and 30 μL of DMSO-d_6 supplemented with 0.5 mM deuterated 4,4-dimethyl-4-silapentane-1-sulfonic acid (DSS-d_6). To elucidate its structural characteristics, I acquired 2D ^1H - ^{13}C heteronuclear single quantum coherence (HSQC) and 2D ^1H - ^{13}C heteronuclear multiple bond correlation (HMBC) spectra at 298 K, employing standard Bruker pulse sequences ‘hsqcetgpprsisp2.2’ and ‘hmbcgp1pndqf’, respectively. A 2D ^1H - ^{13}C HSQC spectrum was recorded for GGE only, acting as a control.

All NMR spectra were recorded at 298 K using a Bruker Avance III HD 600 MHz instrument equipped with a 5 mm cryogenic probe and Z gradient (Bruker BioSpin, MA, USA). To calibrate the chemical shifts of the acquired HSQC spectra, I used DMSO as a reference with δ_C 39.5 ppm and δ_H 2.49 ppm. Data processing, signal assignment, and volume integration were performed using Bruker TopSpin 3.6.4 software. Each signal volume was normalized based on the signal volume for DSS-d_6 .

2.4.7 Polymerization of KL by *CsMnP*

Polymerization of KL (471003, Sigma-Aldrich) was carried out using *CsMnP*. The reaction was conducted in a 50 mL reaction mixture consisting of 50 mM sodium malonate (pH 5), 0.5 g KL, 5 U *CsMnP*, and 2 mM MnSO_4 at 25 °C. To initiate the enzymatic reaction, 0.25 mM H_2O_2 was added. The reaction proceeded for 12 h, after which an additional 0.25 mM H_2O_2 was added, and the reaction was allowed to continue for another 12 h. Subsequently, the pH of the reaction mixture was adjusted to 2.5 using hydrochloric acid, resulting in the formation of a precipitate comprising the reaction products. This precipitate was collected by centrifugation at $10,000 \times g$ for 10 min and subjected to three washes with

acidified water (pH 2.5).^{7,44} The resulting sample was then lyophilized. A control experiment was also conducted following the same procedure but omitting CsMnP. The characteristics of KL and CsMnP-treated KL (CsMnP-KL) were then compared.

2.4.8 Estimation of total phenolic content in KL

The total phenolic content of the samples was determined using the Folin-Ciocalteu method, following the procedure described by Luisa et al.⁴⁵ The samples were dissolved in DMSO to achieve a concentration of 0.2 mg/mL. Subsequently, 100 μ L aliquots of these prepared samples were combined with 500 μ L of Folin-Ciocalteu reagent, followed by the addition of 400 μ L of 0.7 M Na₂CO₃. The resulting mixture was incubated at 50 °C for 10 min. Afterward, it was cooled to room temperature, and the absorbance at 760 nm was measured using an Infinite® 200 PRO spectrophotometer. The total phenolic contents of the samples were determined by comparing the absorbance values to a calibration curve generated from a standard solution of gallic acid (1 to 200 mg/L). The results were expressed as milligrams of gallic acid equivalent (GAE) per one gram of either KL or CsMnP-KL.

2.4.9 Molecular weight analysis of KL by SEC

To determine the molecular weights of KL and CsMnP-KL, the samples were dissolved in a 10 mM NaOH solution and subsequently filtered through a 0.2 μ m PTFE filter. The filtered samples were then injected into a HPLC system equipped with an SPD-20A UV-Vis detector. Detection was carried out at 280 nm. For the analysis, I utilized a TSKgel G3000PW_{XL} analytical column (7.8 \times 300 mm, Tosoh, Japan), which was maintained at a

constant temperature of 35 °C. The mobile phase used in the chromatographic separation was a 10 mM NaOH solution, and the flow rate was set at 0.5 mL/min. To estimate the molecular weights of the samples, a calibration curve was constructed using a series of polystyrene sulfonate sodium salt standards with known peak molecular weights (M_p) of 891 to 151000.

2.4.10 Structural analysis of KL by 2D NMR

For NMR analysis, I dissolved 20 mg of the samples in 300 μ L of DMSO- d_6 containing 0.5 mM DSS- d_6 . To acquire the 2D ^1H - ^{13}C HSQC spectra, I employed the standard Bruker pulse sequence ‘hsqcetgpprsisp2.2’ at 298 K. To calibrate the chemical shifts of the acquired HSQC spectra, I used DMSO as a reference with δ_C 39.5 ppm and δ_H 2.49 ppm. Data processing, signal assignment, and signal volume integration were performed using Bruker TopSpin 3.6.4 software. To normalize each signal volume, I used the signal volume for DSS- d_6 as a reference.

I estimated the amounts of β -O-4', phenylcoumaran, and resinol by analyzing the volumes of their C_α - H_α correlation peaks.^{46,47} Similarly, the amount of diaresinol was estimated from the volume of the C_β - H_β correlation peak. To estimate the amount of xylan, I analyzed the volume of C_3 - H_3 correlation peak. Lastly, the amount of a G-unit was estimated based on the volume of the C_2 - H_2 correlation peak.

2.5 References

1. Liu, Q.; Luo, L.; Zheng, L. Lignins: Biosynthesis and Biological Functions in Plants. *Int. J. Mol. Sci.* 2018, **19**(2), 335.

2. Eswaran, S. C. D.; Subramaniam, S.; Sanyal, U.; Rallo, R.; Zhang, X. Molecular structural dataset of lignin macromolecule elucidating experimental structural compositions. *Sci. Data.* 2022, **9**, 647.
3. Rosini, E.; Molinari, F.; Miani, D.; Pollegioni, L. Lignin Valorization: Production of High Value-Added Compounds by Engineered Microorganisms. *Catalysts* 2023, **13** (3), 555.
4. Alekhina, M.; Ershova, O.; Ebert, A.; Heikkinen, S.; Sixta, H. Softwood Kraft Lignin for value-added applications: Fractionation and structural characterization. *Ind. Crops Prod.* 2015, **66**, 220-228.
5. Zerpa, A.; Pakzad, L.; Fatehi, P. Hardwood Kraft Lignin-Based Hydrogels: Production and Performance. *ACS Omega* 2018, **3**, 8233-8242.
6. Rico-García, D.; Ruiz-Rubio, L.; Pérez-Alvarez L., Hernández-Olmos, S. L.; Guerrero-Ramírez, G. L.; Vilas-Vilela, J. L. Lignin-Based Hydrogels: Synthesis and Applications. *Polymers* 2020, **12**(1), 81.
7. Ibarra, D.; García-Fuentevilla, L.; Domínguez, G.; Martín-Sampedro, R.; Hernández, M.; Arias, M. E.; Santos, J. I.; Eugenio, M. E. NMR Study on Laccase Polymerization of Kraft Lignin Using Different Enzymes Source. *Int. J. Mol. Sci.* 2023, **24**(3), 2359.
8. Yadav, V. K.; Gupta, N.; Kumar, P.; Dashti, M. G.; Tirth, V.; Khan, S. H.; Yadav, K. K.; Islam, S.; Choudhary, N.; Algahtani, A.; Bera, S. P.; Kim, D.; Jeon, B. Recent Advances in Synthesis and Degradation of Lignin and Lignin Nanoparticles and Their Emerging Applications in Nanotechnology. *Materials*, 2022, **15**(3), 953.

9. Xu, H.; Guo, M.; Gao, Y.; Bai, X.; Zhou, X. Expression and characteristics of manganese peroxidase from *Ganoderma lucidum* in *Pichia pastoris* and its application in the degradation of four dyes and phenol. *BMC Biotechnol.* 2017, **17**, 19.
10. Kumar, A.; Arora, P. K. Biotechnological Applications of Manganese Peroxidases for Sustainable Management. *Front. Environ. Sci.* 2022, **10**, 875157.
11. Asina, F.; Brzonova, I.; Kozliak, E.; Kubátová, A.; Ji, Y. Microbial treatment of industrial lignin: Successes, problems and challenges. *Renew. Sustain. Energy Rev.* 2017, **77**, 1179-1205.
12. Saikia, S.; Yadav, M.; Hoque, R. A.; Yadav, H. S. Bioremediation mediated by manganese peroxidase – An overview. *Biocatal. Biotransformation* 2022, **41**, 161-173.
13. Fernández-Fueyo, E.; Ruiz-Dueñas, F. J.; Miki, Y.; Martínez, M. J.; Hammel, K. E.; Martínez, A. T. Lignin-degrading Peroxidases from Genome of Selective Ligninolytic Fungus *Ceriporiopsis subvermispora*. *J. Biol. Chem.* 2012, **287**(20), 16903-16916.
14. Lin, M.; Nagata, T.; Katahira, M. High yield production of fungal manganese peroxidases by *E. coli* through soluble expression, and examination of the activities. *Protein Expr. Purif.* 2018, **145**, 45-52.
15. E, G. V.; Wang, J.; Sun, P.; Waard, P. D.; Putten, J. V. D.; Frissen, G. E.; Gosselink, R. J. A.; Zinovyev, G.; Potthast, A.; Berkel, W. J. H. V.; Kabel, M. A. Structural Motifs of Wheat Straw Lignin Differ in Susceptibility to Degradation by the White-

- Rot Fungus *Ceriporiopsis subvermispora*. *ACS Sustainable Chem. Eng.* 2019, **7**, 20032–20042.
16. Floudas, D.; Binder, M.; Riley, R.; Barry, K.; Blanchette, R. A.; Henrissat, B.; Martínez, A. T.; Otilar, R.; Spatafora, J. W.; Yadav, J. S. The *Paleozoic* origin of enzymatic lignin decomposition reconstructed from 31 fungal genomes. *Science* 2012, **336**, 1715-1719.
17. Hori, C.; Gaskell, J.; Igarashi, K.; Kersten, P.; Mozuch, M.; Samejima, M.; Cullen, D. Temporal Alterations in the Secretome of the Selective Ligninolytic Fungus *Ceriporiopsis subvermispora* during Growth on Aspen Wood Reveal This Organism's Strategy for Degrading Lignocellulose. *Appl. Environ. Microbiol.* 2014, **80**, 2062-2070.
18. Wang, N.; Ren, K.; Jia, R.; Chen, W.; Sun, R. Expression of a fungal manganese peroxidase in *Escherichia coli*: a comparison between the soluble and refolded enzymes. *BMC Biotechnol.* 2016, **16**, 87.
19. Hilgers, R.; Vincken, J.; Gruppen, H.; Kabel, M. A. Laccase/Mediator Systems: Their Reactivity toward Phenolic Lignin Structures. *ACS Sustainable Chem. Eng.* 2018, **6**, 2037–2046.
20. Hilgers, R.; Twentyman-Jones, M.; Dam, A. V.; Gruppen, H.; Zuilhof, H.; Kabel, M. A.; Vincken, J. The impact of lignin sulfonation on its reactivity with laccase and laccase/HBT. *Catal. Sci. Technol.* 2019, **9**, 1535-1542.
21. Zeng, J.; Mills, M. J. L.; Simmons, B. A.; Kent, M. S.; Sale, K. L. Understanding factors controlling depolymerization and polymerization in catalytic degradation of

- β -ether linked model lignin compounds by versatile peroxidase. *Green Chem.* 2017, **19**, 2145-2154.
22. Ando, D.; Ralph, J. Method to Regioselectively Iodine-Tag Free-Phenolic Aromatic End-Groups in Lignin for ^1H - ^{13}C -HSQC NMR Analysis. *ACS Sustainable Chem. Eng.* 2019, **7**, 18624–18629.
23. Liu, Y.; Liu, Y.; Lyu, G.; Ji, X.; Yang, G.; Chen, J.; Lucia, L. A. Analytical pyrolysis pathways of guaiacyl glycerol- β -guaiacyl ether by Py-GC/MS. *BioRes.* 2016, **11**(3), 5816-5828.
24. Ralph, S.; Ralph, J. NMR Database of Lignin and Cell Wall Model Compounds. 2009.
25. Kulikova, N. A.; Klein, O. I.; Stepanova, E. V.; Koroleva, O. V. Use of Basidiomycetes in Industrial Waste Processing and Utilization Technologies: Fundamental and Applied Aspects (Review). *Appl. Biochem. Microbiol.* 2011, **47**, 565-579.
26. Hofrichter, M. Review: lignin conversion by manganese peroxidase (MnP). *Enzyme Microb. Technol.* 2002, **30**, 454-466.
27. Fakoussa, RM.; Hofrichter, M. Biotechnology and microbiology of coal degradation. *Appl. Microbiol. Biotechnol.* 1999, **52**(1), 25-40.
28. Mayr, S. A.; Subagia, R.; Weiss, R.; Schwaiger, N.; Weber, H. K.; Leitner, J.; Ribitsch, D.; Nyanhongo, G. S.; Guebitz, G. M. Oxidation of Various Kraft Lignins with a Bacterial Laccase Enzyme. *Int. J. Mol. Sci.* 2021, **22**(23), 13161.

29. Gouveia, S.; Otero, L. A.; Fernández-Costas, C.; Filgueira, D.; Sanromán, Á.; Moldes, D. Green Binder Based on Enzymatically Polymerized Eucalypt Kraft Lignin for Fiberboard Manufacturing: A Preliminary Study. *Polymers* 2018, **10**(6), 642.
30. Fillat, Ú.; Ibarra, D.; Eugenio, M. E.; Moreno, A. D.; Tomás-Pejó, E.; Martín-Sampedro, R. Laccases as a Potential Tool for the Efficient Conversion of Lignocellulosic Biomass: A Review. *Fermentation* 2017, **3**(2), 17.
31. Huber, D.; Pellis, A.; Daxbacher, A.; Nyanhongo, G. S.; Guebitz, G. M. Polymerization of Various Lignins via Immobilized *Myceliophthora thermophila* Laccase (MtL). *Polymers* 2016, **8**, 280.
32. Gouveia, S.; Fernández-Costas, C.; Sanromán, M.A.; Moldes, D. Polymerisation of Kraft lignin from black liquors by laccase from *Myceliophthora thermophila*: Effect of operational conditions and black liquor origin. *Bioresour. Technol.* 2013, **131**, 288-294.
33. Wang, L.; Tan, L.; Hu, L.; Wang, X.; Koppolu, R.; Tirri, T.; Bochove, B. V.; Ihalainen, P.; Sobhanadhas, L. S. S.; Seppälä, J. V.; Willför, S.; Toivakka, M.; Xu, C. On Laccase-Catalyzed Polymerization of Biorefinery Lignin Fractions and Alignment of Lignin Nanoparticles on the Nanocellulose Surface via One-Pot Water-Phase Synthesis. *ACS Sustainable Chem. Eng.* 2021, **9**, 8770–8782
34. García-Fuentevilla, L.; Domínguez, G.; Martín-Sampedro, R.; Hernández, M.; Arias, M. E.; Santos, J. I.; Ibarra, D.; Eugenio, M. E. Enzyme-Catalyzed Polymerization of

- Kraft Lignin from *Eucalyptus globulus*: Comparison of Bacterial and Fungal Laccases Efficacy. *Polymers* 2023, **15**(3), 513.
35. Eugenio, M. E.; Martín-Sampedro, R.; Santos, J. I.; Wicklein, B.; Martín, J. A.; Ibarra, D. Properties versus application requirements of solubilized lignins from an elm clone during different pre-treatments. *Int. J. Biol. Macromol.* 2021, **181**, 99-111.
36. Saito, T.; Brown, R. H.; Hunt, M. A.; Pickel, D. L.; Pickel, J. M.; Messman, J. M.; Baker, F. S.; Kellerd, M.; Naskar, A. K. Turning renewable resources into value-added polymer: development of lignin-based thermoplastic. *Green Chem.* 2012, **14**, 3295-3303.
37. Giummarella, N.; Pylypchuk, I. V.; Sevastyanova, O.; Lawoko, M. New Structures in Eucalyptus Kraft Lignin with Complex Mechanistic Implications. *ACS Sustainable Chem. Eng.* 2020, **8**, 10983–10994.
38. Lancefield, C. S.; Wienk, H. L.; Boelens, R.; Weckhuysen, B. M.; Bruijninx, P. C. A. Identification of a diagnostic structural motif reveals a new reaction intermediate and condensation pathway in Kraft lignin formation. *Chem. Sci.* 2018, **9**, 6348-6360.
39. Giummarella, N.; Lindén, P. A.; Areskog, D.; Lawoko, M. Fractional Profiling of Kraft Lignin Structure: Unravelling Insights on Lignin Reaction Mechanisms. *ACS Sustainable Chem. Eng.* 2020, **8**, 1112–1120.
40. Prasetyo, E. N.; Kudanga, T.; Østergaard, L.; Rencoret, J.; Gutiérrez, A.; Río, J. C. D.; Santos, J. I.; Nieto, L.; Jiménez-Barbero, J.; Martínez, A. T.; Li, J.; Gellerstedt, G.; Lepifre, S.; Silva, C.; Kim, S. Y.; Cavaco-Paulo, A.; Klausen, B. S.; Lutnaes, B. F.; Nyanhongo, G. S.; Guebitz, G. M. Polymerization of lignosulfonates by the

- laccase-HBT (1-hydroxybenzotriazole) system improves dispersibility. *Bioresour. Technol.* 2010, **101**, 5054-5062.
41. Gillgren, T.; Hedenström, M.; Jönsson, L. J. Comparison of laccase-catalyzed cross-linking of organosolv lignin and liginosulfonates. *Int. J. Biol. Macromol.* 2017, **105**, 438-446.
42. Purnomo, A. S.; Mori, T.; Kamei, I.; Nishii, T.; Kondo, R. Application of mushroom waste medium from *Pleurotus ostreatus* for bioremediation of DDT-contaminated soil. *Int. Biodeterior. Biodegradation* 2010, **64**, 397-402.
43. Tokunaga, Y.; Nagata, T.; Kondo, K.; Katahira, M.; Watanabe, T. Complete NMR assignment and analysis of molecular structural changes of β -O-4 lignin oligomer model compounds in organic media with different water content. *Holzforschung* 2020, **75**(4), 379-389.
44. Jardim, J. M.; Hart, P. W.; Lucia, L. A.; Jameel, H.; Chang, H. The Effect of the Kraft Pulping Process, Wood Species, and pH on Lignin Recovery from Black Liquor. *Fibers* 2022, **10**(2), 16.
45. García-Fuentevilla, L.; Domínguez, G.; Martín-Sampedro, R.; Hernández, M.; Arias, M. E.; Santos, J. I.; Ibarra, D.; Eugenio, M. E. Enzyme-Catalyzed Polymerization of Kraft Lignin from *Eucalyptus globulus*: Comparison of Bacterial and Fungal Laccases Efficacy. *Polymers* 2023, **15**(3), 513.
46. García-Fuentevilla, L.; Rubio-Valle, J. F.; Martín-Sampedro, R.; Valencia, C.; Eugenio, M. E.; Ibarra, D. Different Kraft lignin sources for electrospun

nanostructures production: Influence of chemical structure and composition. *Int. J. Biol. Macromol.* 2022, **214**, 554-567.

47. Strassberger, Z.; Prinsen, Pepijn.; Klis, F. V. D.; Es, D. S. V.; Tanase, S.; Rothenberg, G. Lignin solubilization and gentle fractionation in liquid ammonia†. *Green Chem.* 2015, **17**, 325-334.

Chapter 3

Enhanced depolymerization of beech wood lignin and its removal with peroxidases through continuous separation of lignin fragments

Reproduced from Ref. *Green Chem.*, 2023, **25**, 7682-7695 with permission from the Royal Society of Chemistry. (DOI: 10.1039/D3GC01246H)

3.1 Introduction

Woody biomass, a second-generation biomass packed with valuable organic compounds such as cellulose, hemicelluloses and lignin, is abundantly available on earth.¹ Recent consensus on the success of future biorefineries relies on the complete valorization of all these organic compounds in the biomass. Although high-value-added products from polysaccharides are extensively realized, lignin is heavily underutilized due to the absence of an economically feasible lignin depolymerization technique.² When an effective lignin depolymerization process is developed, a complete biorefinery process involving lignin valorization will result.³⁻⁷

Currently available lignin depolymerization processes can be classified into physical, chemical, and biological treatments.⁸⁻¹¹ Biological treatment exhibits excellent potential as it bypasses the need of harsh chemicals and reaction conditions. In nature, lignin is biologically degraded by microorganisms such as fungi and bacteria, fungi being the major lignin degraders.¹²⁻¹⁴ White-rot fungi are particularly intriguing as they are able to degrade lignin by secreting a variety of lignin-degrading enzymes, such as laccase,¹⁵⁻²⁰ manganese peroxidase (MnP), lignin peroxidase (LiP), and versatile peroxidase (VP).²¹⁻²⁵

One of the major obstacles for lignin depolymerization by these enzymes is the co-occurrence of lignin depolymerization and repolymerization reactions.^{26,27} The radical formation catalyzed by ligninolytic enzymes lead to either the cleavage of lignin interunit linkages or undesirable repolymerization of lignin fragments through free radical coupling. The occurrence of radical coupling seriously limits the efficacy of enzymatic depolymerization.^{28,29}

To date, various ingenious strategies have been developed to improve the efficiency of lignin depolymerization, such as the stabilization or suppression of reactive intermediates using an auxiliary enzyme,²⁴ base-catalyst,³⁰ and solvent,^{31,32} or by limiting the accessibility and mobility of reactive lignin moieties by performing the reaction in the solid-state.³³ Recently, a membrane bioreactor that was designed for a laccase-catalyzed reaction by Steinmetz *et al.*³⁴ successfully shifted the technical lignin reaction from polymerization to depolymerization. In the membrane bioreactor, reactive lignin fragments generated by laccase were continuously isolated from the reaction system, which reduced the repolymerization reaction and enhanced the efficiency of lignin depolymerization. This approach is expected to be favorable also for a peroxidase-catalyzed reaction. Here, the effects of lignin fragment isolation on not only lignin depolymerization but also lignin removal through the peroxidase-catalyzed reaction were examined using various analytical methods. It is also notable that the effect of the peroxidase-catalyzed reaction was examined for a natural woody biomass in this study.

Here, I investigate the benefit of separating lignin fragments for the peroxidase-catalyzed lignin depolymerization of a natural woody biomass, beech wood, by comparing the reaction in a conventional batch bioreactor and that in the membrane bioreactor. For the reaction, heterologously-expressed white-rot fungal peroxidases, MnP of *Ceriporiopsis subvermispota* (also known as *Gelatoporia subvermispota*) and LiP of *Phanerochaete chrysosporium*, were used. In order for a sustainable and economical approach, both enzymes are used without any chromatographic purification and the reaction is performed at room temperature with a low enzyme dosage (2 U per 1 g of beech wood).

Size-exclusion chromatography (SEC) analysis of the products released into the aqueous phase demonstrated a tremendous increase in the total amount of water-soluble lignin fragments attained by using the membrane bioreactor. Gas chromatography mass spectrometry (GCMS) analysis on the fragments revealed the presence of a variety of short aliphatic and aromatic compounds as constituents.

Then, the solid residues in the reaction vessels for batch and membrane bioreactors were analyzed. Lignin quantification by Klason lignin and UV-Vis spectroscopic methods indicated the enhanced lignin removal for the membrane bioreactor. Furthermore, the SEC analysis demonstrated the significant enhancement of lignin depolymerization achieved by applying the membrane bioreactor, which results in an increase in the yield of low molecular weight lignin. Additionally, two-dimensional nuclear magnetic resonance spectroscopy (2D NMR) also supported the significant lignin removal from the solid residues for the membrane bioreactor.

Overall, this study demonstrated remarkable improvement in peroxidase-catalyzed depolymerization of beech wood lignin when performed in the membrane bioreactor as opposed to the batch bioreactor. Isolation of highly reactive lignin fragments is suggested to be the key to accomplish greater lignin depolymerization of a native biomass without the requirement of harsh chemicals or solvents.

3.2 Results and discussion

3.2.1 Peroxidase-catalyzed lignin depolymerization in batch and membrane bioreactors

Milled beech wood (MBW), prepared by size reduction and extractives removal, was used as a natural lignocellulosic substrate for evaluating peroxidase-catalyzed lignin depolymerization using either a batch or membrane bioreactor. Crude MnP or LiP, which were heterologously expressed in *Pichia pastoris*, was used for this evaluation. The reaction using the batch or membrane bioreactor was performed for eight hours, as illustrated in Figure 3.1. In the batch bioreactor (Figure 3.1a), the enzymatic reaction proceeded without any separation of reaction components. 0.2 mM H₂O₂ was added at the beginning and 0.1 mM after four hours of reaction for the batch bioreactor. On the other hand, in the reaction using the membrane bioreactor (Figure 3.1b), low molecular weight components including depolymerized products were continuously separated from the reaction mixture by ultrafiltration through a regenerated cellulose (RC) membrane with a 3000 molecular weight cut off (MWCO). 80 mL of buffer containing 0.2 mM H₂O₂ and 1 mM MnSO₄ was added every hour of reaction for the membrane bioreactor. The pressure inside the membrane bioreactor was kept constant, the filtration rate remaining constant at around 80 mL h⁻¹ throughout the reaction, indicating no fouling or clogging of the RC membrane.

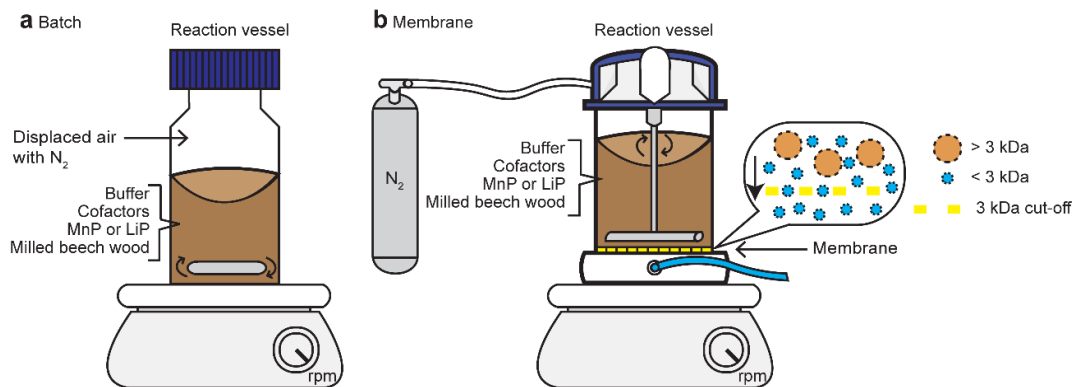


Figure 3.1. Schematic drawing of bioreactors used for the enzymatic reaction. (a) Batch bioreactor. (b) Membrane bioreactor.

3.2.2 Analysis of aromatic products released into the aqueous phase

Water-soluble products that were released into the aqueous phase through a peroxidase-catalyzed reaction were analyzed by SEC with UV absorbance detection at 280 nm. For the batch bioreactor, the water-soluble products were obtained from the supernatant of the reactant after 8 h incubation of MBW with either MnP (Figure 3.2a, black line) or LiP (Figure 3.2b, black line). In the case of both MnP and LiP, a peak (denoted as B_19 in Figure 3.2) was detected at 18.8 min. As B_19 was not detected for the control sample, which was obtained by performing the experiments without either a peroxidase (Figure 3.2a and 3.2b, cyan line) or MBW (Figure 3.2c), B_19 is regarded as being a peak of a reaction product derived from MBW through a peroxidase-catalyzed reaction. The UV absorbance at 280 nm of the product indicated that it contains aromatic groups. This suggests that the product is a lignin fragment derived from MBW. Sulfonated polystyrene whose molecular weight is 894 appeared at 14.2 min in the same SEC experiment, while guaiacol whose molecular weight is 124 did at 21.0 min. This indicates that the molecular weights of products corresponding

to B_19 are between 124 and 894. These results indicate that both MnP and LiP successfully catalyzed the depolymerization of MBW in the batch bioreactor and produced a water-soluble lignin fragment.

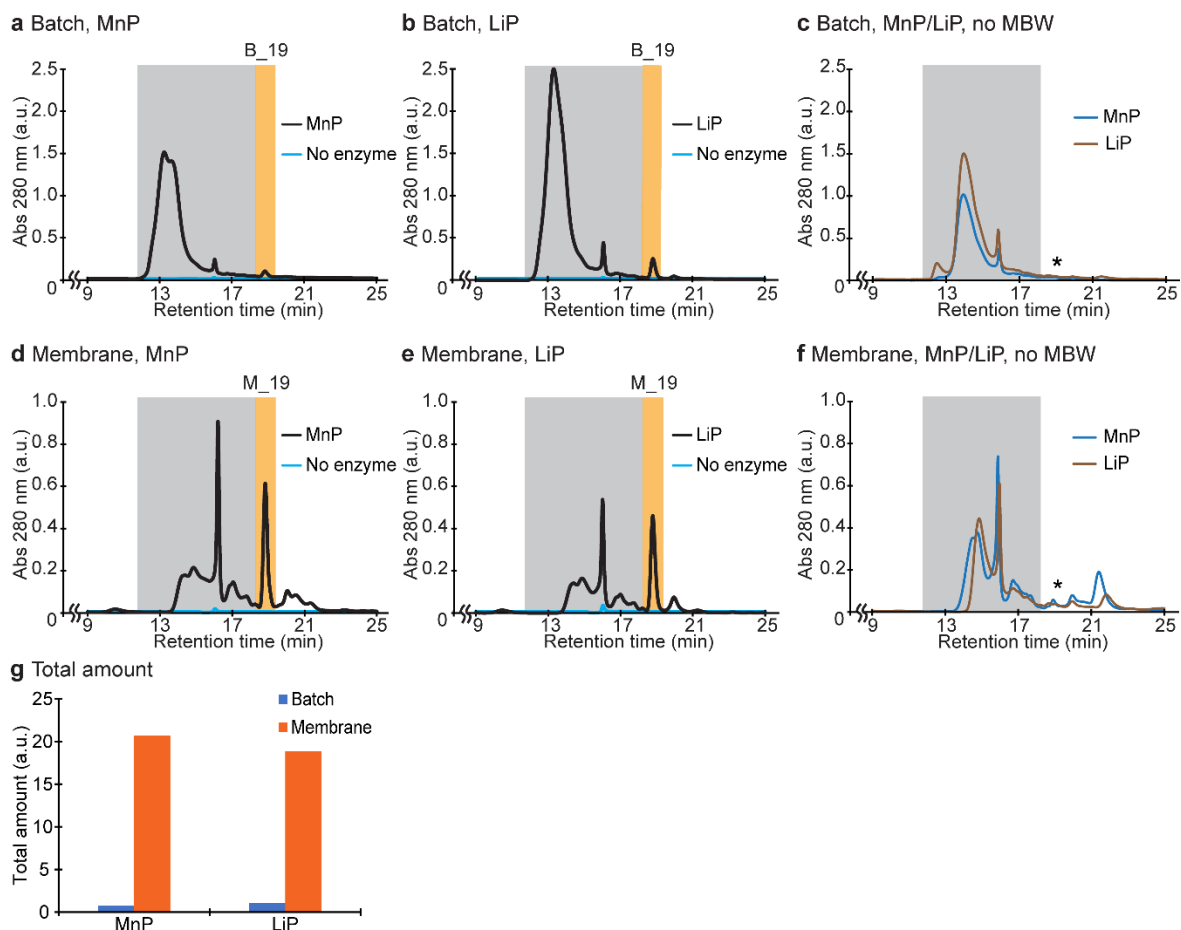


Figure 3.2. SEC analyses of the reaction products released into the aqueous phase of milled beech wood (MBW) treated with peroxidases in batch and membrane bioreactors. (a-c) The SEC profiles for the reaction products released into the aqueous phase for the batch bioreactor. MBW was reacted with either MnP (a) or LiP (b) for 8 h. The cyan lines in (a) and (b) are controls; MBW was incubated without an enzyme for 8 h. Either MnP or LiP was also incubated without MBW for 8 h (c), which is also a control. (d-f) The SEC profiles for the reaction products released into the aqueous phase for the membrane bioreactor. MBW was reacted with either MnP (d) or LiP (e), and for each of them, the SEC profile of the filtrate collected after 1 hour is shown. The cyan lines

in (d) and (e) are controls; MBW incubated without an enzyme and filtrate was collected after 1 h. Either MnP or LiP was incubated without MBW and the filtrates were collected after 1 h (f), which were also controls. The major peak at 18.8 min is highlighted in orange. The asterisks in (c) and (f) denote the position of B_19 and M_19, respectively. Peaks highlighted in gray are not of interest as they were also detected for the control sample without MBW. (g) The total amounts for B_19 and M_19 estimated according to Eqs. (3.1) and (3.2).

For the membrane bioreactor, the filtrate, which passed through the 3000 MWCO membrane during the depolymerization of MBW by either MnP or LiP, was collected every one-hour. The filtrate obtained after the first one-hour for either MnP (Figure 3.2d, black line) or LiP (Figure 3.2e, black line) was analyzed by SEC. In both chromatograms, a product peak (denoted as M_19) was detected at 18.8 min. A corresponding peak was not detected for the control sample, which was obtained by performing the experiment without either a peroxidase (Figure 3.2d and 3.2e, cyan line) or MBW (Figure 3.2f). M_19 was also detected in the filtrate fractions collected at following time points (Figure 3.3). It was noticed that the retention time of M_19 matched that of B_19 detected in the case of the batch bioreactor. These results confirmed that a water-soluble lignin fragment with a molecular weight between 124 and 894 was also produced in the membrane bioreactor. This indicated that the water-soluble lignin fragment could be separated from the reaction system through the RC membrane over the course of the reaction. As the intensity of M_19 peak decreased monotonically over the incubation time (Figure 3.3), the reaction was suggested to occur mainly at an early stage of incubation.

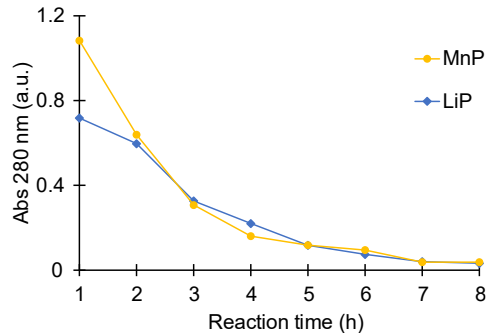


Figure 3.3. Evolution of product M₁₉ in the filtrate fraction during the incubation of MBW with either MnP (yellow line) or LiP (blue line) as analyzed by SEC.

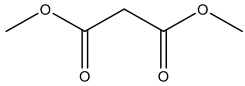
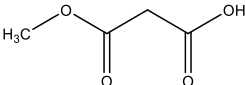
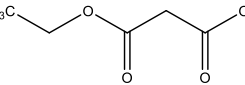
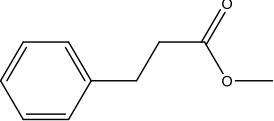
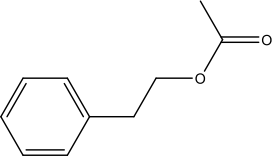
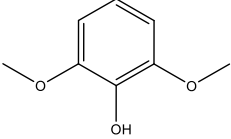
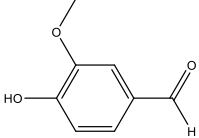
The total amounts of the products detected at 18.8 min were quantified on the basis of their absorbance at 280 nm. The total amount of products at 18.8 min for the batch bioreactor, $TA_{B_{19}}$, was deduced using Eq. (3.1). The total amount of products at 18.8 min for the membrane bioreactor, $TA_{M_{19}}$, was deduced using Eq. (3.2). As the molar extinction coefficient differs for each product, only a rough estimation of amounts of products can be obtained by this method. $TA_{M_{19}}$ reached 28-fold of $TA_{B_{19}}$ in the case of the MnP-catalyzed reaction (Figure 3.2g). Similarly, in the case of the LiP-catalyzed reaction, $TA_{M_{19}}$ reached 18-fold of $TA_{B_{19}}$ (Figure 3.2g). Thus, in the cases of both MnP and LiP, the ability to produce water-soluble lignin fragments from MBW was significantly enhanced by applying continuous product separation using the membrane bioreactor.

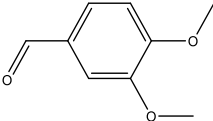
3.2.3 Identification of the depolymerized products in the filtrate

To identify the products obtained after the depolymerization of MBW catalyzed either by MnP or LiP, I performed a GCMS analysis. The depolymerized products in the filtrate fraction, M₁₉ (Figure 3.2d and 3.2e), were concentrated and analyzed. I employed a

similarity search approach by comparing the product spectrum with those available in the NIST mass spectra library, using a similarity index threshold of 80% or higher. The identified compounds are listed in Table 3.1.

Table 3.1. The main depolymerized products of beech wood lignin obtained in the filtrate fraction

No.	Structural formula	Name	Molecular formula	Involved enzyme
1		Propanedioic acid, dimethyl ester	C ₅ H ₈ O ₄	LiP
2		Monomethyl malonate	C ₄ H ₆ O ₄	LiP
3		Ethyl hydrogen malonate	C ₅ H ₈ O ₄	MnP LiP
4		Benzenepropanoic acid, methyl ester	C ₁₀ H ₁₂ O ₂	MnP LiP
5		Acetic acid, 2-phenylethyl ester	C ₁₀ H ₁₂ O ₂	MnP LiP
6		Syringol	C ₈ H ₁₀ O ₃	MnP
7		Vanillin	C ₈ H ₈ O ₃	MnP LiP

8		Veratryl aldehyde	C ₉ H ₁₀ O ₃	LiP
---	---	-------------------	---	-----

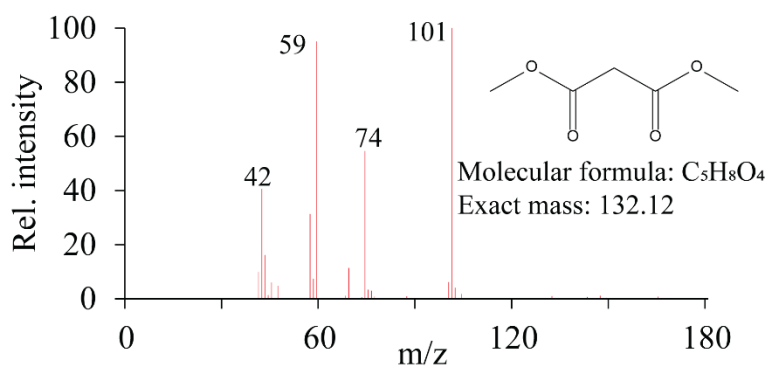
For MnP-catalyzed depolymerization of MBW, an aliphatic compound (No. 3) and several aromatic compounds (No. 4-7) were identified. MnP-catalyzed reaction produced aromatic products like syringol and vanillin, which were subsequently isolated from the reaction vessel through the membrane.

For LiP-catalyzed depolymerization of MBW, a variety of aliphatic (No. 1-3) and aromatic (No. 4-5 and 7-8) compounds were identified. The products such as vanillin and veratryl aldehyde were produced from the LiP-catalyzed reaction and isolated from the reaction vessel.

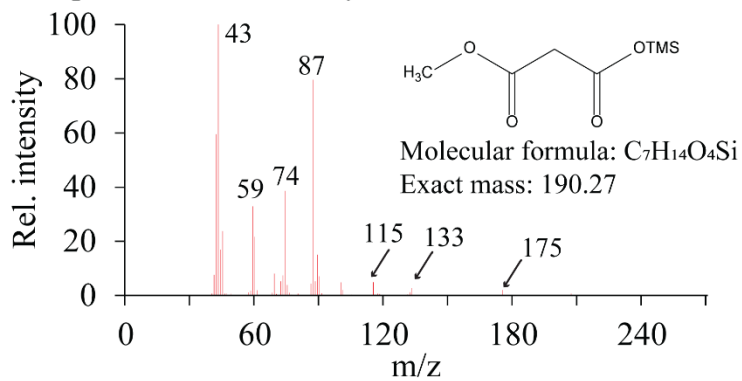
It is worth nothing that syringol was obtained only for MnP-catalyzed depolymerization of MBW, whereas veratryl aldehyde was obtained only for LiP-catalyzed depolymerization of MBW.

Furthermore, methylated compounds like No. 4, 5, 7, and 8 were observed. Such methylated compounds have been reported in a study by Zhang *et al.*, where methyl vanillate, methyl 3-(3,5-di-tert-butyl-4-hydroxyphenyl)propionate, and veratryl alcohol were formed from the enzymatic hydrolysis of corn stover lignin using laccase, MnP and LiP.³⁶

Compound 1: Propanedioic acid, dimethyl ester



Compound 2: Monomethyl malonate



Compound 3: Ethyl hydrogen malonate

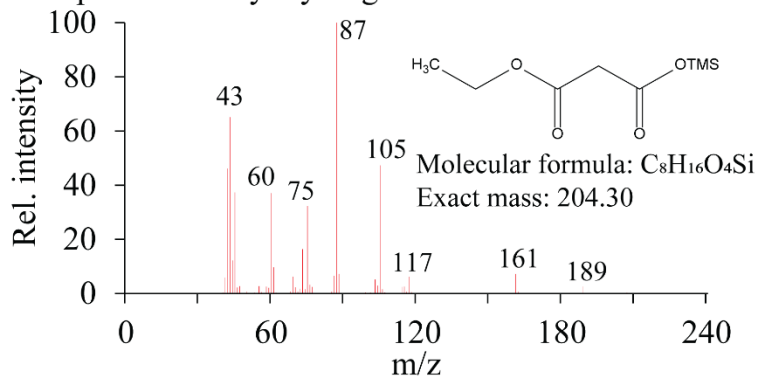


Figure 3.4 The EI mass spectra of the main depolymerized products of beech wood lignin obtained in the filtrate fraction.

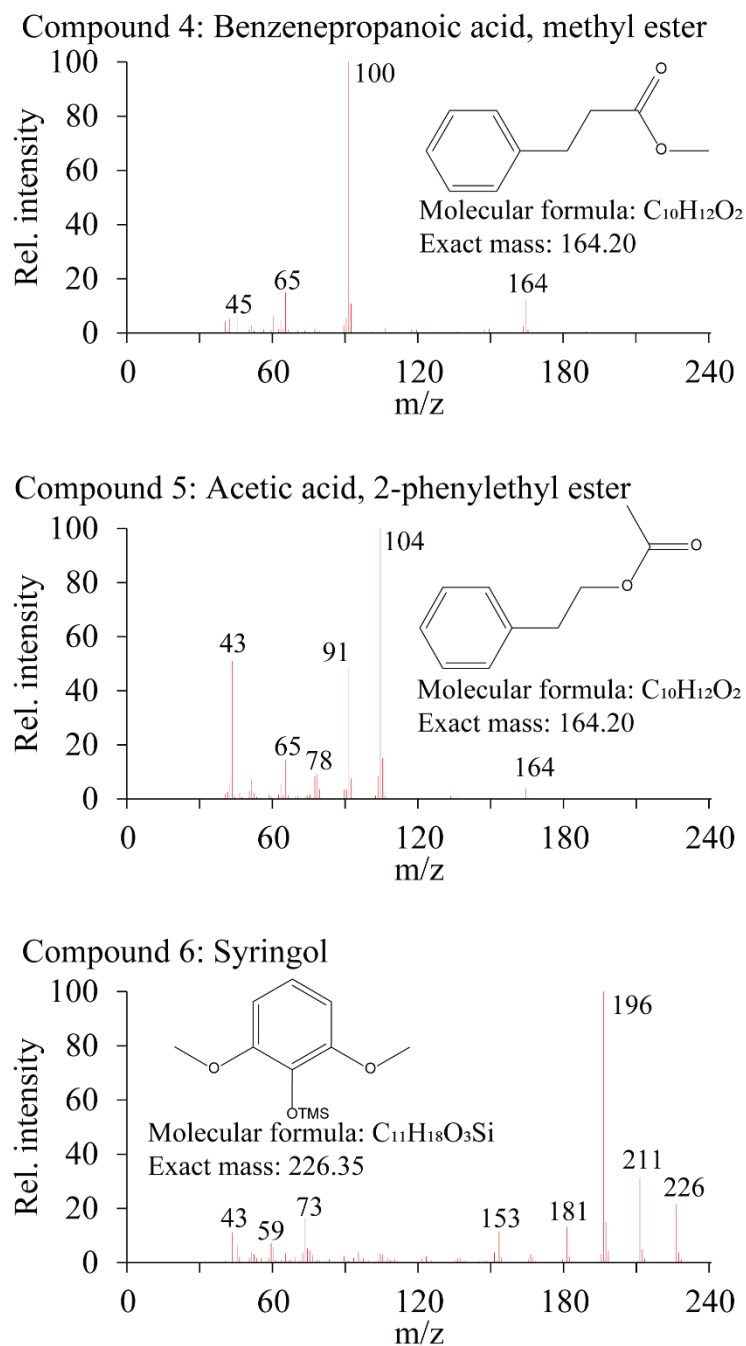


Figure 3.5 The EI mass spectra of the main depolymerized products of beech wood lignin obtained in the filtrate fraction.

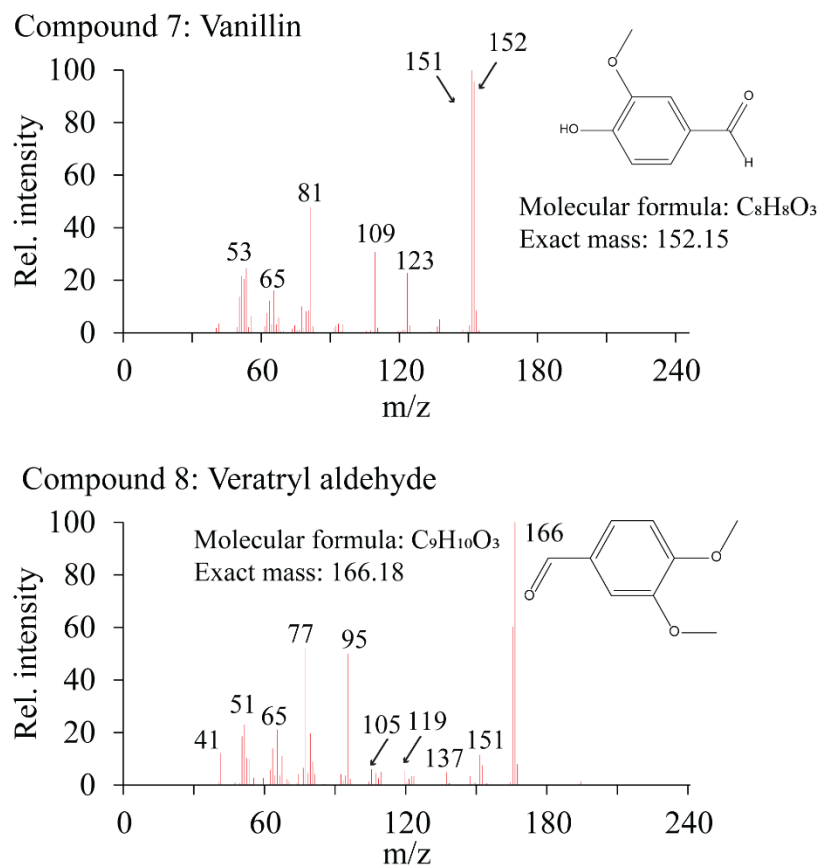


Figure 3.6 The EI mass spectra of the main depolymerized products of beech wood lignin obtained in the filtrate fraction.

3.2.4 Lignin removal from MBW through the peroxidase-catalyzed reaction

As the release of water-soluble lignin fragments through the peroxidase-catalyzed reaction in the batch and membrane bioreactors was confirmed, I next calculated the percentages of lignin (LP) in the solid residues (RES) in the reaction vessels for the batch and membrane bioreactors, RES_{batch} and RES_{membrane}, respectively. Here, the LPs of RES_{batch} and RES_{membrane} were quantified by a conventional Klason lignin method and a recently reported UV-Vis spectroscopic method (Table 3.2 and Table 3.3).³⁷ Firstly, the LP of MBW before the reaction was found to be 24.5 ± 0.4 and $26.9 \pm 0.3\%$ by the Klason lignin

and UV-Vis spectroscopic methods, respectively. In the case of the batch bioreactor, the LP of RES_{batch} obtained for MnP (RES_{batch}^{MnP}) decreased to $21.4 \pm 0.6\%$ ($22.3 \pm 0.7\%$) according to the Klason lignin method (UV-Vis spectroscopic method). The change in LP relative to MBW was calculated using Eq. (3.4) as being $-12.6 \pm 0.6\%$ ($-17.3 \pm 1.7\%$) (Table 3.3 and Figure 3.7). On the other hand, the LP of RES_{batch} obtained for LiP (RES_{batch}^{LiP}) decreased to $19.8 \pm 0.3\%$ ($19.4 \pm 0.9\%$) according to the Klason lignin method (UV-Vis spectroscopic method). The change in LP correspond to $-19.2 \pm 0.8\%$ ($-27.7 \pm 2.5\%$). On the contrary, the LP of RES_{batch} of a control sample that was obtained for the experiment without a peroxidase ($RES_{batch}^{No\ enzyme}$) was much closer to the LP of MBW; the change in LP was $-6.9 \pm 0.8\%$ ($-0.4 \pm 1.0\%$) according to the Klason lignin method (UV-Vis spectroscopic method). This indicates that the decreases of the LP of RES_{batch}^{MnP} and RES_{batch}^{LiP} were achieved through the catalytic activities of MnP and LiP. This indicates that both MnP and LiP could catalyze the lignin removal from MBW even in the batch bioreactor to some extent.

Table 3.2. Chemical composition of solid residues based on Klason lignin analysis

Sample	Recoveries ^a (%)	Cellulose (%)	Hemicellulose (%)	Lignin content (%)
MBW	-	36.4 ± 1.6	31.7 ± 2.3	24.5 ± 0.4
Batch bioreactor				
No enzyme	96.5	36.1 ± 1.9	31.4 ± 1.5	22.8 ± 0.4
MnP	92.5	36.7 ± 1.0	31.9 ± 0.8	21.4 ± 0.6
LiP	92.9	36.5 ± 2.2	31.7 ± 1.2	19.8 ± 0.3
Membrane bioreactor				
No enzyme	96.1	36.2 ± 1.7	31.6 ± 0.4	22.9 ± 0.2
MnP	89.6	37.8 ± 1.4	31.5 ± 0.9	16.9 ± 0.6
LiP	88.3	38.6 ± 0.6	32.1 ± 2.1	14.3 ± 0.5

^aRecoveries (%) of the residues after the reaction relative to the starting material.

Table 3.3. Quantification of lignin in solid residues (RES)^a

Sample	Klason lignin (%)	UV-vis spectroscopy lignin (%)	Change in LP (%) ^b	
			Klason lignin	UV-vis lignin
MBW	24.5 ± 0.4	26.9 ± 0.3	-	-
Batch bioreactor				
No enzyme	22.8 ± 0.4	26.8 ± 0.3	-6.9 ± 0.8	-0.4 ± 1.0
MnP	21.4 ± 0.6	22.3 ± 0.7	-12.6 ± 0.9	-17.3 ± 1.7
LiP	19.8 ± 0.3	19.4 ± 0.9	-19.2 ± 0.8	-27.7 ± 2.5
Membrane bioreactor				
No enzyme	22.9 ± 0.2	26.8 ± 0.3	-6.6 ± 0.8	-0.1 ± 2.1
MnP	16.9 ± 0.6	16.2 ± 0.5	-31.1 ± 2.4	-39.7 ± 1.7
LiP	14.3 ± 0.5	14.2 ± 1.0	-41.5 ± 1.9	-46.7 ± 3.4

^aMeans ± SD (standard deviation) were obtained from technical duplicates. ^bChange in percentage of lignin (LP) was calculated according to Eq. (3.4).

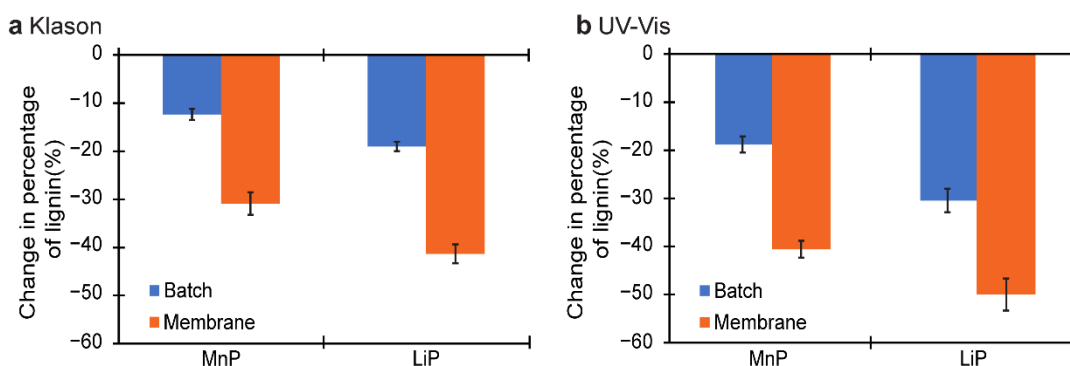


Figure 3.7. The change in percentage of lignin (LP) of MBW achieved through peroxidase treatment in the batch and membrane bioreactors. (a and b) The change in LP achieved through the MnP and LiP treatments, which was calculated using Eq. (3.4), based on the LP of the initial MBW and the LP after the treatment with a peroxidase. The LP was determined by the Klason lignin (a) and UV-Vis spectroscopy (b) methods.

In the case of the membrane bioreactor, the LP of RES_{membrane} obtained for MnP ($RES_{\text{membrane}}^{\text{MnP}}$) was $16.9 \pm 0.6\%$ ($16.2 \pm 0.5\%$) according to the Klason lignin method (UV-Vis spectroscopic method); the change in LP corresponds to $-31.1 \pm 2.4\%$ ($-39.7 \pm 1.7\%$). A

comparison of the decrease in LP obtained for the batch bioreactor and membrane bioreactors showed that the latter is 2.5-fold (2.3-fold) more effective for MnP.

Meanwhile, the LP of RES_{membrane} obtained for LiP ($RES_{\text{membrane}}^{\text{LiP}}$) was $14.3 \pm 0.5\%$ ($14.2 \pm 1.0\%$) according to the Klason lignin method (UV-Vis spectroscopic method); the change in LP corresponds to $-41.5 \pm 1.9\%$ ($-46.7 \pm 3.4\%$). A comparison of the decrease in LP obtained for the batch and membrane bioreactors showed that the latter is 2.2-fold (1.7-fold) more effective for LiP. Therefore, the lignin removal from MBW catalyzed by both MnP and LiP using the membrane bioreactor significantly outperformed that with the batch bioreactor. Notably, the lignin removal was higher in the reaction catalyzed by LiP than that by MnP in both bioreactors.

3.2.5 Molecular weight distribution of lignin in the solid residues

Next, the distribution of the molecular weights of lignin contained in the solid fraction was investigated by SEC analysis. Firstly, cellulolytic enzyme lignin (CEL) was isolated through enzymatic digestion of polysaccharides from untreated MBW, $RES_{\text{batch}}^{\text{MnP}}$, $RES_{\text{batch}}^{\text{LiP}}$, $RES_{\text{membrane}}^{\text{MnP}}$, and $RES_{\text{membrane}}^{\text{LiP}}$, individually. Then the obtained CELs were acetylated. The molecular weight distribution of the acetylated CEL of MBW appeared to be bimodal (Figure 3.8, cyan line). Similarly, the molecular weight distribution of the acetylated CELs of both $RES_{\text{batch}}^{\text{MnP}}$ and $RES_{\text{batch}}^{\text{LiP}}$ was also bimodal (Figure 3.8, orange line). Therefore, I drew a line at a retention time corresponding to the molecular weight of 1000 in Figure 3.8 (dotted line), and defined the fractions larger and smaller than 1000 as the high molecular weight lignin (HML) and low molecular weight lignin (LML), respectively. The relative amount, or

proportion, of HML and LML was estimated from the peak area of each fraction (Table 3.4). The proportion of HML in MBW was 88.2%. The proportions of HML for RES_{batch}^{MnP} and RES_{batch}^{LiP} turned out to be decreased to 68.0 and 74.3%, respectively. This is equivalent to the increases in the proportions of LML for RES_{batch}^{MnP} and RES_{batch}^{LiP} to 32.0 and 25.7%, respectively, from 11.8% for MBW. Such changes in the proportions of HML and LML were not observed for $RES_{batch}^{No\ enzyme}$, for which MBW was similarly incubated in the batch bioreactor without a peroxidase. Therefore, the peroxidase-catalyzed reaction led to a shift of the molecular-weight distribution from HML to LML, which indicates the depolymerization of HML had proceeded through a peroxidase-catalyzed reaction. Next, the weight-average molecular weight (M_w) of each fraction was calculated. The M_w of HML for RES_{batch}^{MnP} and RES_{batch}^{LiP} decreased to 7968 and 8501 $g\ mol^{-1}$, respectively, from 11336 $g\ mol^{-1}$ for MBW, which also indicates the depolymerization of HML had proceeded through a peroxidase-catalyzed reaction. On the other hand, the M_w of LML was not drastically different before and after the reaction. The M_w of LML of around 230 $g\ mol^{-1}$ is in the range of the molecular weights of monomeric and dimeric lignin units. Overall, both MnP and LiP were demonstrated to catalyze the lignin depolymerization in MBW even in the batch bioreactor.

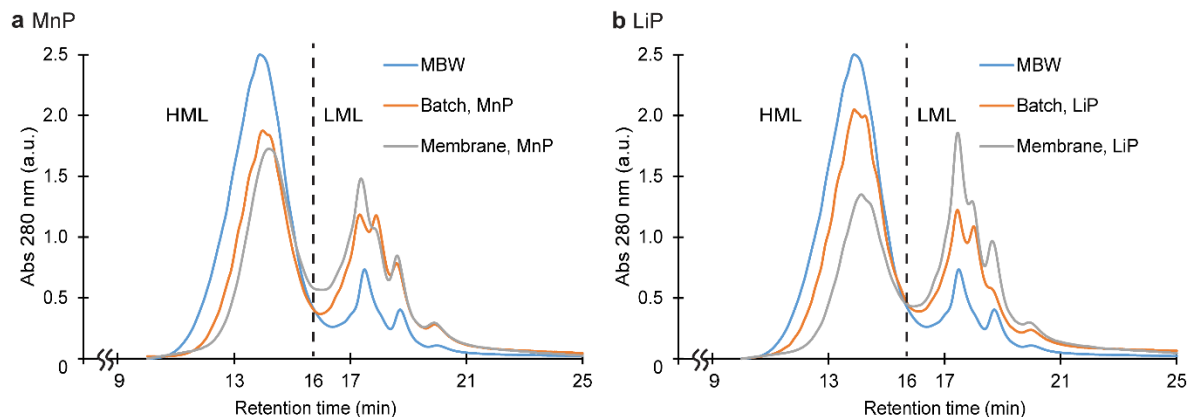


Figure 3.8. Molecular weight distributions of lignin in the solid residue (RES) after peroxidase treatment of MBW. (a) SEC profiles of the acetylated cellulolytic enzyme lignin (CEL) extracted from the RES after treatment with MnP in batch (RES_{batch}^{MnP} , orange line) and membrane ($RES_{membrane}^{MnP}$, gray line) bioreactors. (b) SEC profiles of the acetylated CEL extracted from the RES after treatment with LiP in the batch (RES_{batch}^{LiP} , orange line) and membrane ($RES_{membrane}^{LiP}$, gray line) bioreactors. SEC profiles of the acetylated CEL extracted from the initial MBW supplied to the bioreactors are presented in (a) and (b) (blue line). The high molecular weight lignin (HML) and low molecular weight lignin (LML) fractions are defined as lignin with molecular weights greater and lower than 1000 (elution time at 16 min, dotted line), respectively.

Table 3.4. Molecular weight analysis of HML and LML fractions based on SEC of acetylated CEL obtained from solid residues (RES) of MBW

Sample	Fraction	%	M_w (g mol ⁻¹)	M_n (g mol ⁻¹)	PDI (M_w/M_n)
MBW	HML	88.2	11336	5497	2.1
	LML	11.8	224	151	1.5
Batch bioreactor					
No enzyme	HML	90.7	11090	5466	2.0
	LML	9.3	213	153	1.4
MnP	HML	68.0	7968	5059	1.6
	LML	32.0	243	172	1.4
LiP	HML	74.3	8501	5102	1.7
	LML	25.7	232	174	1.3
Membrane bioreactor					
No enzyme	HML	89.8	11890	5922	2.0
	LML	10.2	218	153	1.4
MnP	HML	62.6	6155	4416	1.4
	LML	37.4	255	182	1.4
LiP	HML	49.0	6313	4518	1.4
	LML	51.0	235	169	1.4

Likewise, a bimodal-shaped molecular weight distribution was also observed in the case of the membrane bioreactor (Figure 3.8, gray line). The proportions of HML for $RES_{\text{membrane}}^{\text{MnP}}$ and $RES_{\text{membrane}}^{\text{LiP}}$ turned out to be decreased to 62.6 and 49.0%, respectively, from 88.2% for MBW. This is equivalent to the increases in the proportions of LML for $RES_{\text{membrane}}^{\text{MnP}}$ and $RES_{\text{membrane}}^{\text{LiP}}$ to 37.4 and 51.0%, respectively, from 11.8% for MBW. Additionally, the M_w of HML for $RES_{\text{batch}}^{\text{MnP}}$ and $RES_{\text{batch}}^{\text{LiP}}$ decreased to 6155 and 6313 g mol⁻¹, respectively, from 11336 g mol⁻¹ for MBW. It is apparent that the decreases in the

proportion and M_w of HML were more drastic for the membrane bioreactor than for the batch bioreactor.

3.2.6 Analysis of lignin substructures in the solid residues by NMR spectroscopy

To obtain chemical and structural insights into lignin contained in untreated MBW, RES_{batch}^{MnP} , RES_{batch}^{LiP} , $RES_{membrane}^{MnP}$, and $RES_{membrane}^{LiP}$, I performed gel-state 2D 1H - ^{13}C heteronuclear single-quantum coherence (HSQC) analysis (Figures 3.9 and 3.10). In the spectrum of $RES_{batch}^{No\ enzyme}$, typical signals of S-, G-, and α -oxidized S (S'-) units were detected in the aromatic region (Figure 3.9a, upper panel). Meanwhile, typical signals of lignin interunit linkages, β -O-4', β - β' , and β -5', and polysaccharide signals were detected in the aliphatic region (Figure 3.9a, lower panel). No new peak was observed in the spectrum of either RES_{batch}^{MnP} (Figure 3.9b) or RES_{batch}^{LiP} (Figure 3.9c) when compared with the spectrum of $RES_{batch}^{No\ enzyme}$ (Figure 3.9a). This suggests that there is no notable structural modification of either lignin or polysaccharide in the solid residues caused by the peroxidase-catalyzed reaction.

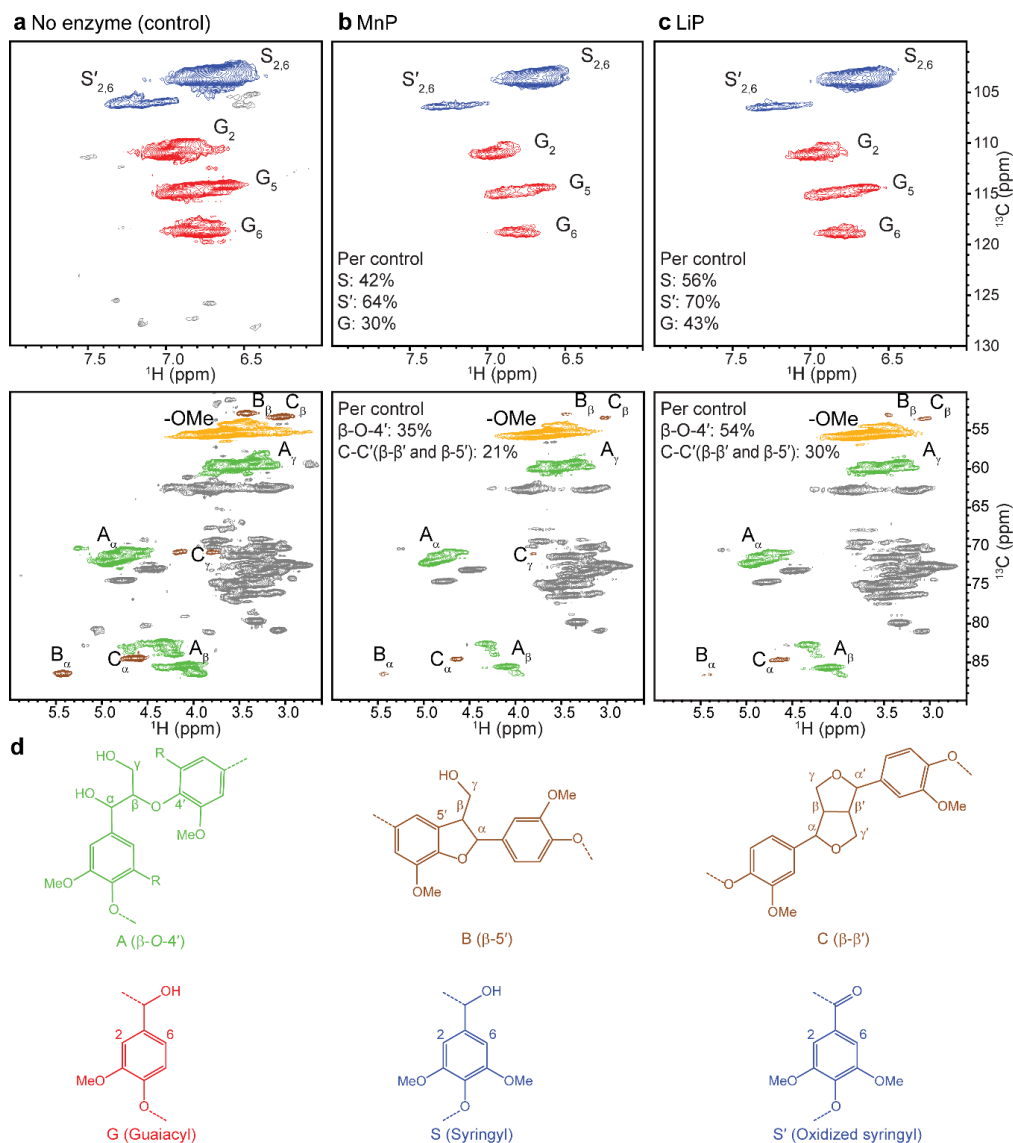


Figure 3.9. NMR analysis of RES after the peroxidase treatment in the batch bioreactor. (a-c) 2D ^1H - ^{13}C HSQC spectra of the RES obtained after the treatment of MBW with the batch bioreactor in three different solution conditions; no enzyme (a), and with either MnP (b) or LiP (c). The upper and lower panels in (a-c) are the aliphatic and aromatic regions of each HSQC spectrum, respectively. (d) The main lignin substructures identified in HSQC spectra, which are color-coded as for the spectra. Gray signals represent unassigned signals, which mainly originated from polysaccharides. A complete list of the identified substructures can be found in Table 3.5. Relative amounts of lignin substructures (S, G, S', β -O-4' and C-C') in RES obtained after treatment with MnP (a) and LiP (b) relative to RES treated without an enzyme determined by Eq. (3.7).

Table 3.5. Assignment of the lignin ^1H - ^{13}C correlation signals of the HSQC NMR spectrum

Label	$\delta_{\text{C}}/\delta_{\text{H}}$ (ppm/ppm)	Assignment
B $_{\beta}$	53.3/3.46	C $_{\beta}$ -H $_{\beta}$ in phenylcoumaran substructures
C $_{\beta}$	53.5/3.06	C $_{\beta}$ -H $_{\beta}$ in resinol substructures
-OMe	55.6/3.73	C-H in methoxy groups
A $_{\gamma}$	59.5-59.7/3.4-3.7	C $_{\gamma}$ -H $_{\gamma}$ in β -O-4' substructures
B $_{\gamma}$	62.6/3.73	C $_{\gamma}$ -H $_{\gamma}$ in phenylcoumaran substructures
A $_{\alpha}$ (G)	70.9/4.71	C $_{\alpha}$ -H $_{\alpha}$ in β -O-4' substructures linked to a guaiacyl unit
C $_{\gamma}$	71.0/3.79 and 4.16	C $_{\gamma}$ -H $_{\gamma}$ in resinol substructures
A $_{\alpha}$ (S)	71.8/4.81	C $_{\alpha}$ -H $_{\alpha}$ in β -O-4' substructures linked to a syringyl unit
A $_{\beta}$ (G)	83.5/4.27	C $_{\beta}$ -H $_{\beta}$ in β -O-4' substructures linked to a guaiacyl unit
C $_{\alpha}$	84.9/4.64	C $_{\alpha}$ -H $_{\alpha}$ in resinol substructures
A $_{\beta}$ (S)	85.9/4.09 and 86.9/3.97	C $_{\beta}$ -H $_{\beta}$ in β -O-4' substructures linked to a syringyl unit
B $_{\alpha}$	86.8/5.46	C $_{\alpha}$ -H $_{\alpha}$ in phenylcoumaran substructures
S $_{2,6}$	103.8/6.71	C $_{2,6}$ -H $_{2,6}$ in syringyl unit
S' $_{2,6}$	106.2/7.23 and 7.07	C $_{2,6}$ -H $_{2,6}$ in C $_{\alpha}$ -oxidized syringyl unit
G $_2$	110.9/6.98	C $_2$ -H $_2$ in guaiacyl unit
G $_5$	114.9/6.77	C $_5$ -H $_5$ in guaiacyl unit
G $_6$	119.0/6.80	C $_6$ -H $_6$ in guaiacyl unit

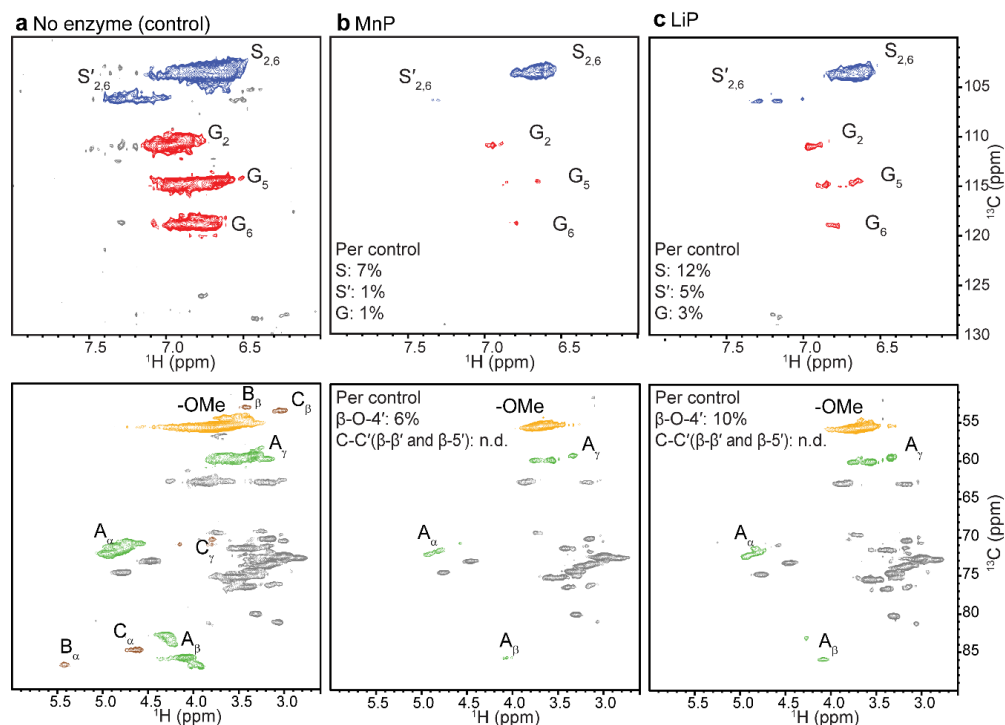


Figure 3.10. NMR analysis of RES after the peroxidase treatment in the membrane bioreactor. 2D ^1H - ^{13}C HSQC spectra of the RES obtained after the treatment of MBW with the membrane bioreactor in three different solution conditions; no enzyme (a), and with either MnP (b) or LiP (c). The upper and lower panels in (a-c) are the aliphatic and aromatic regions of each HSQC spectrum, respectively. Gray signals represent unassigned signals, which mainly originated from polysaccharides. Relative amounts of lignin substructures (S, G, S', β -O-4' and C-C') in RES obtained after treatment with MnP (a) and LiP (b) relative to RES treated without an enzyme determined by Eq. (3.7).

The contents of β -O-4', β - β' , and β -5' interunit linkages were estimated from the volume of their C_α - H_α correlations in the aliphatic region (β -O-4' from A_α ; β - β' from C_α ; β -5' from B_α). Then, I expressed the amount of each interunit linkage as a fraction of the total lignin interunit linkages with reference to literatures (Table 3.6).³⁸⁻³⁹

Table 3.6. Lignin interunit linkages from integration of ^1H - ^{13}C correlation peaks in the HSQC spectra of the residues after enzymatic reaction in batch and membrane bioreactor^a

	Batch bioreactor			Membrane bioreactor		
	No enzyme	MnP	LiP	No enzyme	MnP	LiP
Interunit linkages (%)^b						
β -O-4' (A)	87.5	91.1	91.5	89.3	100.0	100.0
β -5' (B)	4.1	3.2	2.5	3.2	nd	nd
β - β' (C)	8.4	5.7	6.0	7.5	nd	nd

^aThe volume of each signal was normalized as to the signal volume of DSS-d₆. ^bExpressed as a percentage of the total lignin interunit linkage types A-C. ^cnd = not detected

Next, relative amounts of lignin substructures (S-, G-, and S'-units, β -O-4' and some of the C-C' interunit linkages, C-C' (β - β' and β -5')) upon peroxidase-catalyzed reaction were estimated based on Eq. (3.7) (Figure 3.11). In the case of $\text{RES}_{\text{batch}}^{\text{MnP}}$, the quantities of S-, G-, and S'- units decreased to 42, 30, and 64%, respectively, of those for $\text{RES}_{\text{batch}}^{\text{No enzyme}}$ (Figure 3.11). The quantities of β -O-4' and C-C' interunit linkages decreased to 35 and 21%, respectively, of those for $\text{RES}_{\text{batch}}^{\text{No enzyme}}$ (Figure 3.11). Likewise, in the case of $\text{RES}_{\text{batch}}^{\text{LiP}}$, the quantities of S-, G-, and S'- units decreased to 56, 43, and 70%, respectively (Figure 3.11). The quantities of β -O-4' and C-C' interunit linkages decreased to 54 and 30%, respectively (Figure 3.11). The decreases in the relative amounts of lignin substructures were suggested to be the result of lignin removal from MBW achieved due to the peroxidase-catalyzed reaction in the batch bioreactor.

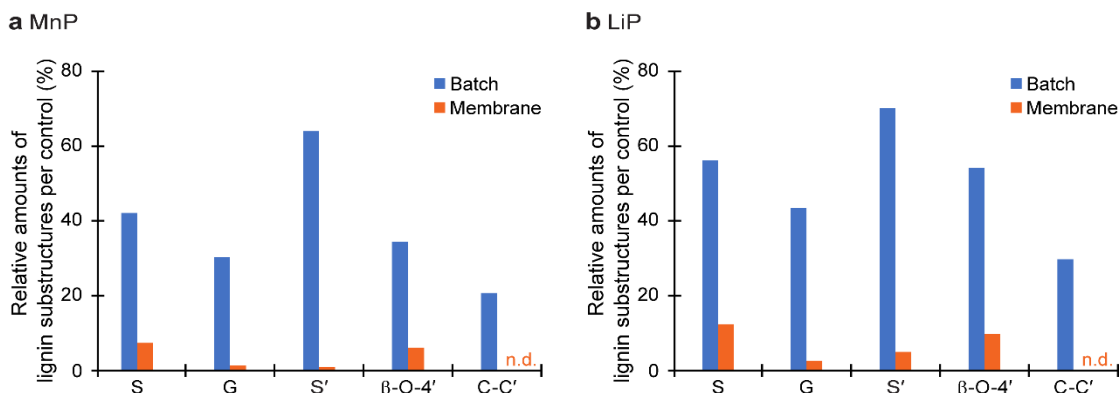


Figure 3.11. Semi-quantitative analysis of the lignin substructures on the basis of 2D ^1H - ^{13}C HSQC experiments. (a and b) Relative amounts of lignin substructures (S, G, S', β -O-4' and C-C') in RES obtained after treatment with MnP (a) and LiP (b) relative to RES treated without an enzyme determined by Eq. (3.7). The relative amount was determined based on the volume integrals of the HSQC correlation peaks. The amounts of β -O-4' and C-C' (β - β' and β -5') interunit linkages were estimated on the basis of the volume of the C_α - H_α correlation. The amounts of S- and S'-units were estimated from the half values of the volumes of the $\text{C}_{2,6}$ - $\text{H}_{2,6}$ correlation, whereas that of the G-unit was estimated from the volume of the C_2 - H_2 correlation. n.d.; not detected.

I then analyzed the spectra of $\text{RES}_{\text{membrane}}$. No new peak was observed in the spectrum of either $\text{RES}_{\text{membrane}}^{\text{MnP}}$ (Figure 3.10b) or $\text{RES}_{\text{membrane}}^{\text{LiP}}$ (Figure 3.10c) when compared with the spectrum of $\text{RES}_{\text{membrane}}^{\text{No enzyme}}$ (Figure 3.10a). Therefore, as was the case in the batch bioreactor, notable structural modification was not observed for either lignin or polysaccharide in the solid fractions.

As for the relative amounts of lignin substructures, the S-, G-, and S'- units for $\text{RES}_{\text{membrane}}^{\text{MnP}}$ decreased to 7, 1, and 1%, respectively, of those for $\text{RES}_{\text{membrane}}^{\text{No enzyme}}$ (Figure 3.11). Whereas, the quantity of the β -O-4' interunit linkage decreased to 6% of that for $\text{RES}_{\text{membrane}}^{\text{No enzyme}}$, and those of C-C' interunit linkages were less than the detection limit (Figure 3.11). In the case of $\text{RES}_{\text{membrane}}^{\text{LiP}}$, the quantities of the S-, G-, and S'- units decreased to 12, 3, and 5%, respectively (Figure 3.11). Whereas, the quantity of the β -O-4' interunit linkage

decreased to 10% and those of C-C' interunit linkages were less than the detection limit (Figure 3.11). Overall, for both MnP and LiP, the reduction in the relative amounts of lignin substructures was much more pronounced for the membrane bioreactor than for the batch bioreactor, which may reflect the higher extent of lignin removal in the case of the membrane bioreactor.

3.2.7 Enzymatic hydrolysis of solid residues

To assess the hydrolysis efficiency following MnP- and LiP-catalyzed lignin depolymerization of MBW, I performed an enzymatic hydrolysis experiment using a commercial cellulase cocktail (CellicCtec2) and quantified the total reducing sugar content produced from the hydrolysis reaction.

For untreated MBW, the measured total reducing sugar content was 0.78 mg mL^{-1} (Figure 3.12). In the batch bioreactor, the production of reducing sugar increased to 1.17 mg mL^{-1} for $\text{RES}_{\text{batch}}^{\text{MnP}}$ and 1.36 mg mL^{-1} for $\text{RES}_{\text{batch}}^{\text{LiP}}$ (Figure 3.12). These results demonstrate that lignin depolymerization by MnP and LiP in the batch bioreactor improved the hydrolysis efficiency of carbohydrates in the residue compared to untreated MBW.

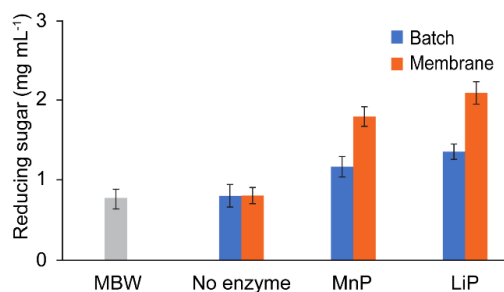


Figure 3.12. The reducing sugar released from the hydrolysis of MBW and RES obtained from batch and membrane bioreactors. Error bars show the standard deviation of three replicates.

In the membrane bioreactor, the production of reducing sugar further increased to 1.80 mg mL^{-1} for $\text{RES}_{\text{membrane}}^{\text{MnP}}$ and 2.11 mg mL^{-1} for $\text{RES}_{\text{membrane}}^{\text{LiP}}$ (Figure 3.12).

This finding suggests that lignin depolymerization by MnP and LiP in the membrane bioreactor resulted in additional enhancements in hydrolysis efficiency for the carbohydrates in the residue, surpassing both untreated MBW and the batch bioreactor.

3.3 Discussions

For the enzymatic depolymerization of grass lignin using laccase, accumulation of water-soluble lignin upon the reaction was reported by Hilgers *et al.*¹⁶ Similar to that report, in the present study, water-soluble lignin fragments were also detected in the aqueous phase after the MnP- and LiP-catalyzed reactions in the batch bioreactor (Figures. 3.2a and 3.2b). Therefore, both MnP and LiP used in this study successfully catalyzed the lignin depolymerization to produce water-soluble lignin fragments. However, such lignin fragments produced through enzymatic depolymerization are reportedly highly reactive and hence undergo a series of complex reactions, which leads to either further depolymerization of lignin chains, or radical recoupling resulting in lignin repolymerization.⁴⁰⁻⁴² Thereby, the yield of the lignin fragments in the batch bioreactor was supposed to be highly dependent on the balance between depolymerization and repolymerization. To overcome this problem, I used the membrane bioreactor to continuously isolate the reactive lignin fragments to enhance the lignin depolymerization efficiency. As expected, the total amounts of water-soluble lignin fragments significantly increased with the membrane bioreactor, 28-fold for

MnP and 18-fold for LiP, respectively (Figure 3.2g), indicating that the isolation of lignin fragments could increase the efficiency of lignin depolymerization.

The GCMS analysis on M₁₉ in the filtrate fractions revealed the presence of depolymerized products produced by either MnP- or LiP-catalyzed depolymerization of MBW, which were subsequently isolated from the reaction vessel through the membrane (Table 3.1). Among the products, monomeric aromatic compounds such as syringol and vanillin have various industrial applications. This makes the continuous isolation of these fine chemicals from the reaction vessel through the membrane desirable especially for large-scale biocatalytic lignin depolymerization process. However, it should be noted that the use of a membrane bioreactor is associated with lower concentrations of the targeted products due to the larger reaction volumes involved. Although I successfully detected the presence of these fine chemicals using a high-sensitivity GCMS system, it was still necessary to concentrate M₁₉ for accurate GCMS analysis. Therefore, further research is necessary to develop a more cost-effective method for the efficient separation and purification of these products, ultimately enhancing their overall yield.

The quantification of lignin in RES showed a decrease in LP of MBW due to MnP- and LiP-catalyzed reactions. A higher degree of lignin removal was achieved in the membrane bioreactor relative to in the batch bioreactor for both MnP and LiP (Figure 3.7 and Table 3.3). These results suggested that the aforementioned higher production of water-soluble lignin fragments in the membrane bioreactor led to the greater lignin removal from MBW. Additionally, the quantification of lignin in RES indicated a significant improvement in the efficiency of lignin depolymerization achieved by the membrane bioreactor.

Upon the MnP- and LiP-catalyzed reactions, a reduction in the HML proportion for RES was observed (Figure 3.8 and Table 3.4). This finding suggests the depolymerization of HML by both MnP and LiP. The reduction was more significant for the membrane bioreactor than for the batch bioreactor. These observations further supported that the efficiency of lignin depolymerization was highly improved by the membrane bioreactor.

Compared to untreated MBW, the increase in the amounts of reducing sugar produced from MBW after treatment with MnP and LiP in both batch and membrane bioreactors indicates the positive effect of reduced lignin content in the sample on enhancing the hydrolysis efficiency of lignocellulosic biomass. Notably, the hydrolysis efficiency of sample obtained from the membrane bioreactor is higher than those from the batch bioreactor. This observation aligns with findings from a previous study, where the improved hydrolysis yield was attributed to the enhanced accessibility of carbohydrates to the hydrolytic enzymes.⁴³ These results underscore the possible application of RES obtained after treatment with MnP and LiP, particularly for membrane bioreactor, as a promising approach for efficient lignocellulosic biomass hydrolysis.

In this study, my primary objective was to investigate the potential advantages of continuous separation of lignin fragments from the reaction medium using a membrane bioreactor, in comparison to a conventional batch bioreactor. Thus, I employed a lower biomass loading to ensure proper biomass dispersion in the reaction vessel and faster separation of lignin fragments through the membrane. Although I did not specifically examine the standard conditions utilized in industrial batch-scale processes, I anticipate that

an improvement in lignin depolymerization would likely be observed under such industrial reaction conditions as well.

Upon the MnP- and LiP-catalyzed reactions, a reduction in the M_w of HML for RES was also observed (Figure 3.8 and Table 3.4). The reduction was more significant for the membrane bioreactor as well than for the batch bioreactor. This is another indication of the higher efficiency of lignin depolymerization by the membrane bioreactor. I did not insist that my system reduced the condensation of lignin. I did not argue whether the amount of the condensation of lignin formed through the C-C' bonds increases or not, by my system. My intention was to propose the enhanced depolymerization of lignin and its removal by my system on the basis of the SEC profile (Figure 3.8) and quantification of lignin by Klason lignin/UV-vis spectroscopy lignin (Table 3.3), respectively.

The NMR spectroscopic analysis of RES also demonstrated the enhanced lignin removal by the membrane bioreactor, because a more drastic reduction in the lignin signal volume was observed for the membrane bioreactor than for the batch bioreactor (Figures 3.9 and 3.10). It is noteworthy that the solubilities of the samples in DMSO may vary due to their different chemical compositions. Even though I used the same sample preparation method, if the residues obtained from the membrane bioreactor had lower solubility in DMSO, this could have also contributed to the lower lignin signal intensity observed in the NMR spectra. As a result, there may have been an underestimation of the relative amount of lignin substructures, which may result in an overestimation of lignin removal.

As far as the spectra observed are concerned, the extent of the reduction in signal volume does not drastically differ between the interunit linkage and aromatic regions (Figure

3.11). This means aromatic rings of lignin are not cleaved by the reaction. Additionally, NMR analysis of lignin substructures suggested that no notable structural modification occurred for the lignin remaining in RES. It is deduced that most of the remaining lignin in RES still maintains its native structure.

For the membrane bioreactor, MnP- and LiP-catalyzed reactions were compared. Firstly, the lignin removal was more effective for the LiP-catalyzed reaction (Figure 3.7 and Table 3.3). Secondly, the reduction in the HML proportion was more drastic for the LiP-catalyzed reaction (Table 3.4). LiP seems to be superior to MnP.

In addition to the lignin repolymerization issue, acquiring a large quantity of peroxidase for biological lignin valorization is another task to be overcome.²⁶ Heterologous expression using a yeast like *Pichia pastoris* is generally superior to homologous expression in terms of large-scale protein production. In this study, lignin depolymerization was successfully achieved with heterologously expressed peroxidases. Furthermore, these peroxidases had the ability to depolymerize lignin even without costly purification and at a low enzyme load relative to the reported enzymatic lignin removal.¹⁵⁻¹⁷ These results imply that enzymatic depolymerization is an applicable approach for economical biomass utilization.

3.4 Conclusions

In summary, I demonstrated the advantage of the membrane bioreactor for lignin depolymerization through the peroxidase-catalyzed reaction. The isolation of lignin fragments using the membrane bioreactor can significantly enhance the depolymerization of

beech wood lignin and its removal. To the best of my knowledge, this is the first report of a significant enhancement of biocatalytic lignin depolymerization of a natural lignocellulosic biomass realized with a membrane bioreactor using MnP and LiP. Furthermore, while my investigation focused on the enzymatic aspect, I firmly believe that the membrane bioreactor concept holds promise for broader applications in lignin conversion, including chemical processes.

Additionally, the enhanced lignin removal from MBW in membrane bioreactors catalyzed by either MnP or LiP must be favorable from the biorefinery perspective, where a lesser inhibitory effect of lignin on the saccharification of carbohydrates is expected, ultimately yielding a higher saccharification efficiency. Overall, the enzymatic reaction carried out with continuous isolation of reactive lignin fragments should be a huge milestone towards a sustainable yet efficient biorefinery.

3.5 Experimental procedures

3.5.1 Preparation of milled beech wood

Beech wood chips (Shinseisangyo, Japan) were pulverized and sieved to a particle size of less than 40-mesh. After being Soxhlet-extracted with acetone for 24 h, the wood powder was dried overnight at 40 °C. The resulting powder was ball-milled using a Fritsch P-6 planetary mono mill, 1 g of the sample being added to an 80 mL agate jar containing 100 g of 3 mm ZrO₂ beads. The milling was performed under a nitrogen environment at 550 rpm for 1.5 h (90 cycles of 1 min milling with 1 min intervals). The milled solid was repeatedly

washed with Milli-Q at a loading of 5% (w/w) until a near-colorless supernatant was obtained, which was lyophilized to yield MBW.

3.5.2 Preparation of crude MnP and LiP

MnP and LiP were expressed in *Pichia pastoris*. The genes encoding MnP of *Ceriporiopsis subvermispora* (Joint Genome Institute (JGI) protein code: 117436) and LiP of *Phanerochaete chrysosporium* (JGI protein code: 2989894) were codon-optimized for *P. pastoris* and synthesized by Thermo Fisher Scientific. The genes were each subcloned into the pPICZ α A (Invitrogen, USA) vector to obtain pPICZ α A-MnP and pPICZ α A-LiP vectors. These vectors were linearized with *SacI* restriction enzyme and introduced individually into *P. pastoris* X-33 (Invitrogen, USA) by electroporation. Transformed clones for MnP and LiP were confirmed by colony PCR, a small-scale expression check, and activity assaying. The cloned transformants for MnP and LiP were used for the preparation of crude MnP and crude LiP solutions; the same procedure was used for their preparation. The transformant for either MnP or LiP was cultivated on YPDS agar medium (1% yeast extract, 2% peptone, 2% glucose, 1 M sorbitol, 2% agar, and 100 $\mu\text{g mL}^{-1}$ zeocin) for 3 days at 30 °C. An isolated zeocin-resistant colony was cultured in BMGY medium (1% yeast extract, 2% peptone, 1.34% yeast nitrogen base with ammonium sulfate, 0.1 M potassium phosphate (pH 6), 0.4 $\mu\text{g mL}^{-1}$ biotin, and 1 vol% glycerol) at 30 °C with 200 rpm shaking until OD₆₀₀ reached 6. The cells were collected by centrifugation at 3,500 \times g for 5 min, and resuspended to an OD₆₀₀ of 1.0 in BMMY medium (1% yeast extract, 2% peptone, 1.34% yeast nitrogen base with ammonium sulfate, 0.1 M potassium phosphate (pH 6), 0.4 $\mu\text{g mL}^{-1}$ biotin, and 0.5 vol% methanol) to

induce protein expression. The induction was conducted at 15 °C. During the induction, methanol and a hemin stock (10 mg mL⁻¹ hemin in a 0.1 M ammonia solution) were added to give final concentrations of 0.5% and 0.35%, respectively; this was repeated every twenty-four hours. After three days the culture was centrifuged at 4,400 × g for 30 min to obtain a supernatant containing the secreted enzyme. Then the supernatant was filtered with a 300-kDa cut-off membrane (Pall, USA), concentrated 20-fold, and buffer-exchanged to 50 mM sodium malonate (pH 4.5) with a 10-kDa cut-off membrane (Pall), all using a Minimate TFF system (OAPMP110, Pall). The resulting solution, either the crude MnP or crude LiP, is used for further experiments.

The enzymatic activities of the obtained crude MnP and crude LiP were assayed using 2,6-dimethoxyphenol as a substrate. The enzymatic reaction was performed at 25 °C for 30 min. The formation of the product (coerulignone) was monitored spectroscopically as the increase in the visible light absorbance at 469 nm using Infinite[®] 200 PRO (TECAN). One unit of peroxidase activity was defined as the formation of 1 μmol of coerulignone ($\epsilon_{469 \text{ nm}} = 53.2 \text{ mM}^{-1} \text{ cm}^{-1}$) per min. Peroxidase was prepared freshly before each enzymatic reaction.

3.5.3 Peroxidase-catalyzed lignin degradation in the batch bioreactor

Peroxidase-catalyzed reactions for MBW were carried out in screw-capped glass bottles containing 500 mg of MBW, 1 mM MnSO₄, and 2 U of either MnP or LiP (Figure 3.1a). The total volume of the solution was adjusted to 200 mL with sodium malonate (pH 4.5). The air in the bottle was replaced with nitrogen gas to mimic the environment in the later mentioned membrane bioreactor. The enzymatic reaction was initiated by the addition

of hydrogen peroxide (H_2O_2) at 0.2 mM and conducted with magnetic stirring at room temperature. After four hours, fresh H_2O_2 (half of the original dose, i.e., 0.1 mM) was added followed by incubation for another four hours. In control experiments, the same procedures were performed with solutions, that did not contain either peroxidase or MBW. After eight hours of incubation, a supernatant and solid residue ($\text{RES}_{\text{batch}}$) were separated by centrifugation. The supernatant was frozen until analysis. The $\text{RES}_{\text{batch}}$ obtained for MnP ($\text{RES}_{\text{batch}}^{\text{MnP}}$), LiP ($\text{RES}_{\text{batch}}^{\text{LiP}}$), and without peroxidases ($\text{RES}_{\text{batch}}^{\text{no enzyme}}$), were washed with Milli-Q by repeated suspension at a loading of 2% (w/w) and centrifugation ($4,400 \times g$ for 10 min) until a near-colorless supernatant was obtained, which was lyophilized.

3.5.4 Peroxidase-catalyzed lignin degradation in the membrane bioreactor

Peroxidase-catalyzed reactions for MBW were also carried out in a membrane bioreactor, which comprised a 400 mL ultrafiltration stirred cell (Millipore 5124, Merck) equipped with a 3000 cut-off RC membrane disc (PLBC07610, Merck) with a diameter of 76 mm (Figure 3.1b). The initial components of the reaction mixture were identical to those for the aforementioned batch bioreactor. The reaction was initiated by the addition of H_2O_2 at 0.2 mM and conducted with magnetic stirring at room temperature for eight hours. Immediately after starting the reaction, the surface of the reaction mixture was pressurized at 4 bars with nitrogen to enhance the filtration, the initial filtration rate being 80 mL h^{-1} . The filtrate passed through the RC membrane was fractionated every one-hour. Every one-hour, 80 mL of sodium malonate (pH 4.5) containing 1 mM MnSO_4 and 0.2 mM H_2O_2 was added to the reactor. In control experiments, the same procedures were performed with solutions

that did not contain either peroxidase or MBW. The collected filtrates were frozen until further analysis. The solid fraction remaining in the membrane bioreactor (RES_{membrane}) was collected. The RES_{membrane} obtained for MnP ($RES_{\text{membrane}}^{\text{MnP}}$), LiP ($RES_{\text{membrane}}^{\text{LiP}}$), and without peroxidases ($RES_{\text{membrane}}^{\text{no enzyme}}$), were washed with Milli-Q by repeated suspension at a loading of 2% (w/w) and centrifugation ($4,400 \times g$ for 10 min) until a near-colorless supernatant was obtained, which was lyophilized.

3.5.5 SEC of the products released into the aqueous phase

The products released into the aqueous phase in the batch and membrane bioreactors were subjected to SEC. A sample was diluted with 10 mM NaOH in a 1:1 ratio and then filtered with a 0.2 μm hydrophilic polytetrafluoroethylene (PTFE) membrane. 20 μL of the sample was injected into a high-performance liquid chromatography (HPLC) system (Shimadzu, Japan) equipped with an SPD-20A UV-Vis detector 280 nm absorbance being used for detection. A TSKgel G3000PW_{XL} (7.8 mm I.D. \times 300 mm, Tosoh, Japan) analytical column was used, which was held at 35 $^{\circ}\text{C}$ throughout the analysis. The mobile phase was a 10 mM NaOH solution at a flow rate of 0.5 mL min^{-1} .

A series of polystyrene sulfonate sodium salt standards (peak molecular weight (M_p) = 891-65400), syringol (M_p = 154), and guaiacol (M_p = 124) were used as calibration standards. The calibration standards were used for estimating the molecular weight of the products.

The total amount of products detected at 18.8 min for the batch bioreactor ($TA_{B_{19}}$) was estimated with Eq. (3.1), where $I_{B_{19}}$ the area of product peak detected at 18.8 min on

SEC, and $V_{\text{supernatant}}$ the total volume of the supernatant collected from the batch bioreactor.

$$TA_{B_{19}} = I_{B_{19}} \times V_{\text{supernatant}} \quad (3.1)$$

The total amount of products detected at 18.8 min for the membrane bioreactor ($TA_{M_{19}}$) was estimated with Eq. (3.2), where i is the number of filtrate fraction collected every one hour, $I_{M_{19},i}$ the area of the product peak detected at 18.8 min on SEC for filtrate fraction i , and $V_{\text{filtrate},i}$ the volume of fraction i .

$$TA_{M_{19}} = \sum_i (I_{M_{19},i} \times V_{\text{filtrate},i}) \quad (3.2)$$

$TA_{B_{19}}$ and $TA_{M_{19}}$ have arbitrary units and are used to compare the amounts of products detected at 18.8 min on SEC.

3.5.6 GCMS analysis of the depolymerized products in the filtrate

To obtain product M_{19} , the filtrate fractions were pooled and lyophilized. The resulting solid was dissolved in 10 mM NaOH and injected into an HPLC system. M_{19} was collected based on the elution profile and subsequently neutralized to pH 7 before being lyophilized again. To prepare for GCMS analysis, the dried M_{19} sample was dissolved in ethyl acetate and trimethylsilylated with N,O-Bis(trimethylsilyl)trifluoroacetamide with 1 vol% chlorotrimethylsilane and pyridine. The trimethylsilylated sample was then concentrated under nitrogen gas for analysis by GCMS.

For the GCMS analysis, 1 μL of the trimethylsilylated sample was injected in split mode into a GCMS-QP2010SE system (Shimadzu, Japan) equipped with a DB-5MS column

(30 m × 0.25 mm id, 0.25 μm film thickness; Agilent Technologies). The injection temperature was set at 250 °C, and the carrier gas was helium at a flow rate of 1.0 mL min⁻¹. The initial column temperature was held at 50 °C for 3 min, then increased to 280 °C at a rate of 6 °C min⁻¹, and held for 3 min. The mass spectrometer was operated in electron impact ionization mode with ionizing energy of 70 eV, an ion source temperature of 250 °C, and an interface temperature of 300 °C. The mass scanning range was set to m/z 40-900.

Putative identification of the lignin depolymerization products was established by comparing the mass spectra of the unknown components to those available in the NIST mass spectral library. Products with a similarity index above 80% were listed in Table 3.1.

3.5.7 Chemical composition analysis of the solid residues

The percentages of lignin (LPs) of MBW, RES_{batch}, and RES_{membrane} were determined by both the Klason lignin method^{16,37,44} and the UV-Vis spectroscopic method.⁴⁵ The quantification by both methods was performed in duplicate.

The Klason lignin method was carried out based on a previously reported method.¹⁶ Briefly, 70 mg of a sample was hydrolyzed with 0.7 mL of 72% w/w sulfuric acid for 1 h at 30 °C. Then, it was diluted with 7.7 mL of hot water and further hydrolyzed for 3 h at 100 °C. After hydrolysis, the sample was filtered and washed extensively with Milli-Q, and then dried at 105 °C until a constant weight was reached. The LP was obtained as a percentage of the dried solid remaining after hydrolysis relative to the initial sample weight.

The UV-Vis spectroscopic method was performed based on the method established by Zhang *et al.* recently, with several modifications.⁴⁵ Measurement was performed using a UV-Vis spectrophotometer (Shimadzu UV-1900i, Japan) with quartz cuvettes of 1 cm path-length. 5 mg of a sample was incubated in 1 mL of 8% LiCl/DMSO (w/w) at room temperature for 24 h with stirring. After the 24 h incubation, the mixture was diluted to 1 mg/mL with 8% LiCl/DMSO and then stirred at 80 °C for another 48 h. The resultant solution was further diluted accordingly to adjust the absorbance to within the range of 0.2-0.8. With the 8% LiCl/DMSO solvent as a blank control, the diluted samples were scanned in the range of 200-800 nm. The absorbance value of each sample was determined at 276 nm. The LP of the sample was calculated with Eq. (3.3) where A is the absorbance at 276 nm for the diluted sample, V the total volume of the diluted sample, d the dilution ratio, ϵ the deduced extinction coefficient of hardwood lignin (13.235 L g⁻¹ cm⁻¹), L the length of the light path (1 cm), and m_0 (5 mg) the weight of the sample incubated in 8% LiCl/DMSO.

$$LP = \frac{A \times V \times d}{\epsilon \times L \times m_0} \times 100\% \quad (3.3)$$

On the basis of the LP value determined by either the Klason lignin or UV-Vis spectroscopic method, the change in LP for each sample was calculated according to the following Eq. (3.4),⁴⁶ where LP_0 is the initial LP of MBW, and LP the LP of each sample.

$$\text{Change in LP} = \frac{LP - LP_0}{LP_0} \times 100\% \quad (3.4)$$

The cellulose and hemicellulose contents were determined using a HPLC system (Shimadzu, Japan) equipped with a refractive index detector (RID-20A, Shimadzu).⁴⁴⁻⁴⁵ The content of cellulose and hemicellulose were determined using Eq. (3.5) and Eq. (3.6),

respectively, from the hydrolysis liquor obtained from the filtration step in the Klason lignin experiment. The content of cellulose (glucan) and hemicellulose (xylan, galactan, arabinan, and mannan) were determined using a HPLC system (Shimadzu, Japan) equipped with a refractive index detector (RID-20A, Shimadzu). The analysis was performed utilizing an Aminex HPX-87H (Bio-Rad Laboratories, Hercules, CA, USA) analytical column maintained at 60 °C. The mobile phase consisted of a 5 mM H₂SO₄ solution at a flow rate of 0.6 ml min⁻¹. To quantify the compounds present in the sample, a calibration curve was established using standards with varying concentration (0.1 to 4 mg mL⁻¹) of glucose, xylose, galactose, arabinose, and mannose. Before analysis, samples were diluted four-fold with 5 mM H₂SO₄ and filtered through a 0.2 μm hydrophilic polytetrafluoroethylene (PTFE) membrane. For analysis, 10 μL of each sample was injected into the HPLC system.

$$\% \text{ Cellulose} = \frac{m_{\text{glucan}}}{m_{\text{substrate,dry}}} \times 100\% \quad (3.5)$$

$$\% \text{ Hemicellulose} = \frac{m_{\text{xylan}} + m_{\text{galactan}} + m_{\text{arabinan}} + m_{\text{mannan}}}{m_{\text{substrate,dry}}} \times 100\% \quad (3.6)$$

3.5.8 SEC for solid residues

The molecular weight distributions of lignin in MBW, RES_{batch}, and RES_{membrane} were determined by SEC. Before being subjected to SEC analysis, a sample was pretreated as follows. 10 mg of the sample was treated twice with 5.6 FPU of a cellulolytic enzyme cocktail (CellicCtec2, Novozymes, Denmark) in 50 mM sodium citrate (pH 5) at 50 °C for 72 h to yield cellulolytic enzyme lignin (CEL). 1 mg of CEL was then acetylated by incubation in 500 μL of a 1:1 v/v mixture of anhydrous pyridine and acetic anhydride for 48 h at room temperature with stirring. The acetylated sample was then co-evaporated with

toluene to remove the reagents. The obtained acetylated CEL was dissolved in tetrahydrofuran, and the soluble fraction was passed through a 0.2 μm PTFE filter. 10 μL of the filtered sample was injected into a HPLC system equipped with an SPD M20A photo diode array detector and three tandemly connected TSKgel SuperMultiporeHZ-M analytical columns (4.6 mm I.D. \times 150 mm, Tosoh). The analysis was performed at 40 $^{\circ}\text{C}$ using tetrahydrofuran as a mobile phase at a flow rate of 0.35 mL min^{-1} .

A series of polystyrene standards (PStQuickC, weight average molecular weight (M_w) = 5970-2110000, Tosoh), 1-(3,4-Dimethoxyphenyl)-2-(2-methoxyphenoxy)-1,3-propanediol (M_w = 334), and vanillin (M_w = 152) were used to construct a calibration curve. M_w , number average molecular weight (M_n), and polydispersity index (PDI) were calculated using a LabSolutions software (Shimadzu).

3.5.9 Structural analysis of MBW solid residue by 2D NMR

The lignin substructures in MBW, $\text{RES}_{\text{batch}}$, and $\text{RES}_{\text{membrane}}$ were analyzed by the gel-state 2D NMR method described by Shawn *et al.*⁴⁶ Without performing cellulase treatment, 60 mg of the sample ($\text{RES}_{\text{batch}}$ and $\text{RES}_{\text{membrane}}$) was transferred to a 5 mm NMR tube and swollen with 500 μL of DMSO-d_6 containing 0.4 mM deuterated 4,4-dimethyl-4-silapentane-1-sulfonic acid (DSS-d_6). The sample was sonicated for 1-5 h, during which the temperature of the ultrasonic bath was maintained below 40 $^{\circ}\text{C}$, to obtain a homogeneous gel. NMR spectra were recorded using a Bruker Avance III HD 600 MHz instrument equipped with a 5 mm cryogenic probe and Z gradient (Bruker BioSpin, MA, USA). Acquisition of 2D ^1H - ^{13}C HSQC spectra was performed using a standard Bruker pulse

sequence 'hsqcetgpsisp2.2' at 313 K. Signals were calibrated using DMSO as a reference (δC 39.5 ppm; δH 2.49 ppm). Data processing, signal assignment, and signal volume integration were performed with Bruker TopSpin 3.6.4 software. DSS-d₆ was used as the internal chemical shift and quantification reference; the volume of each signal was normalized as to the signal volume of DSS-d₆. A semi-quantitative analysis of the volume integrals of the HSQC correlation peaks was performed according to the literatures.⁴⁷⁻⁴⁸ The contents of β -O-4', β - β' , and β -5' interunit linkages were estimated from the volume of their C _{α} -H _{α} correlations in the aliphatic region. The contents of S- and S'-units were estimated from the half values of the volume of their C_{2,6}-H_{2,6} correlations, whereas that of the G-unit was estimated from the volume of the C₂-H₂ correlation in the aromatic region. The signal assignments of the 2D NMR spectra were obtained according to the literatures.^{16,47-48}

The relative amounts of lignin substructures per control was calculated with Eq. (3.7), where $\int S_{\text{ctrl}}$ is the HSQC integral for the lignin substructure for RES_{batch}^{no enzyme} or RES_{membrane}^{no enzyme} and $\int S_{\text{RES}}$ the HSQC integral for the lignin substructure for either RES_{batch}^{MnP}, RES_{batch}^{LiP}, RES_{membrane}^{MnP}, or RES_{membrane}^{LiP}.

$$\text{Relative amounts of lignin substructures per control} = \frac{\int S_{\text{RES}}}{\int S_{\text{ctrl}}} \times 100\% \quad (3.7)$$

3.5.10 Enzymatic hydrolysis of solid residues

The hydrolysis of MBW, RES_{batch}, and RES_{membrane} was conducted using a commercial cellulolytic enzyme cocktail (CellicCtec2, Novozymes, Denmark). 5 mg of the lyophilized dried sample (MBW, RES_{batch}, and RES_{membrane}) was treated with 0.02 FPU of CellicCtec2 in 500 μL of 50 mM sodium citrate (pH 5) at 50 °C for 24 h with shaking.

After the 24 h-incubation, the samples were centrifuged at $10,000 \times g$ for 5 min to separate the hydrolysate. The amount of reducing sugar released in the hydrolysate was determined using the dinitro salicylic acid method, with glucose used as the standard for comparison and quantification.⁴⁹

3.6 References

1. J. Cai, Y. He, X. Yu, S. W. Banks, Y. Yang, X. Zhang, Y. Yu, R. Liu and A. V. Bridgwater, Review of physicochemical properties and analytical characterization of lignocellulosic biomass. *Renewable Sustainable Energy Rev.* 2017, **76**, 309-322.
2. S. Liu, Woody biomass: Niche position as a source of sustainable renewable chemicals and energy and kinetics of hot-water extraction/hydrolysis. *Biotechnol. Adv.* 2010, **28**, 563-582.
3. L. M.C. L. K. Curran, L. T. M. Pham, K. L. Sale and B. A. Simmons, Review of advances in the development of laccases for the valorization of lignin to enable the production of lignocellulosic biofuels and bioproducts. *Biotechnol. Adv.* 2022, **54**, 107809.
4. M. Xie, J. Zhang, T. J. Tschaplinski, G. A. Tuskan, J. Chen and W. Muchero, Regulation of Lignin Biosynthesis and Its Role in Growth-Defense Tradeoffs. *Front. Plant Sci.* 2018, **9**, 1427.
5. V. K. Ponnusamy, D. D. Nguyen, J. Dharmaraja, S. Shobana, J. R. Banu, R. G. Saratale, S. W. Chang and G. Kumar, A review on lignin structure, pretreatments,

- fermentation reactions and biorefinery potential. *Bioresour. Technol.* 2019, **271**, 462-472.
6. E. M. Anderson, M. L. Stone, R. Katahira, M. Reed, W. Muchero, K. J. Ramirez, G. T. Beckham and Y. Román-Leshkov, Differences in S/G ratio in natural poplar variants do not predict catalytic depolymerization monomer yields. *Nat. Commun.* 2019, **10**, 2033.
 7. J. Barros, L. Escamilla-Trevino, L. Song, X. Rao, J. C. Serrani-Yarce, M. D. Palacios, N. Engle, F. K. Choudhury, T. J. Tschaplinski, B. J. Venables, R. Mittler and R. A. Dixon, 4-Coumarate 3-hydroxylase in the lignin biosynthesis pathway is a cytosolic ascorbate peroxidase. *Nat. Commun.* 2019, **10**, 1994.
 8. Q. Liu, L. Luo and L. Zheng, Lignins: Biosynthesis and Biological Functions in Plants. *Int. J. Mol. Sci.* 2018, **19**, 235.
 9. S. Guadix-Montero and M. Sankar, Review on Catalytic Cleavage of C–C Inter-unit Linkages in Lignin Model Compounds: Towards Lignin Depolymerisation. *Top. Catal.* 2018, **61**, 183-198.
 10. Y. Jian, Y. Meng and H. Li, Selectivity Control of C-O Bond Cleavage for Catalytic Biomass Valorization. *Front. Energy Res.* 2022, **9**, 827680.
 11. H. B. Aditiya, T. M. I. Mahlia, W. T. Chong, H. Nur and A. H. Sebayang, Second generation bioethanol production: A critical review. *Renewable Sustainable Energy Rev.* 2016, **66**, 631-653.

12. Y. Su, X. Yu, Y. Sun, G. Wang, H. Chen and G. Chen, Evaluation of Screened Lignin-degrading Fungi for the Biological Pretreatment of Corn Stover. *Sci. Rep.* 2018, **8**, 5385.
13. R. C. Wilhelm, R. Singh, L. D. Eltis and W. W. Mohn, Bacterial contributions to delignification and lignocellulose degradation in forest soils with metagenomic and quantitative stable isotope probing. *ISME J.* 2019, **13**, 413-429.
14. T. Cui, B. Yuan, H. Guo, H. Tian, W. Wang, Y. Ma, C. Li and Q. Fei, Enhanced lignin biodegradation by consortium of white rot fungi: microbial synergistic effects and product mapping. *Biotechnol. Biofuels Bioprod.* 2021, **14**, 162.
15. A. Rico, J. Rencoret, J. C. d. Río, A. T. Martínez and A. Gutiérrez, Pretreatment with laccase and a phenolic mediator degrades lignin and enhances saccharification of Eucalyptus feedstock. *Biotechnol. Biofuels Bioprod* 2014, **7**, 6.
16. R. Hilgers, G. v. Erven, V. Boerkamp, I. Sulaeva, A. Potthast, M. A. Kabel and J. Vincken, Understanding laccase/HBT-catalyzed grass delignification at the molecular level. *Green Chem.* 2020, **22**, 1735-1746.
17. J. Rencoret, A. Pereira, J. C. d. Río, A. T. Martínez and A. Gutiérrez, Laccase-Mediator Pretreatment of Wheat Straw Degrades Lignin and Improves Saccharification. *BioEnergy Res.* 2016, **9**, 917-930.
18. L. Munk, A. M. Punt, M. A. Kabel and A. S. Meyer, Laccase catalyzed grafting of –N–OH type mediators to lignin via radical–radical coupling. *RSC Adv.* 2017, **7**, 3358-3368.

19. P. Baiocco, A. M. Barreca, M. Fabbrini, C. Galli and P. Gentili, Promoting laccase activity towards non-phenolic substrates: a mechanistic investigation with some laccase–mediator systems. *Org. Biomol. Chem.* 2003, **1**, 191-197.
20. L. Munk, A. K. Sitarz, D. C. Kalyani, J. D. Mikkelsen and A. S. Meyer, Can laccases catalyze bond cleavage in lignin? *Biotechnol. Adv.* 2015, **33**, 13-24.
21. P. Nousiainen, J. Kontro, H. Manner, A. Hatakka and J. Sipilä, Phenolic mediators enhance the manganese peroxidase catalyzed oxidation of recalcitrant lignin model compounds and synthetic lignin. *Fungal Genet. Biol.* 2014, **72**, 137-149.
22. E. Fernández-Fueyo, F. J. Ruiz-Dueñas and A. T. Martínez, Engineering a fungal peroxidase that degrades lignin at very acidic pH. *Biotechnol. Biofuels Bioprod.* 2014, **7**, 114.
23. T. Jian, Y. Zhou, P. Wang, W. Yang, P. Mu, X. Zhang, X. Zhang and C. Chen, Highly stable and tunable peptoid/hemin enzymatic mimetics with natural peroxidase-like activities. *Nat. Commun.* 2022, **13**, 3025.
24. B. M. Majeke, F. Collard, L. Tyhoda and J. F. Görgens, The synergistic application of quinone reductase and lignin peroxidase for the deconstruction of industrial (technical) lignins and analysis of the degraded lignin products. *Bioresour. Technol.* 2021, **319**, 124152.
25. E. Liu, F. Segato, R. A. Prade and M. R. Wilkins, Exploring lignin depolymerization by a bi-enzyme system containing aryl alcohol oxidase and lignin peroxidase in aqueous biocompatible ionic liquids. *Bioresour. Technol.* 2021, **338**, 125564.

26. H. Xu, G. M. Scott, F. Jiang and C. Kelly, Recombinant manganese peroxidase (rMnP) from *Pichia pastoris*. Part 1: Kraft pulp delignification. *Holzforschung* 2010, **64**, 017.
27. C. Cagide and S. Castro-Sowinski, Technological and biochemical features of lignin-degrading enzymes: a brief review. *Environ. Sustainability* 2020, **3**, 371-389.
28. T. Warinowski, S. Koutaniemi, A. Kärkönen, I. Sundberg, M. Toikka, L. K. Simola, I. Kilpeläinen and T. H. Teeri, Peroxidases Bound to the Growing Lignin Polymer Produce Natural Like Extracellular Lignin in a Cell Culture of Norway Spruce. *Front. Plant Sci.* 2016, **7**, 01523
29. X. Mu, Z. Han, C. Liu and D. Zhang, Mechanistic Insights into Formaldehyde-Blocked Lignin Condensation: A DFT Study. *J. Phys. Chem. C* 2019, **123**, 8640-8648.
30. S. Dabral, J. Engel, J. Mottweiler, S. S. M. Spoehrle, C. W. Lahive and C. Bolm, Mechanistic studies of base-catalysed lignin depolymerisation in dimethyl carbonate. *Green Chem.* 2018, **20**, 170-182.
31. P. J. Deuss, C. S. Lancefield, A. Narani, J. G. de Vries, N. J. Westwood and K. Barta, Phenolic acetals from lignins of varying compositions via iron(iii) triflate catalysed depolymerisation. *Green Chem.* 2017, **19**, 2774-2782.
32. O. Yu, C. G. Yoo, C. S. Kim and K. H. Kim, Understanding the Effects of Ethylene Glycol-Assisted Biomass Fractionation Parameters on Lignin Characteristics Using a Full Factorial Design and Computational Modeling. *ACS Omega* 2019, **4**, 16103-16110.

33. N. Li, Y. Li, C. G. Yoo, X. Yang, X. Lin, J. Ralph and X. Pan, An uncondensed lignin depolymerized in the solid state and isolated from lignocellulosic biomass: a mechanistic study. *Green Chem.* 2018, **20**, 4224-4235.
34. V. Steinmertz, M. Villain-gambier, A. Klem, I. Ziegler, S. Dumarcay and D. Trebouet, In-situ extraction of depolymerization products by membrane filtration against lignin condensation. *Bioresour. Technol.* 2020, **311**, 123530.
35. M. Lin, T. Nagata and M. Katahira, High yield production of fungal manganese peroxidases by *E. coli* through soluble expression, and examination of the activities. *Protein Expression Purif.* 2018, **145**, 45-52.
36. S. Zhang, Z. Dong, J. Shi, C. Yang, Y. Fang, G. Chen and C. Tian, Enzymatic hydrolysis of corn stover lignin by laccase, lignin peroxidase, and manganese peroxidase. *Bioresour. Technol.* 2022, **361**, 127699.
37. A. Sluiter, B. Hames, R. Ruiz, C. Scarlata, J. Sluiter, D. Templeton, and D. Crocker, Determination of structural carbohydrates and lignin in biomass, Report NREL/TP-510-42618, National Renewable Energy Laboratory, Golden, CO, USA, 2012.
38. S. D. Mansfield, H. Kim, F. Lu and J. Ralph, Whole plant cell wall characterization using solution-state 2D NMR. *Nat. Protoc.* 2012, **7**, 1579-1589.
39. J. del Río, J. Rencoret, P. Prinsen, A. T. Martínez, J. Ralph and A. Gutiérrez, Structural Characterization of Wheat Straw Lignin as Revealed by Analytical Pyrolysis, 2D-NMR, and Reductive Cleavage Methods. *J. Agric. Food Chem.* 2012, **60**, 5922-5935.

40. D. Salvachúa, R. Katahira, N. S. Cleveland, P. Khanna, M. G. Resch, B. A. Black, S. O. Purvine, E. M. Zink, A. Prieto, M. J. Martínez, A. T. Martínez, B. A. Simmons, J. M. Gladden and G. T. Beckham, Lignin depolymerization by fungal secretomes and a microbial sink. *Green Chem.* 2016, **18**, 6046-6062.
41. T. D. H. Bugg and R. Rahmanpour, Enzymatic conversion of lignin into renewable chemicals. *Curr. Opin. Chem. Biol.* 2015, **29**, 10-17.
42. H. Son, H. Seo, S. Han, S. M. Kim, L. T. M. Pham, M. F. Khan, H. J. Sung, S. Kang, K. Kim and Y. H. Kim, Extra disulfide and ionic salt bridge improves the thermostability of lignin peroxidase H8 under acidic condition. *Enzyme Microb. Technol.* 2021, **148**, 109803.
43. M. Nazar, L. Xu, M. W. Ullah, J. M. Moradian, Y. Wang, S. Sethupathy, B. Iqbal, M. Z. Nawaz and D. Zhu, Biological delignification of rice straw using laccase from *Bacillus ligniniphilus* L1 for bioethanol production: A clean approach for agro-biomass utilization. *J. Clean. Prod.* 2022, **360**, 132171.
44. M. M. Abu-Omar, K. Barta, G. T. Beckham, J. S. Luterbacher, J. Ralph, R. Rinaldi, Y. Román-Leshkov, J. S. M. Samec, B. F. Sels and F. Wang, Guidelines for performing lignin-first biorefining. *Energy Environ. Sci.* 2021, **14**, 262-292.
45. H. Zhang, H. Zhao, Y. Yang, H. Ren and H. Zhai, A spectroscopic method for quantitating lignin in lignocellulosic biomass based on the completely dissolved solution of biomass in LiCl/DMSO. *Green Chem.* 2022, **24**, 2212-2221.
46. D. Mikulski and G. Kłosowski, Delignification efficiency of various types of biomass using microwave-assisted hydrotropic pretreatment. *Sci. Rep.* 2022, **12**, 4561.

47. J. Rencoret, P. Prinsen, A. Gutiérrez, A. T. Martínez and J. del Río, Isolation and Structural Characterization of the Milled Wood Lignin, Dioxane Lignin, and Cellulolytic Lignin Preparations from Brewer's Spent Grain. *J. Agric. Food Chem.* 2015, **63**, 603-613.
48. T. Yuan, S. Sun, F. Xu and R. Sun, Characterization of Lignin Structures and Lignin–Carbohydrate Complex (LCC) Linkages by Quantitative ¹³C and 2D HSQC NMR Spectroscopy. *J. Agric. Food Chem.* 2011, **59**, 10604-10614.
49. G. L. Miller, Use of Dinitrosalicylic Acid Reagent for Determination of Reducing Sugar. *Anal. Chem.* 1959, **31**, 3, 426-428.

Chapter 4

Enhancing bioethanol production from rice straw through environmentally-friendly delignification using versatile peroxidase

Reproduced from Ref. *J. Agr. Food. Chem.*, 2024 with permission from the American Chemical Society. (DOI: 10.1021/acs.jafc.3c07998)

4.1 Introduction

In recent years, the global economy has experienced rapid growth and industrialization, leading to a significant increase in energy consumption. Unfortunately, this surge in energy demand has primarily been met by heavily relying on fossil fuels, which are notorious for their harmful impact on the environment.¹ Consequently, there is an urgent need to find an alternative energy source that is both sustainable and environmentally friendly. One promising way to replace fossil fuels in the pursuit of cleaner energy is biofuels such as bioethanol which are known to be carbon-neutral.² Upon combustion, biofuels such as bioethanol produce fewer harmful pollutants such as sulfur dioxide and particulate matter, in comparison to conventional fossil fuels.^{3,4} Besides, bioethanol also exhibits substantial potential as a chemical building block in biorefineries, where it can serve as a precursor for the production of valuable fine chemicals like olefins, gasoline, and syngas.^{5,6}

Bioethanol can be produced from various raw materials, and one with great potential is lignocellulosic biomass. Among the available options, rice straw (RS) stands out as an abundant and promising lignocellulosic biomass resource for bioethanol production.^{7,8} RS possesses a high content of polysaccharides, including cellulose (32-47%) and hemicellulose (19-27%), making it highly suitable for bioethanol production.⁸ For the production of bioethanol, cellulose is required to be converted into fermentable sugars.⁹ One increasingly popular method for this conversion is an enzymatic pathway, which offers advantages such as lower energy requirements and an environmentally friendly process.¹⁰ In this pathway, cellulase, an enzyme with cellulolytic activity, is utilized during the saccharification stage to

convert cellulose into glucose.¹¹ The resulting glucose is then fermented into bioethanol using yeast.^{11,12}

However, saccharification of RS in its untreated state presents a significant challenge due to the presence of lignin.¹³ Lignin impedes cellulase's access to cellulose, resulting in poor saccharification efficiency. To overcome this limitation, pretreatment of RS becomes necessary to break down lignin and to enhance cellulase's accessibility to cellulose.¹⁴ Traditionally, physical and chemical treatments, such as steam explosion, or organosolv, acid, or alkali treatment, have been employed to degrade lignin in RS.¹⁵ However, these processes often require high reaction temperatures and the use of harsh chemicals, leading to several notable drawbacks, including high energy consumption and adverse environmental impacts.^{16,17}

Biological treatment offers a promising alternative to the use of harsh chemicals and reaction conditions. Biological treatment involves the use of fungi, bacteria, or their ligninolytic enzymes to delignify biomass, which has gained significant interest for enhancing enzymatic saccharification and fermentation processes.¹⁸ Lignin degrading microorganisms produce various ligninolytic enzymes, including laccase, lignin peroxidase, manganese peroxidase, and versatile peroxidase (VP; EC 1.11.1.16).^{19,20} VP is a heme-containing ligninolytic peroxidase considered a hybrid of both manganese and lignin peroxidases.²¹ Its functional versatility stems from three distinct active sites for substrate oxidation: the first site converts Mn^{2+} to Mn^{3+} , serving as a diffusible mediator; the second site is a low-redox potential heme-dependent binding pocket; and the third site contains a surface-reactive tryptophan radical with high redox potential, which is connected to the heme

via a long-range electron-transfer pathway.²²⁻²⁴ In the presence of hydrogen peroxide, VP can oxidize a wide range of substances, including phenolic and non-phenolic compounds, dyes, and lignin.²¹

While VP holds great promise for diverse biotechnological applications, its utilization in native biomass delignification and subsequent bioethanol production remains limited. One primary challenge is the efficient production of active VP.²² Although homologous expression systems have been used, they suffer from drawbacks such as low expression levels and time-consuming enzyme production.²⁵ In contrast, heterologous expression systems, particularly in hosts like bacteria and yeast, offer distinct advantages such as rapid large-scale enzyme production compared to homologous systems.²⁶ Among these heterologous expression systems, yeast-based recombinant expression, such as *Pichia pastoris* based expression, offers numerous benefits, including rapid growth, high recombinant protein yields, post-translational modification capabilities, secretory expression, and ease of genetic manipulation.²⁷ This positions *P. pastoris* as an attractive host for recombinant VP production.

In this study, my aim was to express VP in *P. pastoris* and to investigate its potential as a biocatalyst for delignifying raw biomass material, specifically RS. My approach involved several key steps. First, I optimized the expression of soluble VP in *P. pastoris* while ensuring sufficient heme incorporation. Subsequently, I evaluated the catalytic activity of the expressed VP, employing various lignin-like monomeric and dimeric compounds as substrates. Finally, I investigated VP's capability to catalyze the delignification of RS using a membrane bioreactor, which was previously reported to be more effective in catalyzing

lignin depolymerization compared to a batch bioreactor,²⁸ and assessed the resulting enhancements in saccharification yield and bioethanol production.

4.2 Results and Discussion

4.2.1 Optimization of VP expression for activity

Ligninolytic peroxidases, including manganese peroxidase, lignin peroxidase and VP, are heme-containing enzymes crucial for catalyzing the H₂O₂-dependent oxidative degradation of lignin.²⁰ Hence, it is imperative to ensure the sufficient incorporation of hemin into VP during the expression stage to achieve a high level of VP activity. Previous research by Lin *et al.* demonstrated that adequate hemin incorporation into manganese peroxidase significantly increased its activity.²⁵ Given the similarity between VP and manganese peroxidase as ligninolytic peroxidases, I anticipated that VP could similarly benefit from hemin incorporation. To achieve a high level of VP activity, I explored methods for hemin incorporation during cultivation. Different hemin stock solutions were prepared by dissolving hemin in various solvents (Figure 4.1A), and I determined VP expression levels in the culture supernatants using a VP activity assay with DMP as the substrate.

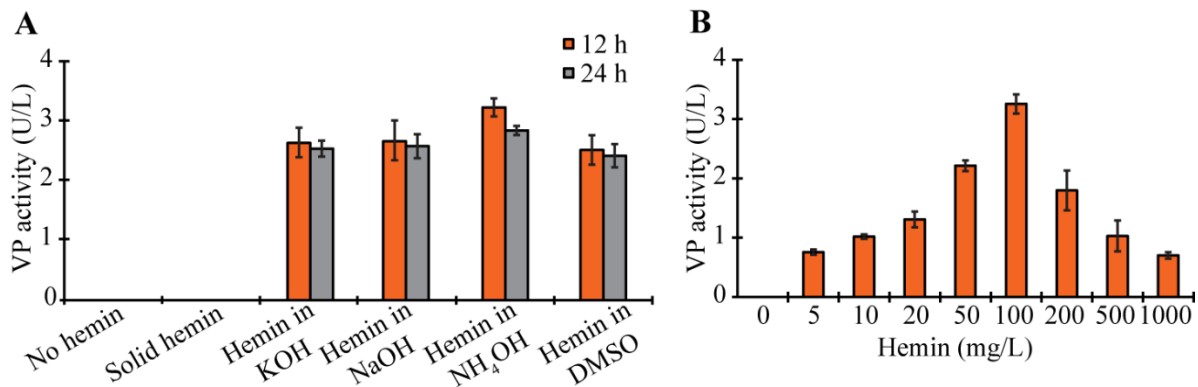


Figure 4.1. Effect of hemin addition strategies on the level of VP activity. (A) The effect of various hemin stocks on the level of VP activity. Four hemin stocks were prepared by dissolving hemin in KOH, NaOH, NH₄OH, and DMSO, respectively. Hemin was introduced cumulatively at 12-hour (orange bars) or 24-hour (grey bars) intervals, resulting in a final concentration of 100 mg hemin/L culture after 72 hours of induction. (B) The effect of the amount of hemin added on the level of VP activity. Hemin stock (dissolved in NH₄OH) was introduced cumulatively at 12-hour intervals, the final concentration reaching 0 to 1,000 mg hemin/L culture after 72 hours of induction. VP activity for (A) and (B) was determined using DMP as the substrate.

Figure 4.1A illustrates that directly introducing solid hemin into the culture medium or using no hemin at all resulted in almost no enzymatic activity towards DMP. This indicates a limited presence of active VP in the culture supernatant, likely due to the poor solubility of solid hemin in the pH range of 4 to 7, which hinders its dispersion in the medium.²⁹ Consequently, hemin incorporation into VP was not accomplished, resulting in almost no expression of active VP.

To address this issue, I explored an alternative approach by preparing four distinct hemin stock solutions through the dissolution of solid hemin in KOH, NaOH, NH₄OH, and DMSO. These hemin stocks, respectively, were sequentially added to the medium during the cultivation, either every 12 hours (indicated by orange bars) or 24 hours (indicated by grey bars). This gradual addition aimed to prevent abrupt pH fluctuations that could harm *Pichia*

cells. Ultimately, after 72 hours of induction, I achieved a final concentration of 100 mg hemin/L culture.

The results, as depicted in Figure 4.1A, showed a significant improvement in active VP expression in *P. pastoris*. The solubilization of hemin in these solvents facilitated its dispersion in the medium, leading to improved hemin incorporation into VP and consequently resulting in elevated levels of VP activity. Several studies have also shown that introducing hemin during the cultivation improved hemin incorporation into manganese peroxidase, resulting in a higher level of manganese peroxidase activity.^{25,29} Notably, the hemin stock solution prepared using NH₄OH and added every 12 hours gave the highest level of VP activity, displaying enzymatic activity of 3.3 U/L.

Next, I explored the impact of the quantity of added hemin on the VP activity (Figure 4.1B). An increase in hemin quantity was positively correlated with VP activity, reaching 3.3 U/L at a final concentration of 100 mg hemin/L culture after 72 hours of induction (Figure 4.1B). However, a further increase in the hemin concentration led to a decline in VP activity.

I applied these optimized conditions for the production of crude VP in the following and evaluated VP's enzymatic activity using both monomeric and dimeric substrates.

4.2.2 Optimizing VP enzymatic activity using monomeric and dimeric substrates

In this section, I aimed to determine the optimal conditions for maximizing VP enzymatic activity. To achieve this, I used three distinct substrates: VA, DMP, and guaiacol (Figure 4.2), and varied the pH from 3 to 7. The findings, summarized in Table 4.1,

demonstrate that VP exhibited enzymatic activity across the entire pH range for all three substrates. The highest enzymatic activity was observed at pH 4 for all substrates.

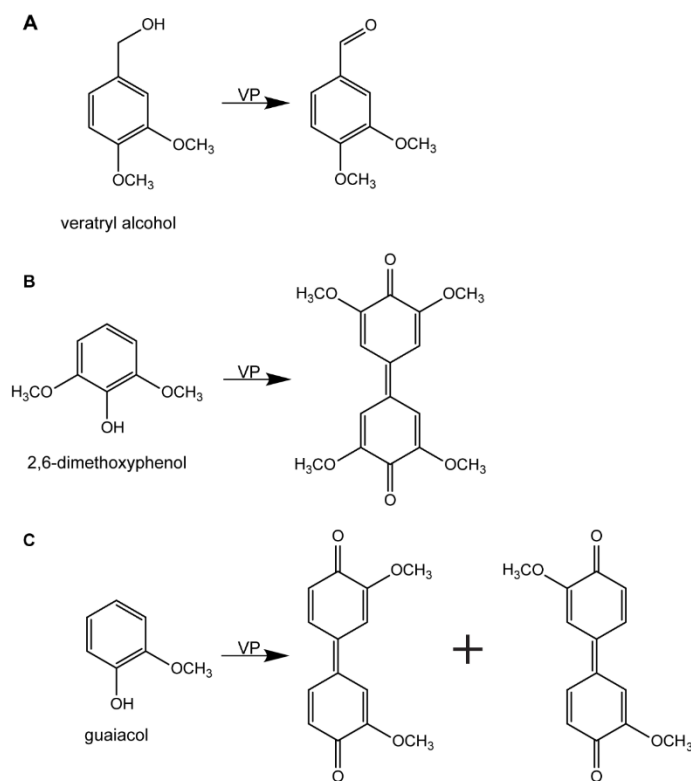


Figure 4.2. Oxidation of veratryl alcohol (A), 2,6-dimethoxyphenol (B), and guaiacol (C) by VP.

Next, I explored the impact of MnSO_4 on VP's enzymatic performance at pH 4. The addition of 2 mM MnSO_4 resulted in a substantial increase in VP's enzymatic activity for all three substrates (Table 4.1). In the presence of manganese ions and their chelators such as malonate, VP oxidizes Mn^{2+} to Mn^{3+} , which, in turn, serves as a diffusible mediator catalyzing the oxidative reaction on the substrates.²¹

Table 4.1. Enzymatic activity of VP towards various substrates^a

Conditions	VP activity (U/L)		
	VA ^b	DMP ^b	Guaiacol
Sodium tartrate 125 mM			
pH 3	26 ± 5	38 ± 1	15 ± 2
Sodium malonate 50 mM			
pH 4	88 ± 7	101 ± 3	35 ± 2
pH 5	40 ± 5	73 ± 3	31 ± 1
pH 6	15 ± 3	52 ± 2	22 ± 1
pH 7	11 ± 3	46 ± 6	21 ± 4
MnSO ₄ (mM)			
0.0	7 ± 3	9 ± 2	2 ± 2
2.0	88 ± 7	101 ± 3	35 ± 2

^aOne unit (U) of VP activity was defined as the amount of enzyme required to catalyze the conversion of 1 μmol of substrate per minute under the assay conditions. All activity assays were performed in 200 μL reaction solution containing 1 mM substrate, 0.5 mM H_2O_2 , 2 mM MnSO_4 , and 10 μL VP (0.1 mU/ μL VP), unless stated otherwise. Activity assays for varying concentrations of MnSO_4 were performed in 50 mM sodium malonate (pH 4). All reactions were performed thrice at 25 °C to obtain the mean and standard deviation. ^bVA, veratryl alcohol; DMP, 2,6-dimethoxyphenol.

Then, I investigated VP's enzymatic performance with phenolic dimer substrates (GGE and SGE, Figure 4.3) while varying the concentration of H_2O_2 (Table 4.2). The results revealed that in the absence of H_2O_2 , there was no conversion of either GGE or SGE, highlighting the essential role of H_2O_2 in VP's enzymatic function. At 1 mM H_2O_2 , the conversion rates of GGE and SGE reached 53% and 27%, respectively (Table 4.2). Increasing the H_2O_2 concentration to 50 mM led to a decline in the conversion rates of both GGE and SGE. This decline can be attributed to VP's deactivation at high H_2O_2 concentrations.²² When

VP was absent from the reaction mixture containing 50 mM H₂O₂, no conversion of GGE and SGE was observed, conclusively attributing the achieved conversion rates in this study to VP's catalytic activity (Table 4.2).

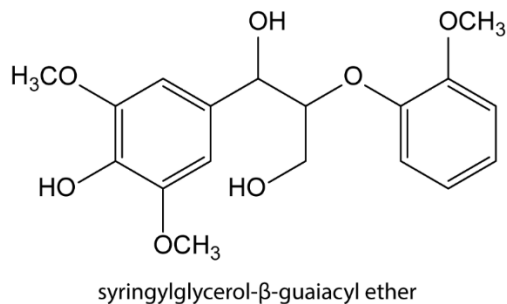
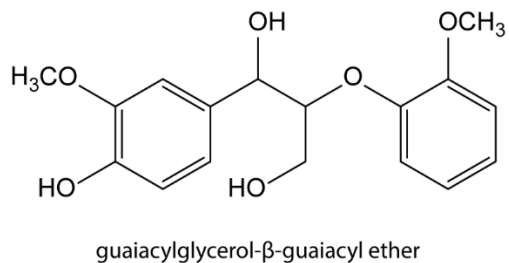


Figure 4.3. Chemical structures of guaiacylglycerol-β-guaiacyl ether (GGE) and syringylglycerol-β-guaiacyl ether (SGE).

Table 4.2. Conversion of GGE and SGE achieved using VP^a

H ₂ O ₂ (mM)	Conversion (%)	
	GGE	SGE
0	n.c.	n.c.
1	53 ± 1	27 ± 2
50	41 ± 3	34 ± 1
50 (no VP)	n.c.	n.c.

^aThe reaction was performed in 50 mM sodium malonate (pH 4) containing 1 mM substrate, 2 mM MnSO₄, and 0.694 mU VP. H₂O₂ was added to the final concentrations given in Table 2. Conversion was estimated based on

the peak areas of the substrates on the RP-HPLC chromatograms after 12 h of reaction. All reactions were performed twice at 30 °C to obtain the mean and standard deviation. ^bGGE, guaiacylglycerol- β -guaiacyl ether; SGE, syringylglycerol- β -guaiacyl ether; n.c., no conversion.

4.2.3 Delignification of RS using VP

In the following experiment, I utilized expressed VP as a biocatalyst to facilitate the delignification of RS using a membrane bioreactor. In this study, a membrane bioreactor was chosen as the reaction vessel due to its established superiority in promoting lignin degradation compared to batch bioreactor systems, as demonstrated in my recent study.²⁸ A membrane bioreactor continuously separates the degraded lignin from the reaction mixture through a regenerated cellulose membrane whose cut-off is 1 kDa to prevent repolymerization and thus improve lignin degradation. The delignification process involved incubating crude VP with RS at 30 °C for 24 hours. To establish a baseline for comparison, I also conducted a parallel incubation without VP. After the 24-hour reaction period, I analyzed the RS residue obtained with both treatments: one with VP (VP-RS) and the other without VP (Ctrl-RS), which served as a control.

I determined the lignin contents in Ctrl-RS and VP-RS and compared them to the initial lignin content in raw RS. With the control treatment (Ctrl-RS), where VP was absent, I observed a negligible change in lignin content, with an insignificant reduction from 22% in raw RS to 21% in Ctrl-RS (Table 4.3). This suggests that, in the absence of VP, lignin removal was minimal. Conversely, when RS was treated with VP (VP-RS), there was a substantial reduction in lignin content, it decreasing from the initial 22% in raw RS to 16% in VP-RS (Table 4.3). The delignification rates, calculated using Eq. (4.1), were 7% and 35% for Ctrl-

RS and VP-RS, respectively (Table 4.3). A similar delignification rate of 32% was achieved in a laccase-mediated system, in which lignin degradation in milled wheat straw was catalyzed at 40 °C in an oxygen gas-pressurized reactor for 24 hours.³⁰

Table 4.3. Composition analysis of raw rice straw (RS), and RS treated with (VP-RS) and without VP (Ctrl-RS)

Sample	Recovery (%) ^a	Glucan (%)	Xylan (%)	Lignin (%)	Delignification (%)
Raw RS	-	29 ± 3	18 ± 2	22 ± 3	-
Ctrl-RS	97	29 ± 1	18 ± 1	21 ± 2	7
VP-RS	90	31 ± 1	18 ± 1	16 ± 2	35

^aRecovery (%) represents the weight of residue obtained after the reaction relative to the weight of starting material.

Overall, my results demonstrate the effectiveness of VP as a biocatalyst in facilitating the degradation of lignin within RS under mild and environmentally friendly reaction conditions at 30 °C.

4.2.4 Effect of VP treatment on enzymatic saccharification of RS

After successfully delignifying RS through VP treatment in the membrane bioreactor, I investigated its impact on enzymatic saccharification efficiency in comparison to Ctrl-RS. I used a cellulolytic enzyme cocktail to saccharify VP-RS and Ctrl-RS, and the resulting saccharified products were analyzed for the glucose (Figure 4.4A) and reducing sugar (Figure 4.4B) contents.

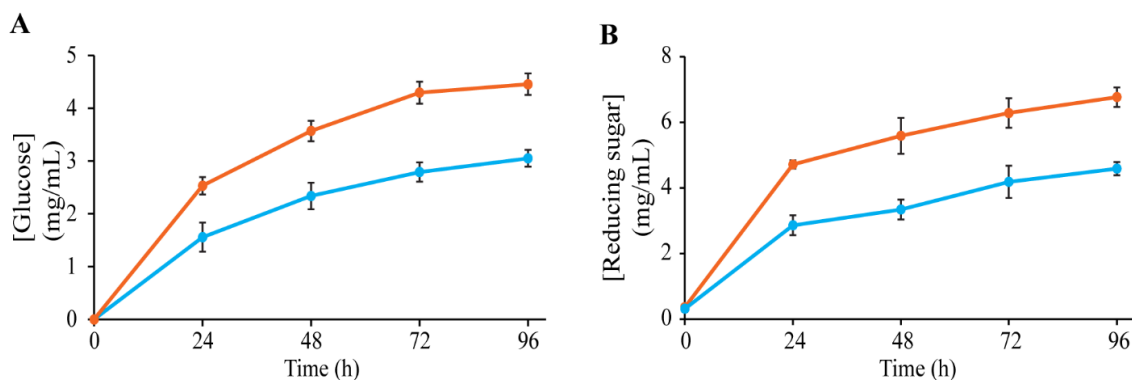


Figure 4.4. Time courses of the concentrations of glucose (A) and reducing sugar (B) produced on saccharification of Ctrl-RS (cyan) and VP-RS (orange) using a cellulolytic enzyme cocktail.

In Figure 4.4A, the cyan line represents the glucose concentration in the saccharified product of Ctrl-RS, while the orange line corresponds to that of VP-RS, throughout the reaction time. The results clearly show an increase in glucose production from VP-RS compared to that from Ctrl-RS. After 96 hours of enzymatic saccharification, VP-RS yielded a glucose concentration of 4.5 mg/mL, whereas Ctrl-RS yielded only 3.1 mg/mL, indicating 1.5-fold enhancement in glucose production for VP-RS (Figure 4.4A).

Figure 4.4B illustrates the production of reducing sugar on the enzymatic saccharification of Ctrl-RS and VP-RS. Reducing sugars serve as intermediary feedstock for downstream bioethanol conversion, and their quantity reflects the depolymerization of cellulose/hemicellulose in RS during the enzymatic saccharification process.³¹ After 96 hours of enzymatic saccharification, VP-RS yielded 6.8 mg/mL of reducing sugar, while Ctrl-RS produced 4.6 mg/mL, indicating 1.5-fold enhancement in reducing sugar production for VP-RS (Figure 4.4B).

The increased levels of glucose and reducing sugars obtained for VP-RS in comparison to those for Ctrl-RS indicate enhancement of the cellulose/hemicellulose saccharification efficiency by the VP treatment. This improvement can be attributed to the degradation and removal of lignin in VP-RS, which likely exposes cellulose to cellulase more effectively, facilitating better cellulase access to cellulose in VP-RS.³² This positive effect of VP treatment on enzymatic saccharification aligns with findings from other studies involving different lignocellulosic materials and enzymes. For instance, studies involving laccase-treated sugarcane bagasse/straw¹⁸ and rice straw³³ demonstrated that delignification of these materials significantly improved cellulase saccharification efficiency. This underscores the pivotal roles of degradation and removal of lignin in enhancing the digestibility of cellulose in lignocellulosic materials.³⁴

It was found in other studies that delignification of lignocellulosic biomass by laccase can mitigate the non-productive adsorption of cellulase to lignin, which results in higher enzymatic saccharification efficiency.^{18,33} It is likely that the delignification of RS by VP might also similarly mitigate the non-productive adsorption of cellulase to lignin, resulting in the higher enzymatic saccharification efficiency observed (Figure 4.4). In these studies, laccase treatment increased the level of carboxylic acids on the lignocellulosic substrate surface, reducing non-specific adsorption of negatively charged cellulase to lignin due to the electrostatic repulsion.^{18,35,36} This reduction in competitive adsorption allows greater cellulase availability, thereby enhancing the efficiency of cellulose breakdown into glucose and reducing sugars.

In conclusion, my findings indicate that VP treatment not only reduces the lignin content in RS but also positively affects the interaction between cellulase and cellulose, resulting in improved enzymatic saccharification efficiency and higher yields of glucose and reducing sugars. This knowledge underscores the potential of VP treatment as a valuable method for enhancing the bioconversion of lignocellulosic biomass into valuable products, such as bioethanol.

4.2.5 Molecular weight analysis of delignified RS

Following the observation of RS delignification through the VP treatment, which was revealed by Klason lignin analysis, I investigated the molecular weight of RS lignin using SEC. As shown in Table 4.4, the results revealed a significant reduction in lignin molecular weight for VP-RS (3737) compared to those for Ctrl-RS (5140). This represented a 27% decrease in lignin molecular weight in VP-RS.

Table 4.4. Number-average (M_n) and weight-average (M_w) molecular weights, and polydispersity (M_w/M_n) of Ctrl-RS and VP-RS

Sample	M_w	M_n	M_w/M_n
Ctrl-RS	5140	2635	2
VP-RS	3737	2204	2

The decrease in lignin molecular weight after VP treatment suggests that VP catalyzed the cleavage of lignin interunit linkages, resulting in a lower lignin molecular weight compared to for Ctrl-RS. This observation is consistent with previous studies on laccase-

treated RS lignin and manganese peroxidase-treated beech wood lignin, both of which also demonstrated a reduction in lignin's molecular weight. This reduction was attributed to the successful depolymerization of lignin into smaller lignin fragments.^{26,37}

4.2.6 FTIR spectroscopy analysis of raw and delignified RS

FTIR spectroscopy was employed to characterize the difference in chemical functional groups present in Ctrl-RS and VP-RS. The spectra, with the cyan line representing Ctrl-RS and the orange line representing VP-RS, are shown in Figure 4.5. I assigned the peaks by referencing literature (Table 4.5).^{33,38-43}

Table 4.5. Absorption peaks for rice straw lignin in the Fourier transform infrared spectrum

Wavenumber (cm ⁻¹)	Bands assignment
3350	Hydroxyl O-H stretching vibration
1650~1507	Aromatic ring C=C stretching
1423	C-H deformation
1325	Syringyl ring C-O stretching
1252	Guaiacyl ring C-O stretching
1032	C-O stretching

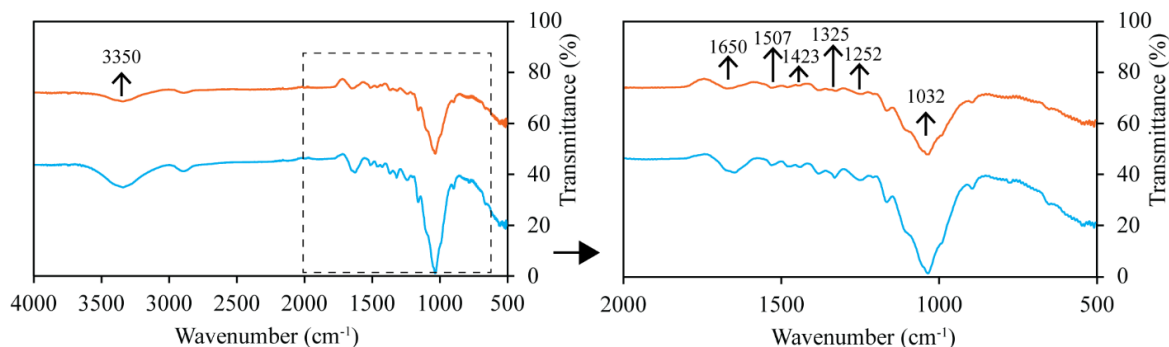


Figure 4.5. Left: FTIR spectra of Ctrl-RS (cyan) and VP-RS (orange). Right: Expansion of the 2000 to 500 cm⁻¹ region of the FTIR spectra.

The broad peak observed at 3350 cm^{-1} was attributed to O-H stretching, arising from hydrogen bonds within cellulose, hemicellulose, and lignin (Figure 4.5).^{33,39,43} The reduction in the intensity of this peak after VP treatment can be explained as the partial removal of lignin from RS and/or the disruption of hydrogen bonds within cellulose/hemicellulose.^{39,43}

Distinct lignin-specific peaks were identified at wavenumbers 1650 cm^{-1} and 1507 cm^{-1} , which correspond to the aromatic skeletal vibration of lignin characterized by conjugated C=C, alkenyl C=C stretch and aryl switched C=C functionalities (Figure 4.5).^{38,39,42} Notably, these peaks exhibited a noticeable decrease in intensity for VP-RS compared to Ctrl-RS, indicating the partial removal of lignin from RS catalyzed by VP.

A characteristic peak at 1423 cm^{-1} was attributed to the C-H deformation within methoxy groups inherent in lignin and hemicellulose (Figure 4.5).^{40,43,44} The decrease in intensity of this peak following VP treatment provides indicative evidence of lignin removal attributed to the VP treatment.⁴³

Characteristic peaks positioned at 1325 cm^{-1} and 1252 cm^{-1} were assigned to C-O stretching vibrations unique to syringyl and guaiacyl lignin, respectively (Figure 4.5).^{41,42} The noticeable reduction in peak intensities for these vibrations after VP treatment provides compelling support for the removal of both syringyl and guaiacyl lignin constituents from RS. Furthermore, a relevant lignin-related peak observed at 1032 cm^{-1} , which signifies C-O stretching, exhibited reduced intensity in VP-RS in comparison to Ctrl-RS, which is also consistent with lignin removal.^{33,38,41}

The outcomes indicated by FTIR analysis conclusively validated the delignification of lignin from RS achieved by VP treatment. Consequently, VP treatment effectively reduces

the recalcitrance of RS, promoting the subsequent enzymatic saccharification discussed in section 4.2.4.

4.2.7 Morphological characterization of raw and delignified RS

SEM images of Ctrl-RS and VP-RS were captured and evaluated (Figure 4.6), revealing distinctive differences in structural appearance between the two samples. Ctrl-RS (Figure 4.6A) exhibits a well-defined, compact, and crystalline structure, with a firm and tightly packed surface. In contrast, VP-RS (Figure 4.6B) displays a markedly different morphology. The structure of VP-RS appears rough, with evident distortions and a porous nature. These observations align with similar findings in other studies, where laccase-induced lignin degradation of rice straw and sugarcane tops resulted in surface disruption, increased porosity, and structural deformation.^{33,42}

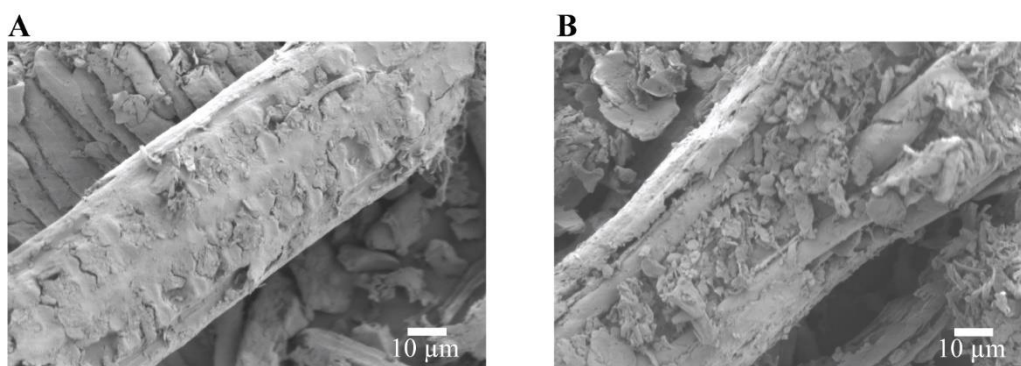


Figure 4.6. SEM images of Ctrl-RS (A) and VP-RS (B).

This distortion can be attributed to the removal of lignin from RS, resulting in the disruption of the cellulose-hemicellulose-lignin matrix following VP treatment.⁴² The higher

porosity observed in VP-RS allows for better permeability and accessibility, resulting in a larger surface area compared to in Ctrl-RS. This increased porosity in VP-RS facilitates improved accessibility of cellulases to the cellulose, explaining the higher yields of glucose and reducing sugars observed during the enzymatic saccharification of VP-RS, as discussed previously in section 4.2.4.

4.2.8 Effect of VP treatment on ethanol production from RS

Having successfully demonstrating the delignification of RS by VP in the previous sections, I investigated its impact on bioethanol production through simultaneous saccharification and fermentation. In this process, I employed a cellulolytic enzyme cocktail comprising a blend of commercial cellulase (Celluclast 1.5L) and glucosidase to convert the cellulose within RS into glucose, which was simultaneously fermented by *S. cerevisiae* into bioethanol.¹¹

The results, depicted in Figures 4.7A, 4.7B, and 4.7C, illustrate the concentrations of glucose, xylose, and ethanol produced during the simultaneous saccharification and fermentation of Ctrl-RS and VP-RS. Remarkably, the concentrations of glucose, xylose, and ethanol derived from VP-RS surpassed those obtained from Ctrl-RS.

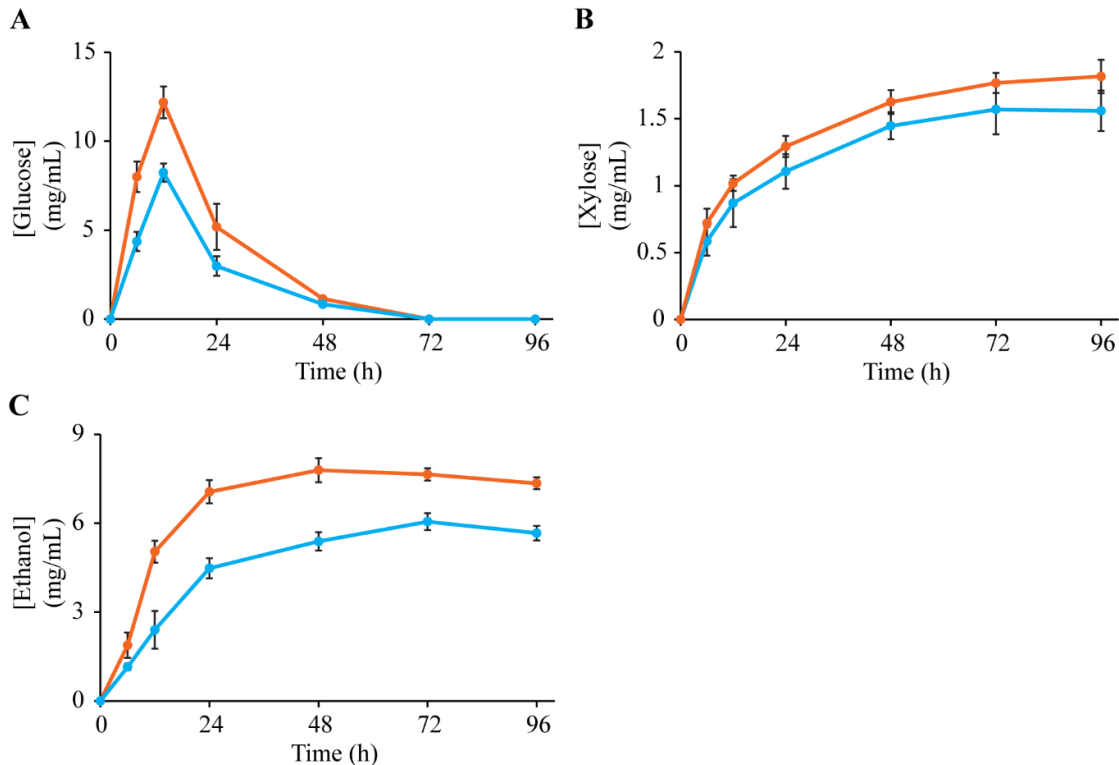


Figure 4.7. Time courses of the concentrations of glucose (A), xylose (B), and ethanol (C) produced on the simultaneous saccharification and fermentation of Ctrl-RS (cyan) and VP-RS (orange).

Figure 4.7A shows that glucose concentrations rapidly increased for both Ctrl-RS and VP-RS in the initial 12 hours of incubation, followed by gradual decreases as the incubation time progressed. At 12 hours of incubation, a substantial difference in glucose production became evident. VP-RS yielded a glucose concentration of 12.2 mg/mL, whereas Ctrl-RS only produced 8.2 mg/mL, indicating 1.5-fold enhancement in glucose production for VP-RS (Figure 4.7A). The decrease in glucose concentration beyond 12-hours for both Ctrl-RS and VP-RS indicates glucose consumption by *S. cerevisiae* surpasses the glucose production.

Meanwhile, the production of xylose from Ctrl-RS and VP-RS displayed a steady increase over the course of incubation (Figure 4.7B). After 96 hours of incubation, VP-RS

yielded a xylose concentration of 1.8 mg/mL, while Ctrl-RS produced 1.6 mg/mL, signifying 1.1-fold enhancement in xylose production for VP-RS (Figure 4.7B). In my study, I used a wild-type *S. cerevisiae* which does not consume xylose for its metabolic activity, hence, the xylose concentration did not decrease over the fermentation period.

The production of ethanol from Ctrl-RS increased steadily until the incubation time of 72 hours, followed by a decline thereafter (Figure 4.7C). Meanwhile, the production of ethanol from VP-RS increased steadily until the incubation time of 48 hours, followed by a decline thereafter (Figure 4.7C). At 48 hours of incubation, VP-RS had produced 7.8 mg/mL ethanol, whereas Ctrl-RS had yielded 5.4 mg/mL, signifying a noteworthy 1.4-fold increase in ethanol production for VP-RS (Figure 4.7C).

The elevated bioethanol production in VP-RS, compared to Ctrl-RS, can be attributed to the effective delignification of RS by the VP treatment, which results in effective saccharification. This was verified through Klason lignin quantification, SEC, FTIR, and SEM analyses. The delignification process disrupted the cellulose-hemicellulose-lignin matrix in RS, as corroborated by the SEM analysis discussed in section 4.2.7. This disruption significantly increased the internal surface area, enhancing cellulose accessibility to cellulase and substantially boosting the fermentable sugar yield. This higher yield of fermentable sugar is supposed to be directly translated into a greater quantity of bioethanol produced from VP-RS.

4.3 Conclusions

In this study, I harnessed the potential of VP, expressed in *P. pastoris*, as a biocatalyst for effectively delignifying RS at 30°C. My results unveiled 35% delignification of RS by VP (Table 4.3), demonstrating its effectiveness as an eco-friendly delignification biocatalyst. Following the delignification process, I conducted enzymatic saccharification for VP-RS, resulting in a 1.5-fold increase in glucose production and a 1.5-fold increase in reducing sugar production compared to those for Ctrl-RS. Additionally, SEC, FTIR, and SEM analyses demonstrated that VP disrupted the cellulose-hemicellulose-lignin matrix within RS. This disruption led to increased porosity and an expanded internal surface area, which, in turn, enhanced the cellulase accessibility to cellulose. These structural changes significantly improved the efficiency of enzymatic saccharification in VP-RS. Furthermore, this heightened efficiency in enzymatic saccharification is directly translated into a substantial 1.4-fold increase in bioethanol production for VP-RS compared to that for Ctrl-RS. In summary, my study highlights the potential of VP as a biocatalyst for both RS delignification and the enhancement of bioethanol production through an environmentally friendly approach.

4.4 Experimental procedures

4.4.1 Cloning and expression of VP gene in *Pichia pastoris*

The VP gene sequence from *Pleurotus eryngii* (UniprotKB/Swiss-Prot: O94753.1, VP) was codon optimized for expression in *Pichia pastoris* and synthesized by Thermo Fisher Scientific. Subsequently, the VP gene was amplified using the polymerase chain reaction (PCR) and ligated into the pPICZαA vector (Invitrogen, USA) at the *KpnI* and *XbaI*

restriction sites. The resulting construct, named pPICZ α A-VP, was linearized with *SacI* and introduced into competent *P. pastoris* X-33 (Invitrogen, USA) through electroporation. Transformants were then cultivated on YPDS agar medium (containing 1% yeast extract, 2% peptone, 2% glucose, 1 M sorbitol, 2% agar, and 100 μ g/mL zeocin) at 30 °C for three days. Positive clones were identified using a combination of colony PCR, a 1 mL-scale expression check, and an activity assay.

4.4.2 Optimizing the expression of VP

For the optimization of VP expression, a single colony of the confirmed transformant was inoculated into 10 mL of BMGY medium (1% yeast extract, 2% peptone, 1.34% yeast nitrogen base with ammonium sulfate, 0.1 M potassium phosphate (pH 6), 0.4 μ g/mL biotin, and 1% glycerol). The culture was then incubated at 30 °C with 200 rpm shaking until the optical density at 600 nm (OD_{600}) reached 4.0. To induce the expression of VP, the cells were harvested by centrifugation at $3,500 \times g$ for 5 min and resuspended in 10 mL of BMMY medium (1% yeast extract, 2% peptone, 1.34% yeast nitrogen base with ammonium sulfate, 0.1 M potassium phosphate (pH 6), 0.4 μ g/mL biotin, and 0.5% methanol) supplemented with 1 mM $CaCl_2$. The induction was carried out at 15 °C.

During the induction phase, hemin dissolved in different solvents was added to the BMMY medium. A total of five different hemin addition methods were tested. Three hemin stock solutions were prepared by dissolving 10 mg of hemin in 1 mL of 0.1 M KOH, 0.1 M NaOH, and 0.1 M NH_4OH . Meanwhile, hemin dissolved in DMSO was prepared by dissolving 32.6 mg of hemin in 1 mL of DMSO. Lastly, solid hemin was added directly to

the BMMY medium. Hemin stock was introduced cumulatively at 12 or 24 h intervals to reach a final concentration of 100 mg hemin per 1 L of BMMY medium after 72 h induction. In parallel, methanol (0.5% of culture volume) was also cumulatively added at 12 h intervals. As a control, induction without any addition of hemin was also performed. After 72 h induction, the supernatant containing the secreted VP was collected by centrifugation at $12,000 \times g$ for 5 min and the enzymatic activity of crude VP was determined using 2,6-dimethoxyphenol (DMP) as the substrate.

Next, optimization of the amount of hemin addition during the induction phase was performed. Hemin stock (10 mg/mL hemin in 0.1 M NH_4OH) was added every 12 h to reach a final concentration of 0 to 1000 mg of hemin per 1 L of BMMY medium after 72 h of induction. In parallel, methanol (0.5% of culture volume) was also cumulatively added at 12 h intervals. After 72 h of induction, the activity of secreted VP was determined using 2,6-dimethoxyphenol (DMP) as the substrate.

4.4.3 Production of VP

To produce VP, a single colony was inoculated into a 1 L baffled flask containing 200 mL of BMGY medium (1% yeast extract, 2% peptone, 1.34% yeast nitrogen base with ammonium sulfate, 0.1 M potassium phosphate (pH 6), 0.4 $\mu\text{g/mL}$ biotin, and 1% glycerol). The culture was maintained at 30 °C with constant agitation at 200 rpm until the optical density at 600 nm (OD_{600}) reached 4.0. At this point, the cells were harvested through centrifugation at $4,500 \times g$ for 5 min and then resuspended in BMMY medium (1% yeast extract, 2% peptone, 1.34% yeast nitrogen base with ammonium sulfate, 0.1 M potassium

phosphate (pH 6), 0.4 µg/mL biotin, and 0.5% methanol) to achieve an OD₆₀₀ of 1.0 to induce VP expression. During induction, a hemin stock solution (10 mg hemin dissolved in 1 mL of 0.1 M NH₄OH) was added cumulatively at either 12-hour or 24-hour intervals, a final concentration of 100 mg hemin per 1 L of BMMY medium being reached after 72 hours of induction. In parallel, methanol (0.5% of culture volume) was also added cumulatively at 12-hour intervals. The induction phase was performed at 15 °C for 72 hours.

After 72 hours, the culture supernatant containing secreted VP was collected by centrifugation at 8,000 × g for 30 minutes. Subsequently, the supernatant was filtered through a 300-kDa cut-off membrane (Pall, USA) using a Minimate TFF system (OAPMP110, Pall) to remove cell debris. The resulting cell-free supernatant was concentrated 40-fold and then underwent buffer exchange to 50 mM sodium malonate (pH 4) using a 10-kDa cut-off membrane (Pall, USA). The resulting solution, referred to as crude VP, was stored at 4 °C for future use.

4.4.4 Enzymatic activity assessment of VP using monomeric substrates

The enzymatic activity of crude VP was evaluated using three monomeric substrates: veratryl alcohol (VA), 2,6-dimethoxyphenol (DMP), and guaiacol (Figure 4.2). The assays were conducted at 25 °C in 200 µL of reaction mixture containing 10 µL of crude VP, 1 mM substrate, MnSO₄ (0 or 2 mM), and 0.5 mM H₂O₂. The pH conditions were adjusted using either 125 mM sodium tartrate (for pH 3) or 50 mM sodium malonate (for pH 4-7).

For VA, the formation of veratryl aldehyde was monitored by measuring the increase in absorbance at 310 nm using a UV-Vis spectrophotometer (Shimadzu UV-1900i, Japan).

For DMP and guaiacol, the formation of the dimeric product was monitored by measuring the increase in absorbance at 469 nm (DMP) and 470 nm (guaiacol) using an Infinite[®] 200 PRO spectrophotometer (TECAN). The product's quantity was determined using the molar absorption coefficient of each product: VA ($\epsilon_{310} = 9,300/\text{M cm}$), DMP ($\epsilon_{469} = 24,800/\text{M cm}$), and guaiacol ($\epsilon_{470} = 26,600/\text{M cm}$).⁴⁵⁻⁴⁸

Enzyme activity was expressed in units (U), defined as the amount of VP required to catalyze the production of 1 μmol of product per minute under the specified assay conditions.

4.4.5 Enzymatic activity assessment of VP using dimeric substrates

The enzymatic activity of crude VP was evaluated using two dimeric substrates: guaiacylglycerol- β -guaiacyl ether (GGE, TCI, Japan) and syringylglycerol- β -guaiacyl ether (SGE, Merck) (Figure 4.3). The reaction was performed at 25 °C in a 1 mL reaction mixture containing 50 mM sodium malonate (pH 4), 1 mM substrate, 0.694 mU VP, and 2 mM MnSO_4 . Reactions were initiated by adding H_2O_2 (0-50 mM), followed by incubation for 12 hours. After 12 hours, the reactions were terminated by heating at 95 °C for 10 minutes.

The resulting products were analyzed using a reverse-phase high-performance liquid chromatography (RP-HPLC) system (Shimadzu, Japan), equipped with an SPD-20A UV-Vis detector set to monitor absorbance at 280 nm. To prepare the samples for RP-HPLC analysis, acetonitrile (ACN) was added to the reaction product (GGE or SGE treated with VP) to adjust the final concentration to 5% ACN, and the resulting mixture was filtered through a 0.2 μm polytetrafluoroethylene (PTFE) membrane. For analysis, 20 μL of the filtered sample was injected into a TSKgel ODS-80T_M (6.0 \times 150 mm, Tosoh, Japan) analytical column, which

was maintained at 45 °C throughout the analysis. The mobile phases consisted of water (eluent A) and ACN (eluent B), both containing 0.1% trifluoroacetic acid. The elution profile used was as follows: an isocratic step at 5% B for 0-5 min, a linear gradient from 5 to 40% B over 5-15 min, a linear gradient from 40 to 95% B over 15-40 min, an isocratic step at 95% B for 40-45 min, a linear gradient from 95 to 5% B over 45-46 min, and an isocratic step at 5% B for 47-52 min. The flow rate was set at 0.5 mL/min.

Conversion of the substrate was estimated based on its peak area on the chromatograms before and after the reaction. Two independent experiments were performed to determine the mean and standard deviation.

4.4.6 Preparation of rice straw

Rice straw (RS) obtained from Nagano, Japan, was finely pulverized and sieved to achieve a particle size smaller than 40-mesh. The resulting straw powder was subjected to Soxhlet extraction with acetone for 24 hours, followed by overnight drying at 40 °C. The resulting solid was thoroughly washed with water until the supernatant became nearly colorless. The solid was subsequently lyophilized, yielding the raw RS used in this study.

4.4.7 VP-catalyzed delignification of rice straw

The delignification of RS using VP was performed using an ultrafiltration stirred cell (UFSC40001, Merck) equipped with a 76 mm diameter, 1 kDa cut-off RC membrane disc (PLAC07610, Merck).²⁸ The reaction mixture was composed of 5 g RS, 2 mM MnSO₄, and 15 U VP, in a total volume of 300 mL, adjusted to a pH of 4 with 50 mM sodium malonate.

The reaction was initiated by adding 1 mM H₂O₂ and conducted with magnetic stirring at 30 °C for 24 hours. At the start of the reaction, the mixture's surface was pressurized to 4 bar with air, which resulted in a filtration rate of approximately 15 mL/h. Every 6 hours, 90 mL of 50 mM sodium malonate (pH 4), containing 2 mM MnSO₄ and 1 mM H₂O₂, was added to the reaction vessel. The same procedure was followed in the control experiment, except VP was omitted.

After 24 hours, the solid residue remaining in the reaction vessel was collected. The solid residue obtained on treatment with VP (VP-RS) and without VP (Ctrl-RS) was thoroughly washed with water until a nearly colorless supernatant was obtained. Subsequently, the washed residue was suspended to a concentration of 0.25 g/mL using 50 mM sodium citrate (pH 4.8) for subsequent saccharification and fermentation experiments. For composition, SEC, SEM, and FTIR analyses, the washed solid residue was lyophilized prior to further analysis.

4.4.8 Composition analysis of rice straw by the Klason lignin method

The cellulose, hemicellulose, and lignin contents of raw RS, Ctrl-RS, and VP-RS were determined using the laboratory analytical procedure (LAP) established by the National Renewable Energy Laboratory (NREL).⁴⁹ In brief, a 100 mg sample was subjected to hydrolysis with 1 mL of 72% w/w H₂SO₄ for 1 hour at 30 °C. Subsequently, the solution was diluted to 4% w/w H₂SO₄ using hot water and then autoclaved for 1 hour at 121 °C. The resulting hydrolyzed sample was filtered to separate the hydrolysis liquor from the acid-insoluble residue.

The hydrolysis liquor was used to determine acid-soluble lignin through UV-spectroscopy at a wavelength of 282 nm.⁵⁰ The glucan and xylan contents of the hydrolysis liquor were measured using a high-performance liquid chromatography (HPLC) system, as detailed in a subsequent section.

The acid-insoluble residue, collected through the filtration was thoroughly washed with water, followed by drying at 105 °C until a constant weight was attained, after which it was weighed. This dried acid-insoluble residue was then subjected to heating at 575 °C for 6 hours in a muffle furnace to determine the ash content. The difference in weight between the acid-insoluble residue and ash content represented acid-insoluble lignin in the sample. The summation of acid-insoluble and acid-soluble lignin represented the total lignin content of the sample.

The extent of delignification achieved was calculated using Eq. (4.1), where $m_{\text{lignin in raw RS}}$ represents the total lignin mass within raw RS, and $m_{\text{lignin in sample}}$ the total lignin mass within the sample (VP-RS and Ctrl-RS).⁵⁰

$$\text{Delignification (\%)} = \frac{m_{\text{lignin in raw RS}} - m_{\text{lignin in sample}}}{m_{\text{lignin in raw RS}}} \times 100 \quad (4.1)$$

4.4.9 HPLC analysis

The contents of glucose, xylose, and ethanol in the samples were determined using a HPLC system (Shimadzu, Japan) equipped with a refractive index detector (RID-20A, Shimadzu). The analysis was performed utilizing an Aminex HPX-87H (Bio-Rad Laboratories, Hercules, CA, USA) analytical column maintained at 60 °C. The mobile phase consisted of a 5 mM H₂SO₄ solution at a flow rate of 0.6 ml/min. To quantify the compounds

present in the samples, a calibration curve was established using standards with varying concentrations of glucose, xylose, and ethanol. Prior to analysis, samples were diluted four-fold with 5 mM H₂SO₄ and filtered through a 0.2 µm hydrophilic polytetrafluoroethylene (PTFE) membrane. Subsequently, 10 µL of each sample was injected into the HPLC system for analysis.

4.4.10 Molecular weight analysis of treated rice straw

The molecular weight distributions of lignin within Ctrl-RS and VP-RS were determined using size-exclusion chromatography (SEC). A sample (Ctrl-RS or VP-RS) was pretreated as follows. The sample was ball-milled using a Fritsch P-6 planetary mono mill, 500 mg of the sample being added to an 80 mL agate jar containing 100 g of 3 mm ZrO₂ beads. The milling was performed under a nitrogen environment at 550 rpm for 1.5 h (90 cycles of 1 min milling with 1 min intervals). The milled solid was repeatedly washed with water and then lyophilized. 10 mg of the lyophilized solid was treated twice with 1.5 FPU of a cellulolytic enzyme cocktail (CellicCtec2, Novozymes, Denmark) in 50 mM sodium citrate (pH 4.8) at 50 °C for 72 h to yield cellulolytic enzyme lignin (CEL). CEL was then acetylated by incubation in 500 µL of a 1:1 v/v mixture of anhydrous pyridine and acetic anhydride for 24 h at 50 °C with shaking. The acetylated sample was then co-evaporated with toluene to remove the reagents. The obtained acetylated CEL was dissolved in tetrahydrofuran, and the soluble fraction was passed through a 0.2 µm PTFE filter. 10 µL of the filtered sample was injected into a HPLC system equipped with an SPD M20A photo diode array detector and three tandemly connected TSKgel SuperMultiporeHZ-M analytical columns (4.6 × 150 mm,

Tosoh, Japan). The analysis was performed at 40 °C using tetrahydrofuran as a mobile phase at a flow rate of 0.35 mL/min.

Calibration curves were constructed using a series of polystyrene standards (PStQuickC, weight-average molecular weight (M_w) = 5970-2110000, Tosoh), 1-(3,4-Dimethoxyphenyl)-2-(2-methoxyphenoxy)-1,3-propanediol (M_w = 334), and vanillin (M_w = 152). LabSolutions software (Shimadzu) was employed to determine the M_w , number-average molecular weight (M_n), and polydispersity index (M_w/M_n) for the samples.

4.4.11 Structural morphology analysis of treated rice straw

The structural morphology of the Ctrl-RS and VP-RS samples was assessed using a scanning electron microscope (SEM). The samples were uniformly spread on a conductive adhesive strip with a thickness of less than 1 cm. Subsequently, a gold coating was applied to the samples, which were then subjected to SEM analysis using a VE-9800 SEM instrument from KEYENCE, Japan.

4.4.12 Fourier transform infrared spectroscopy analysis of treated rice straw

Fourier transform infrared spectroscopy (FTIR) was employed to evaluate changes in functional groups resulting from VP-treatment. FTIR spectra of Ctrl-RS and VP-RS samples were generated using a PerkinElmer UATR Two FTIR spectrometer. Scans were conducted within the spectral range of 4000-400 cm^{-1} with a detector resolution of 2 cm^{-1} .

4.4.13 Enzymatic saccharification of treated rice straw

Enzymatic saccharification of RS was conducted using a cellulolytic enzyme cocktail comprising cellulase (Celluclast 1.5L, Novozymes, Denmark) and glucosidase from *Aspergillus niger*. The saccharification was carried out in a 10 mL reaction mixture in a Falcon tube, containing 50 mM sodium citrate (pH 4.8), 0.3 g sample (Ctrl-RS or VP-RS), 0.4 FPU Celluclast 1.5L (equivalent to 2 FPU/g substrate), and 1.2 U glucosidase (equivalent to 6 U/g substrate). The reaction was performed for 96 hours at 30 °C with continuous shaking. To prevent microbial contamination, sodium azide (20 mg/L) was included in the reaction mixture.

At specific time points (0, 24, 48, 72, and 96 hours), samples were collected and subsequently centrifuged at $12,000 \times g$ for 5 minutes to separate the supernatants for analysis. Glucose concentrations were determined using the HPLC system described earlier. The concentration of reducing sugar was determined using the dinitro salicylic acid method (DNS), with glucose as the standard for quantification.⁵¹

4.4.14 Simultaneous saccharification and fermentation of treated rice straw

The simultaneous saccharification and fermentation (SSF) of RS was conducted using *Saccharomyces cerevisiae* strain D452-2.^{52,53} The process was carried out in a flask, containing a fixed volume of 30 mL of 50 mM sodium citrate (pH 4.8), containing *S. cerevisiae* ($OD_{600} = 0.5$), 1% yeast extract, 2% peptone, 3 g of the sample (Ctrl-RS or VP-RS), 24 FPU of Celluclast 1.5L (equivalent to 8 FPU/g substrate), and 24 U of glucosidase

(equivalent to 8 U/g substrate). The SSF process was conducted at 30 °C with continuous shaking for 96 hours.

Samples were collected at designated time intervals (0, 24, 48, 72, and 96 hours), and subsequently centrifuged at $12,000 \times g$ for 5 minutes to separate the supernatants for analysis. The concentrations of glucose, xylose, and ethanol produced during the SSF were determined using the HPLC system described earlier.

4.5 References

1. Vázquez, V.; Giorgi, V.; Bonfiglio, F.; Menéndez, P.; Gioia, L.; Ovsejevi, K. Lignocellulosic residues from bioethanol production: a novel source of biopolymers for laccase immobilization. *RSC Adv.* 2023, **13**, 13463-13471.
2. Panahi, H. K. S.; Dehhaghi, M.; Kinder, J. E.; Ezeji, T. C. A review on green liquid fuels for the transportation sector: a prospect of microbial solutions to climate change. *Biofuel Res. J.* 2019, **6**, 995-1024.
3. Mostafaeipour, A.; Sedaghat, A.; Hedayatpour, M.; Jahangiri, M. Location planning for production of bioethanol fuel from agricultural residues in the south of Caspian Sea. *Environ. Dev.* 2020, **33**, 100500.
4. Ibarra, D.; Eugenio, M. E.; Alvira, P.; Ballesteros, I.; Ballesteros, M.; Negro, M. J. Effect of Laccase Detoxification on Bioethanol Production from Liquid Fraction of Steam-Pretreated Olive Tree Pruning. *Fermentation* 2023, **9**(3), 214.

5. Xiang, H.; Xin, R.; Prasongthum, N.; Natewong, P.; Sooknoi, T.; Wang, J.; Reubroycharoen, P.; Fan, X. Catalytic conversion of bioethanol to value-added chemicals and fuels: A review. *RCM* 2022, **1**, 47-68.
6. Dagle, R. A.; Winkelman, A. D.; Ramasamy, K. K.; Dagle, V. L.; Weber, R. S. Ethanol as a Renewable Building Block for Fuels and Chemicals. *Ind. Eng. Chem. Res.* 2020, **59**(11), 4843-4853.
7. Kumar, V.; Patel, S. K. S.; Gupta, R. K.; Otari, S. V.; Gao, H.; Lee, J.; Zhang, L. Enhanced saccharification and fermentation of rice straw by reducing the concentration of phenolic compounds using an immobilized enzyme cocktail. *Biotechnol. J.* 2019, **14**(6), 1800468.
8. Kumari, D.; Singh, R. Rice straw structure changes following green pretreatment with petha wastewater for economically viable bioethanol production. *Sci. Rep.* 2022, **12**, 10443.
9. Bušić, A.; Marđetko, N.; Kundas, S.; Morzak, G.; Belskaya, H.; Šantek, M. I.; Komes, D.; Novak, S.; Šantek, B. Bioethanol Production from Renewable Raw Materials and Its Separation and Purification: A Review. *Food Technol. Biotechnol.* 2018, **56**(3), 289-311.
10. Wang, F.; Jiang, Y.; Guo, W.; Niu, K.; Zhang, R.; Hou, S.; Wang, M.; Yi, Y.; Zhu, C.; Jia, C.; Fang, X. An environmentally friendly and productive process for bioethanol production from potato waste. *Biotechnol. Biofuels* 2016, **9**, 50.

11. Takano, M.; Hoshino, K. Bioethanol production from rice straw by simultaneous saccharification and fermentation with statistical optimized cellulase cocktail and fermenting fungus. *Bioresour. Bioprocess.* 2018, **5**, 16.
12. Park, J. M.; Oh, B.; Seo, J.; Hong, W.; Yu, A.; Sohn, J.; Kim, C. H. Efficient production of ethanol from empty palm fruit bunch fibers by fed-batch simultaneous saccharification and fermentation using *Saccharomyces cerevisiae*. *Appl. Biochem. Biotechnol.* 2013, **170**(8),1807-14.
13. Terrett, O. M.; Dupree, P. Covalent interactions between lignin and hemicelluloses in plant secondary cell walls. *Curr. Opin. Biotechnol.* 2019, **56**, 97-104.
14. Sawhney, D.; Vaid, S.; Bangotra, R.; Sharma, S.; Dutt, H. C.; Kapoor, N.; Mahajan, R.; Bajaj, B. K. Proficient bioconversion of rice straw biomass to bioethanol using a novel combinatorial pretreatment approach based on deep eutectic solvent, microwave irradiation and laccase. *Bioresour. Technol.* 2023, **375**, 128791.
15. Li, H.; Xiao, W.; Liu, J.; Ran, Q.; Wang, R.; Yu, C.; Zhang, X.; Song, H.; Jiang, Z. Combination strategy of laccase pretreatment and rhamnolipid addition enhance ethanol production in simultaneous saccharification and fermentation of corn stover. *Bioresour. Technol.* 2022, **345**, 126414.
16. Sharma, S.; Tsai, M.; Sharma, V.; Sun, P.; Nargotra, P.; Bajaj, B. K.; Chen, C.; Dong, C. Environment Friendly Pretreatment Approaches for the Bioconversion of Lignocellulosic Biomass into Biofuels and Value-Added Products. *Environments* 2023, **10**(1), 6.

17. Haq, I.; Qaisar, K.; Nawaz, A.; Akram, F.; Mukhtar, H.; Zohu, X.; Xu, Y.; Mumtaz, M. W.; Rashid, U.; Ghani, W. A. W. A. K.; Choong, T. S. Y. Advances in Valorization of Lignocellulosic Biomass towards Energy Generation. *Catalysts* 2021, **11**(3), 309.
18. Rencoret, J.; Pereira, A.; Río, J. C.; Martínez, Á. T.; Gutiérrez, A. Delignification and Saccharification Enhancement of Sugarcane Byproducts by a Laccase-Based Pretreatment. *ACS Sustainable Chem. Eng.* 2017, **5**(8), 7145–7154.
19. Ruiz-Dueñas, F. J.; Martínez, A. T. Microbial degradation of lignin: how a bulky recalcitrant polymer is efficiently recycled in nature and how we can take advantage of this. *Microb. Biotechnol.* 2009, **2**(2), 164-77.
20. Wang, X.; Yao, B.; Su, X. Linking Enzymatic Oxidative Degradation of Lignin to Organics Detoxification. *Int. J. Mol. Sci.* 2018, **19**(11), 3373.
21. Ruiz-Dueñas, F. J.; Morales, M.; García, E.; Miki, Y.; Martínez, M. J.; Martínez, A. T. Substrate oxidation sites in versatile peroxidase and other basidiomycete peroxidases. *J. Exp. Bot.* 2009, **60**(2), 441-52.
22. Barber-Zucker, S.; Mindel, V.; Garcia-Ruiz, E.; Weinstein, J. J.; Alcalde, M.; Fleishman, S. J. Stable and Functionally Diverse Versatile Peroxidases Designed Directly from Sequences. *J. Am. Chem. Soc.* 2022, **144**(8), 3564-3571.
23. Tsukihara, T.; Honda, Y.; Sakai, R.; Watanabe, T.; Watanabe, T. Mechanism for Oxidation of High-Molecular-Weight Substrates by a Fungal Versatile Peroxidase, MnP2. *Appl. Environ. Microb.* 2008, **74**, 9.

24. Kamitsuji, H.; Watanabe, T.; Honda, Y.; Kuwahara, M. Direct oxidation of polymeric substrates by multifunctional manganese peroxidase isoenzyme from *Pleurotus ostreatus* without redox mediators. *Biochem. J.* 2005, **386**(2), 387-393.
25. Lin, M.; Nagata, T.; Katahira, M. High yield production of fungal manganese peroxidases by *E. coli* through soluble expression, and examination of the activities. *Protein Expr. Purif.* 2018, **145**, 45-52.
26. Lambertz, C.; Garvey, M.; Klinger, J.; Heesel, D.; Klose, H.; Fischer, R.; Commandeur, U. Challenges and advances in the heterologous expression of cellulolytic enzymes: a review. *Biotechnol. Biofuels* 2014, **7**, 135.
27. Karbalaei, M.; Rezaee, S. A.; Farsiani, H. *Pichia pastoris*: A highly successful expression system for optimal synthesis of heterologous proteins. *J. Cell Physiol.* 2020, **235**(9), 5867-5881.
28. Teo, K. S. K.; Kondo, K.; Saito, K.; Iseki, Y.; Watanabe, T.; Nagata, T.; Katahira, M. Enhanced depolymerization of beech wood lignin and its removal with peroxidases through continuous separation of lignin fragments. *Green Chem.* 2023, **25**, 7682-7695.
29. Jiang, F.; Kongsaree, P.; Charron, R.; Lajoie, C.; Xu, H.; Scott, G.; Kelly, C. Production and Separation of Manganese Peroxidase from Heme Amended Yeast Cultures. *Biotechnol. Bioeng.* 2008, **99**(3), 540-9.

30. Hilgers, R.; Erven, G.; Boerkamp, V.; Sulaeva, I.; Potthast, A.; Kabel, M. A.; Vincken, J. Understanding laccase/HBT-catalyzed grass delignification at the molecular level. *Green Chem.* 2020, **22**, 1735-1746.
31. Li, J.; Tang, X.; Chen, S.; Zhao, J.; Shao, T. Ensiling pretreatment with two novel microbial consortia enhances bioethanol production in sterile rice straw. *Bioresour. Technol.* 2021, **339**, 125507.
32. Das, N.; Jena, P. K.; Padhi, D.; Mohanty, M. K.; Sahoo, G. A comprehensive review of characterization, pretreatment and its applications on different lignocellulosic biomass for bioethanol production. *Biomass Convers. Biorefin.* 2023, **13**, 1503-1527.
33. Nazar, M.; Xu, L.; Ullah, M. W.; Moradian, J. M.; Wang, Y.; Sethupathy, S.; Iqbal, B.; Nawaz, M. Z.; Zhu, D. Biological delignification of rice straw using laccase from *Bacillus ligniniphilus* L1 for bioethanol production: A clean approach for agro-biomass utilization. *J. Clean. Prod.* 2022, **360**, 132171.
34. Sannigrahi, P.; Miller, S. J.; Ragauskas, A. J. Effects of organosolv pretreatment and enzymatic hydrolysis on cellulose structure and crystallinity in Loblolly pine. *Carbohydr. Res.* 2010, **345**(7), 965-970.
35. Heap, L.; Green, A.; Brown, D.; Dongen, B.; Turner, N. Role of laccase as an enzymatic pretreatment method to improve lignocellulosic saccharification. *Catal. Sci. Technol.* 2014, **4**, 2251-2259.

36. Palonen, H.; Viikari, L. Role of Oxidative Enzymatic Treatments on Enzymatic Hydrolysis of Softwood. *Biotechnol. Bioeng.* 2004, **86**(5), 550-7.
37. Zhang, W.; Wang, W.; Wang, J.; Shen, G.; Yuan, Y.; Yan, L.; Tang, H.; Wang, W. Isolation and Characterization of a Novel Laccase for Lignin Degradation, LacZ1. *Appl. Environ. Microbiol.* 2021, **87**, 23.
38. Bhardwaj, N.; Kumar, B.; Agrawal, K.; Verma, P. Bioconversion of rice straw by synergistic effect of in-house produced ligno-hemicellulolytic enzymes for enhanced bioethanol production. *Bioresour. Technol. Rep.* 2020, **10**, 100352.
39. Zhao, C.; Shao, Q.; Ma, Z.; Li, B.; Zhao, X. Physical and chemical characterizations of corn stalk resulting from hydrogen peroxide presoaking prior to ammonia fiber expansion pretreatment. *Ind. Crops Prod.* 2016, **83**, 86-93.
40. Bhattacharyya, P.; Bhaduri, D.; Adak, T.; Munda, S.; Satapathy, B.S.; Dash, P.K.; Padhy, S.R.; Pattanayak, A.; Routray, S.; Chakraborti, M.; Baig, M.J.; Mukherjee, A.K.; Nayak, A.K.; Pathak, H. Characterization of rice straw from major cultivars for best alternative industrial uses to cut off the menace of straw burning. *Ind. Crops Prod.* 2020, **143**, 111919.
41. Nazar, M.; Xu, Q.; Zahoor; Ullah, M. W.; Khan, N. A.; Iqbal, B.; Zhu, D. Integrated laccase delignification with improved lignocellulose recalcitrance for enhancing enzymatic saccharification of ensiled rice straw. *Ind. Crops Prod.* 2023, **202**, 116987.

42. Sherpa, K. C.; Ghangrekar, M. M.; Banerjee, R. A green and sustainable approach on statistical optimization of laccase mediated delignification of sugarcane tops for enhanced saccharification. *J. Environ. Manage.* 2018, **217**, 700-709.
43. Ma, Y.; Chen, X.; Khan, M. Z.; Xiao, J.; Liu, S.; Wang, J.; Alugongo, G. M.; Cao, Z. Biodegradation and hydrolysis of rice straw with corn steep liquor and urea alkali pretreatment. *Front. Nutr.* 2022, **9**, 989239.
44. Guo, G.; Chen, W.; Chen, W.; Men, L.; Hwang, W. Characterization of dilute acid pretreatment of silver grass for ethanol production. *Bioresour. Technol.* 2008, **99**(14), 6046-6053.
45. Forootanfar, H.; Faramarzi, M. A. Insights into Laccase Producing Organisms, Fermentation States, Purification Strategies, and Biotechnological Applications. *Biotechnol Prog.* 2015, **31**(6), 1443-63.
46. Roy, J. J.; Abraham, T. E. Preparation and characterization of cross-linked enzyme crystals of laccase. *J. Mol. Catal., B Enzym.* 2006, **38**(1), 31-36.
47. Durão, P.; Bento, I.; Fernandes, A. T.; Melo, E. P.; Lindley, P. F.; Martins, L. O. Perturbations of the T1 copper site in the CotA laccase from *Bacillus subtilis*: structural, biochemical, enzymatic and stability studies. *J. Biol. Inorg. Chem.* 2006, **11**(4), 514-26.
48. Mester, T.; Field, J. A. Characterization of a Novel Manganese Peroxidase-Lignin Peroxidase Hybrid Isozyme Produced by *Bjerkandera* Species Strain BOS55 in the Absence of Manganese. *J. Biol. Chem.* 1998, **273**(25), 15412-15417.

49. Sluiter, A.; Hames, B.; Ruiz, R.; Scarlata, C.; Sluiter, J.; Templeton, D.; Crocker, D. Determination of Structural Carbohydrates and Lignin in Biomass. National Renewable Energy Laboratory 2008.
50. Mukherjee, A.; Banerjee, S.; Halder, G. Parametric optimization of delignification of rice straw through central composite design approach towards application in grafting. *J. Adv. Res.* 2018, **14**, 11-23.
51. Miller, G. L. Use of Dinitrosalicylic Acid Reagent for Determination of Reducing Sugar. *Anal. Chem.* 1959, **31**(3), 426–428.
52. Khattab, S. M. R.; Kodaki, T. Efficient bioethanol production by overexpression of endogenous *Saccharomyces cerevisiae* xylulokinase and NADPH-dependent aldose reductase with mutated strictly NADP⁺-dependent *Pichia stipitis* xylitol dehydrogenase. *Process Biochem.* 2014, **49**(11), 1838-1842.
53. Hosaka, K.; Nikawa, J.; Kodaki, T.; Yamashita, S. A dominant mutation that alters the regulation of INO1 expression in *Saccharomyces cerevisiae*. *J. Biochem.* 1992, **111**(3), 352-8.

Chapter 5

Conclusions

In this study, I successfully expressed three distinct ligninolytic enzymes: MnP, LiP, and VP in *Pichia pastoris* and demonstrated their catalytic activities across various substrates. My investigation primarily centered on evaluating their potential for the valorization of lignocellulosic biomass, shedding light on new possibilities for sustainable biomass valorization.

Chapter 2 delves into the intricate catalytic mechanisms of CsMnP, with a specific emphasis on its application in the valorization of Kraft lignin. Through a rigorous exploration of CsMnP's enzymatic characteristics using a phenolic-type lignin model dimer (GGE) as the substrate, I uncovered valuable insights. Notably, I observed that CsMnP's catalytic activity requires the presence of hydrogen peroxide (H_2O_2) and can be further enhanced by the addition of $MnSO_4$. My analysis of reaction products, facilitated by RP-HPLC, SEC, and 2D NMR techniques, unveiled the formation of polymerized products derived from GGE. Additionally, I successfully identified a predominant product as a biphenyl GGE linked at the 5-5' position of the phenolic ring. Furthermore, my examination of CsMnP's application in the polymerization of Kraft lignin unveiled a significant reduction in phenolic content and a substantial increase in molecular weight compared to the pre-reaction state. NMR analysis provided further support for this successful polymerization. Overall, Chapter 2 presents novel insights into CsMnP's enzymatic properties and its potential as a biocatalyst for synthesizing lignin-based products through polymerization reactions.

Chapter 3 presents a pivotal investigation into the application of MnP and LiP as biocatalysts for lignin depolymerization in beech wood. Addressing the challenge of reactive lignin fragments repolymerization, I introduced a membrane bioreactor equipped with a 3

kDa membrane to efficiently separate these fragments from the reaction medium. The results were impressive, with up to a 2.5-fold increase in lignin removal compared to conventional batch bioreactors, all achieved without the need for additional chemicals or solvents. This enhanced depolymerization process, coupled with the successful isolation of valuable aromatics like vanillin, holds great promise for downstream applications in the production of valuable biochemicals. Moreover, the saccharification efficiency of the remaining lignocellulosic materials significantly improved, highlighting the substantial advantages of employing a membrane bioreactor for lignin depolymerization.

Chapter 4 introduces a promising approach utilizing versatile peroxidase (VP) for lignin removal from rice straw, a valuable agricultural residue with substantial potential for bioethanol production. VP's selective lignin removal, facilitated within a membrane bioreactor, resulted in a remarkable 35% delignification of rice straw at 30 °C. This process disrupted the cellulose-hemicellulose-lignin matrix within rice straw, increasing porosity and the internal surface area, ultimately enhancing cellulase accessibility to cellulose. As a result, glucose and bioethanol production exhibited remarkable increases, with VP-treated rice straw outperforming its counterpart by up to 1.5-fold and 1.4-fold, respectively. These findings emphasize the environmentally friendly potential of VP for delignifying rice straw and significantly improving bioethanol production.

In summary, my study successfully developed methodologies for the expression of MnP, LiP, and VP using *Pichia pastoris* and confirmed their catalytic activity. The applications of these peroxidases for the valorization of technical lignin and lignocellulosic biomass open exciting avenues for sustainable biomass utilization. Looking forward, my

research aims to further manipulate the outcomes of peroxidase-catalyzed reactions towards high-value bioproducts. Additionally, I intend to explore the synergistic potential of MnP, LiP, and VP to achieve even more efficient lignin delignification. This research paves the way for greener and more sustainable pathways in biomass utilization.

List of publications

1. Understanding manganese peroxidase-catalyzed conversion of the lignin structure and its application for the polymerization of Kraft lignin

Kenneth Sze Kai TEO, Keiko Kondo, Takashi Watanabe, Takashi Nagata, Masato Katahira

ACS Sustainable Chemistry & Engineering, 2024

DOI: 10.1021/acssuschemeng.3c05635

(Chapter 2)

2. Enhanced depolymerization of beech wood lignin and its removal with peroxidases through continuous separation of lignin fragments

Kenneth Sze Kai TEO, Keiko Kondo, Kaori Saito, Yu Iseki, Takashi Watanabe, Takashi Nagata, Masato Katahira

Green Chemistry, 2023, **25**, 7682-7695

DOI: 10.1039/D3GC01246H

(Chapter 3)

3. Enhancing bioethanol production from rice straw through environmentally-friendly delignification using versatile peroxidase

Kenneth Sze Kai TEO, Keiko Kondo, Sadat Mohamed Rezk Khattab, Takashi Watanabe, Takashi Nagata, Masato Katahira

Journal of Agricultural and Food Chemistry, 2024

DOI: 10.1021/acs.jafc.3c07998

(Chapter 4)

List of other publications

1. Fermentation of Microalgae Biomass through Mild Acid Pretreatment for Bioethanol Production

Lee Muei Chng, **Kenneth Sze Kai TEO**, Derek Juinn Chieh Chan, Keat Teong Lee, Pey Yi Toh

Journal of Energy and Safety Technology, **1**, 2

DOI: 10.11113/jest.v1n2-2.27

2. Structure-based characterization and improvement of an enzymatic activity of

Acremonium alcalophilum feruloyl esterase

Apisan Phienluphon, Keiko Kondo, Bunzo Mikami, **Kenneth Sze Kai TEO**, Kaori Saito, Takashi Watanabe, Takashi Nagata, Masato Katahira

ACS Sustainable Chemistry & Engineering (under review)

List of presentations

1. Heterologous expression and oxidative activity of four fungal ligninolytic enzymes by *Pichia pastoris*

Kenneth Sze Kai TEO, Keiko Kondo, Takashi Nagata, Masato Katahira

The 2020 Annual Meeting of The Japan Society for Bioscience, Biotechnology and Agrochemistry (日本農芸化学会 2020 年度大会)

2. Enzymatic treatment of lignin from rice straw with heterologously expressed fungal ligninolytic enzymes

Kenneth Sze Kai TEO, Keiko Kondo, Takashi Nagata, Masato Katahira

The 70th Annual Meeting of The Japan Wood Research Society in TOTTORI (第 70 回 日本木材学会大会 2020)

3. Boost in beech wood's lignin degradation by heterogeneously expressed manganese peroxidase by using a semi-continuous bioreactor system

Kenneth Sze Kai TEO, Keiko Kondo, Takashi Nagata, Masato Katahira

The 72nd Annual Meeting of Japan Wood Research Society (第 72 回 日本木材学会大会 2022)

4. Boost in beech wood's lignin degradation by heterogeneously expressed manganese peroxidase by using a semi-continuous bioreactor system

Kenneth Sze Kai TEO, Keiko Kondo, Kaori Saito, Yu Iseki, Takashi Watanabe, Takashi Nagata, Masato Katahira

The 22nd Young NMR Research Group (第 22 回 若手 NMR 研究会 2022)

5. The molecular level elucidation of a *Ceriporiopsis subvermispora* manganese peroxidase-catalyzed conversion of a phenolic lignin dimer

Kenneth Sze Kai TEO, Keiko Kondo, Takashi Watanabe, Takashi Nagata, Masato Katahira

The 73rd Annual Meeting of Japan Wood Research Society in Fukuoka (第 73 回 日本木材学会大会 2023)

6. Highly efficient lignin decomposition of beech using lignin peroxidase performed in a membrane reactor

Kenneth Sze Kai TEO, Keiko Kondo, Kaori Saito, Yu Iseki, Takashi Watanabe, Takashi Nagata, Masato Katahira

The 68th Lignin conference in Nagaoka (第 68 回リグニン討論会 2023)

Acknowledgements

I would like to sincerely express my profound gratitude to Professor Masato Katahira for giving me the invaluable opportunity to join his research group. Throughout the span of six years, which included six months as a research student, two years as a master's student, and three and a half years as a doctoral student, Prof. Katahira consistently offered me invaluable guidance, unwavering support, academic insight, and more. While maintaining a strict and professional demeanor in our pursuit of research excellence, he also fostered a friendly and enjoyable atmosphere during laboratory gatherings, such as welcome parties and year-end celebrations. My journey alongside Prof. Katahira has not only enriched me academically but has also shaped my personal growth.

I extend my deepest gratitude to Professor Takashi Nagata for his continuous mentorship during my postgraduate studies in Katahira Laboratory. Prof. Nagata has been a constant source of invaluable guidance, consistently presenting challenging research ideas, offering constructive criticism, and sharing his unique insights, including memorable dining experiences. His exemplary work ethic and professionalism have been a continual source of inspiration throughout my academic journey. I consider myself truly privileged to have had Prof. Nagata as my secondary research supervisor, and I am deeply appreciative of the immense benefit I have gained from his mentorship and support.

I also wish to convey my appreciation to Professor Keiko Kondo for her unwavering support and guidance in the realm of biomass research. As my mentor in Katahira Laboratory, Prof. Kondo has patiently nurtured my research skills from the ground up, imparting countless techniques and equipment handling expertise that have been instrumental in

shaping my current research capabilities. Beyond research techniques, her dedication to improving my proficiency in the Japanese language through continuous conversation has been instrumental in my personal development.

I seize this opportunity to thank Professor Takashi Morii and Professor Haruo Kawamoto for their invaluable time and constructive criticism, which greatly contributed to the refinement of this thesis.

Additionally, I express my gratitude to Professor Yudai Yamaoki for his consistent technical and emotional support within the laboratory. His professionalism and dedication to his work have served as a model for me. I also extend my thanks to Dr. Keisuke Kamba for offering valuable critiques during my presentations in the laboratory.

To all my fellow research members in the field of biomass in Katahira Laboratory, including Dr. Sadat Mohamed Rezk Khattab, Dr. Lin Meng-I, Dr. Wan Hasnidah Wan Osman, Mr. Mohammed Oksh Mohammed Mousa, Mr. Apisan Phienluphon, Mr. Yusei Yagi, Mr. Andry Wangsamihardja, Mr. Yuta Sakai, Mr. Ryosuke Ono, Ms. Yuka Yonezawa, Mr. Dai Weire, Mr. Ji Chen Chen, Ms. Eri Oga, and Mr. Yuto Goto, I am deeply grateful for your presence and the wealth of knowledge and ideas you shared throughout my research journey in Katahira Laboratory. As a cohesive team, we collectively tackled the challenge of advancing biomass valorization, and your contributions significantly enhanced the quality of my thesis while keeping my research motivation high.

To all the other members of Katahira Laboratory, including Dr. Nesreen Hamad Abdelgawwad, Mr. Tomohito Igaki, Ms. Lin Kuan-Heng, Mr. Shohei Takami, Ms. Wang Ning-Xin, Ms. Tu Wei-Hsun, Dr. Mohammed Mahmoud Afaf Sobhi Eladl, Mr. Mohammed

Mahmoud Omar Sobhi Eladl, Mr. Sakamoto Tomoki, Ms. Zheng Chuyu, Ms. Chaithanya Pudushery Kunjiveedu, Mr. Kentarou Tozawa, Mr. Taisei Masunaga, Ms. Makoto Shimizu, Ms. Aika Kawakami, Mr. Souichiro Matsuo, and Mr. Taiki Morita, I am truly thankful for the enjoyable moments we shared during my research tenure in Katahira Laboratory.

I take this occasion to express my gratitude to Ms. Naomi Murakami, the secretary of Katahira Laboratory, for her continuous support and assistance throughout my student life at Kyoto University. Equally, I appreciate the support provided by Ms. Mayako Saito and Ms. Tomomi Komiyama in handling administrative matters at Kyoto University.

I am profoundly thankful for the generous MEXT scholarships provided by the Japanese government over five and a half years. Without this financial support, pursuing my studies at Kyoto University would have been unfeasible. I am forever indebted for their trust and kindness, and I am committed to fostering stronger ties between Malaysia and Japan throughout my life.

To my research collaborators, especially Professor Takashi Watanabe, I extend my heartfelt appreciation for facilitating access to their analytical equipment, which was instrumental in generating valuable research data. Prof. Watanabe's collaboration has also provided invaluable feedback and critique that enhanced the quality of my research articles. I would also like to thank members of Watanabe Laboratory, including Professor Hiroshi Nishimura, Dr. Kaori Saito, Dr. Yutaka Makimura, Dr. Mei Sano, and Mr. Yu Iseki, for their support and assistance during my research in Watanabe Laboratory.

I wish to extend my profound gratitude to my parents and sister, Mr. Teo Kong Wan, Ms. Yip Siew Fune, and Ms. Joycelyn Teo Sze Ling, for their unwavering support in my

pursuit of a Doctoral degree at Kyoto University, Japan. Their consistent encouragement has been the cornerstone of my journey thus far, and I consider myself incredibly fortunate to have them by my side.

Lastly, I would like to express my heartfelt appreciation to my friends, also at Kyoto University, Dr. Jia Zhen Yap and Ms. Yang Hsien Li, for continually providing encouragement and being a cherished travel companion as we explored Japan together. Your friendship and unwavering support have enriched my experience, and I am truly thankful for your presence in my life in Japan.

Kenneth Sze Kai TEO

Laboratory of Bioenergy,
Department of Fundamental Energy Science,
Graduate School of Energy Science,
Kyoto University
December 2023